UNIVERSITY OF NAPLES "FEDERICO II"

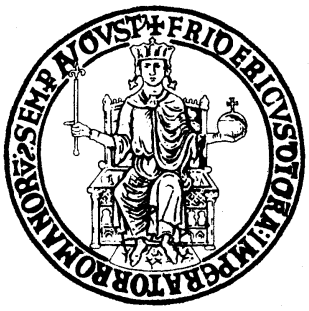

SCHOOL OF MEDICINE AND SURGERY

DEPARTMENT OF NEUROSCIENCES,

REPRODUCTIVE SCIENCES AND ODONTOSTOMATOLOGY

PhD Program in Neuroscience – XXIX

Director: Prof. Lucio Annunziato

PhD THESIS

INSIGHT IN THE PHYSIOPATHOLOGY OF THE DEVELOPING BRAIN: PRENATAL IMAGING AND EXPERIMENTAL MODELS

SUPERVISORS

Prof. Pasquale Martinelli

Prof. Daniel Surbek

CANDIDATE

Marialuigia Spinelli

ACADEMIC YEAR 2015/2016

Für meine geliebte Schweiz und
die Menschen die ich hier kennengelernt habe

"Es gibt zur zwei Arten zu leben. Entweder so als wäre nichts ein Wunder oder so als wäre alles ein Wunder".

Albert Einstein

Index

Preface

The development of this phD Thesis has its roots a three - year study across two Countries. The first half of the project has been realized in Italy, in Naples, at the private Centre "*Diagnostica ecografica prenatale Aniello Di Meglio s.r.l.*", with the collaboration of the Department of Radiologic, Oncologic and Pathologic Sciences at La Sapienza University, in Rome, while the second half of the research has been conducted in Switzerland, in Bern, at the "*Prenatal Ultrasound Unit*" of the Department of Obstetrics and Gynaecology, with the collaboration of the Department of Diagnostic and Interventional Neuroradiology, as well as at the "*Prenatal Medicine Research Laboratory*" of the Department of Obstetrics and Gynaecology and the Department of Clinical Research of the University of Bern.

The opportunity to combine clinical activity with in-vitro research has raised the challenge of the integration between two different, but at the same time, complementary and synergic points of view: from one side, the pragmatism of the clinician, dedicated to prenatal diagnosis in an OB/GYN facility in the routine practice and, from the other side, the vision of the pre-clinical researcher, that looks far, beyond the everyday feasibilities, to the exiting possibilities of widening prenatal therapy.

In relation to the pathophysiology of the developing human brain, these two approaches embrace two big chapters of this interesting field of medicine, including the study of brain malformations from one side (the clinical side), and the study of acquired brain injuries from the other side (the pre-clinical side).

The development of the brain is a fascinating but at the same time an exceptionally complicated process, which still today remains a challenge to the neurologists, neuroscientists and neuropathologists. Pathological noxae that may impair this physiological development are related to a number of events involving internal and/or external causative agents, that lead to brain malformations or to acquired brain injuries.

A malformation is defined as an aberration of normal organ development occurring as a consequence of a genetic disposition, infection, exposition to a teratogenic agent, or sporadically. Fetal brain malformations have an incidence of 0.36% of life-births and can be, depending on the involved pathophysiological mechanism, subsequent to the failure of (a) ventral induction, (b) dorsal induction, (c) neuronal proliferation, differentiation, histogenesis, (d) neuronal migration.

Acquired fetal brain injuries are a consequence of damage to a previously normally formed structure, so they must be differentiated from malformations (where a structure is not normally formed). In a neuropathological series of intrauterine or neonatal deaths, 20.4% showed evidence of prenatal brain injury. Acquired brain injury may be subsequent to (a) maternal disease, acute maternal impairment, (b) exposition to toxic/iatrogenic agents (c) disorders of the placenta and\or of the umbilical cord (d) fetal metabolic or hematologic disease/malformations.

Guided by a genuine combination of interest in the subject, curiosity, challenge, but also adaptability to the circumstances as well as a pinch of "*serendipity*", this phD research line has been developed into 3 branches as follows:

- the main part (A) focused on a specific aspect of the ventral induction and its failure: the developing cerebellum, with a special insight in the midline structures of the posterior fossa. This main part explores the diagnostic potentialities of prenatal imaging such as ultrasound and magnetic resonance imaging (MRI), which, thanks to the ongoing technical and scientific progress, have evolved from almost exclusively experimental examinations to clinically important tools, which impact decision making in the field of pre- and perinatal medicine;

- the second part (B) has been dedicated to the prenatal ultrasonographic imaging of neuronal migration, with special attention to the growing fetal cortex, whose fissures and sulci mark progressively its development throughout gestation;

- an ancillary part (C) has dealt with experimental translational stem cell research in acquired fetal brain injuries. This is a currently ongoing project, including in-vitro experiments as well as in- vivo-transplantation of stem cells and stem cell derivates for peripartum neuro-regeneration in an experimental model. Only the little contribution of this thesis to this ongoing project has here briefly reported.

It is important to underline that all the here reported data represent a starting point rather than a conclusion of a research trajectory. Indeed, the final, most important aim of this project, across its 3 branches, is to open new ways for further, new investigations as well as to raise the interest of the scientific community to these still understudied and challenging fields of Prenatal Medicine.

A) Main project: The developing cerebellum: insight in the midline structures of the posterior fossa

A 1. Introduction

A 1.a The cerebellum: historical overview

Throughout the history of Medicine, the cerebellum has always been recognized as a distinct subdivision of the brain. Its special feature is that it is not visible when looking down at the surface of the human brain, since it is overlaid by the occipital lobe of the cerebral cortex. In many animals, the cortex does not extend over the cerebellum, so it can be seen from the top. This species difference lay at the root of Vesalius' (1514–1564) questioning an earlier description by Galen. Vesalius (1543) wrote: "*Anatomists describe the site of the cerebellum as if it filled the whole region of that prominence of the occiput, that swelling which the mass of the people consider a measure of the power of memory and talent. The very highest part of the cerebellum extends only to the middle [the middle here refers to the occiput; ed.] although some, deluded by oxen and asses or by dreams, have written that the cerebellum ascends from the posterior site of the foramen, to the lambdoid suture*".

Vesalius was one of the first in a long tradition in cerebellar research of questioning the worth of his predecessor's contribution. Vesalius suggested that Galen's descriptions were false, probably because he based his descriptions, not on the human cerebellum, but on that of an ox.

The earliest anatomical descriptions were limited by the usual procedure of dissecting brain structures from above. Costanzo Varolio (1543–1575) introduced the practice of dissecting from below (Varolio, 1573). He described and illustrated the pons, a massive structure in humans which is intimately related to the cerebellum, and often referred to as "*the Pons of Varolius*."

After this discovery, followed an increasingly accurate portrayal of the gross anatomical structure of the cerebellar cortex and recognition of the cerebellar nuclei which are encased within its white matter.

Marcello Malpighi (1628–1694) wrote (1665): "*All the fibres dispersed through the brain and cerebellum seem to have origin from the trunk of the spinal marrow contained within the cranium like a noteworthy collection of fibres: for they ramify hither and thither from four reflected crura of the marrow until they end in the cortex in branching extremities. This course is more apparent in the cerebellum because the fibres are extended in the form of a tree and on the extreme branches, almost like leaves, the cortex is delicately placed. It is not attached to anything so it resembles a free leaf*."

Shortly thereafter, the cerebellar nuclei were recognized by Raymond de Vieussens (1641–1716) as an ash grey area of glandular substance, buried within the white matter of the cerebellum. Félix Vicq dÁzyr (1746–1794) provided a more realistic drawing of the corpus rhomboideum, and renamed it as the corps dentelé (Moreau de la Sarthe, 1805) (**Fig.1**). The other cerebellar nuclei were first labelled as the emboliform, globose and fastigial nuclei

by Stilling (1864). Vicq dÁzyr drew attention to the distinctness of the indentation on the superior surface of the dentate and their relative absence on its inferior surface, corresponding to the two divisions of the human dentate now known as the dorsal microgyric division or palaeodentatum and its ventral, macrogyric division, also known as the neodentatum, the latter receiving its name from the large undulations of the cell band in this part of the nucleus. A division of the monkey dentate into a dorsal (motor) and ventral (nonmotor) portions, with projections to (pre-)motor and pre-frontal cortical areas and eye fields recently was proposed by Dum and Strick (2002).

In the 18th Century took place a succession of increasingly accurate anatomical descriptions in which subdivisions of the cerebellum began to be named. Vincenzo Malacarne (1744–1816) published the first work entirely devoted to the cerebellum in 1776 (**Fig.2**). He dissected the brain from all approaches, and gave a far more accurate description of the cerebellar cortex and nuclei than any of his predecessors.

Furthermore, interestingly, he first described accurately the midline structures of the cerebellum and the posterior fossa, i.e. the currently so called "*vermis*". Curiously, he named the cerebellar parts and the vermis itself - as well as its further subdivisions - for their resemblance to some other known structures, e.g. lingula (Italian: linguetta, a cat's tongue) uvula (Italian: ugola). He wrote: *". . . is seen a thick pyramidal eminence . . . I have called the laminate pyramid . . . to these lateral tangles . . . I give the name of tonsils of the cerebellum and to the conical eminence uvula, because they greatly resemble the parts of the same names located in the human body*."

In Malacarne's time congenital hypotyroidism was widespread in the Po valley due to a lack of iodine in this region of Italy. He described two cases of cretinism that came to autopsy in which the cerebellum was smaller than normal, and with fewer folia. Malacarne also suggested that the cerebellum might be involved in plastic changes. In his book on the anatomy of the cerebellum, he described the presence of variability in the number of folia from 500 to 780. In a case of an intellectually disabled they were 340. In a series of letters that he exchanged with the Swiss anatomist Carlo Bonnet, Malacarne (1791) discussed whether such variability is innate or was acquired by experience. He proposed raising animal twins in poor and enriched environments and determining the number of folia. If the experiment was ever done, it has not been reported.

By the end of the 18th Century there was an accurate picture of the gross anatomy of the cerebellum, and there were speculations about its functions. Although the anatomical descriptions were accurate, early claims for cerebellar functions remained speculative; typically based on very little evidence. Johann Christian Reil (1759–1813) and Karl Friedrich Burdach (1776–1847) used alcohol fixation to verify and extend Malacarne's earlier description, resulting in the classical nomenclature for the lobules of the human cerebellum, still in use today (Reil, 1807-1808; Burdach, 1819–1826). Reil's paper contains a meticulous description of the cerebellar lobules. Beautiful engravings illustrate this paper.

At the time that these anatomical studies were being reported, Volta's discovery of a bimetallic source of electricity was the newest thing in physics. Reil suggested that the alternating layers of grey and white matter

constitute a sort of voltaic pile, generating animal electricity. Other interpretations were based on even less-well-founded evidence.

Curiously, the phrenologists Gall (1757–1828) and his followers (Combe and Combe, 1838) started to consider the cerebellum as the organ of sexuality: "*philoprogenitiveness*" (love of making babies). The claim was taken seriously, some authors supporting the proposed role of the cerebellum in sexual functions, others rejecting it. In this lectures on diseases of the brain, reported in The Lancet, Andral cited M. Voisin who had studied the heads of 372 convicts sentenced to the galleries at Toulon. On the basis of the shape of their skulls he identified 20 of these as potential sex offenders. Voisin wrote that "*thirteen of these twenty had actually been confined for rape or attempts upon female chastity*." Voisin also cited Dr. Ferroresi of Torino who had obtained the cure of a young girl afflicted with nymphomania and two young men who suffered from a habit of masturbation by the simple application of ice to the back of the head, below the occipital protuberance. Gall's speculations about cerebellar function attracted supporters, even though experimental evidence began to be available.

At the beginning of the 19th Century, animal experiments began to give a more accurate functional understanding. Luigi Rolando (1773–1831) identified the specifically motor symptoms which follow cerebellar lesion (1809). The lesions impaired motor and not sensory or intellectual functions.

Rolando concluded that the cerebellum was the brain region responsible for initiating movement, but his experiments were rather crude. With the development of increased surgical skill and later of aseptic technique, more accurate evaluation of the effects of cerebellar lesions became possible. Two of the great experimenters of the 19th Century were Pierre Flourens and Luigi Luciani.

Flourens (1794–1867) made the fundamental observation that animals are not paralyzed. Movements are not completely lost after cerebellar ablation. He argued that it is the coordination of movement, a property which had not previously been considered by physiologists. Flourens also noted there may be considerable recovery from the initial symptoms caused by a cerebellar lesion.

Flourens (1824) wrote: ". . . *All movements persist following ablation of the cerebellum: all that is missing is that they are not regular and coordinated. From this I have been induced to conclude that the production and the coordination of movements form two classes of essentially distinct phenomena and that they reside in two classes of organs also essentially distinct: with coordination in the cerebellum and production in the spinal cord and medulla oblongata*."

Flourens dismissed definitively as unfounded the claims for the sexual functions of the cerebellum. He removed the cerebellum of a mature rooster. The animal was still deeply interested in the hens, but motor dysfunction made it difficult for him to express his feelings towards them. The animal's deficit seemed to be entirely motor in character. Flourens' descriptions of the effects of cerebellar lesions remained as the definitive work for much of the remainder of the 19th century, and many of his conclusions remain valid today.

Towards the end of the Century Luigi Luciani (1840– 1919) used improved operative technique and sterile procedures to re-address the question of cerebellar symptoms.

Luciani (1891) (**Fig. 3**) distinguished between the immediate transient effects of lesions (un-stabilized deficiency), and their more permanent effects (stabilized deficiency). He emphasized that the permanent effects of cerebellar lesions could be understood in terms of elementary deficits in muscle control. The three cardinal symptoms according to Luciani were asthenia, or weakness, atonia, lack of normal muscle tone, and "astasia". Luciani characterized "astasia" as an inability to maintain normal fusion and continuity of movement, reflected in the intention tremor that is seen in cerebellar patients. He wrote: "*To this group of phenomena which include tremor, titubation and rhythmical oscillating movements, we gave the name astasia for the sake of brevity and owing to their probable common origin*."

During the last Century the technical and technological advancements have allowed a thorough and a deep study of the cerebellum, its functions, its interactions with all the other parts of the brain. Today, we can affirm that the cerebellum is one of the best studied parts of the brain.

One of the most interesting and fashioned progresses of this last Century has been the possibility to study the cerebellum also during prenatal life, and investigate the cerebellar embryogenesis and morphogenesis throughout gestation, thanks to the recent enormous development of prenatal imaging.

A 1.b Embryogenesis and morphogenesis of the cerebellum

The cerebellum develops over a long period, extending from the early embryonic period until the first postnatal years, arising bilaterally from the alar layers of the so called "first rhombomere" (**Fig. 4**). Early in the fetal period, the two cerebellar primordia were said to unite dorsally to form the vermis. However, Sidman and Rakic (1982) advocated Hochstetter's (1929) view that such a fusion does not take place, and hypothesized the presence of only one cerebellar primordium (the tuberculum cerebelli). Today this last theory is the most accredited. The tuberculum cerebelli consists of a band of tissue in the dorsolateral part of the alar plate that straddles the midline in the shape of an inverted V. The arms of the V are directed caudally as well as laterally, and thicken enormously, accounting for most of the early growth of the cerebellum. The rostral, midline part of the V, however, remains small and relatively inconspicuous.

The further morphogenesis of the cerebellum can be summarized as follows (**Fig. 5**): (1) the caudally and laterally directed limbs of the tuberculum cerebelli thicken rapidly early during the 6th postovulatory week and bulge downwards into the fourth ventricle (on each side the internal cerebellar bulge or "*innerer Kleinhirnwulst*" of Hochstetter, which together form the corpus cerebelli) ; (2) during the following weeks, the rapidly growing cerebellum bulges outwards as the external cerebellar bulges ("*äusserer Kleinhirnwulst*" of Hochstetter) which represent the flocculi, delineated by the posterolateral fissures; (3) during the third month of development the growth of the midline component accelerates and begins to fill the gap between the limbs of the V, thereby forming

the vermis. It is important to underline this latter point: currently, has been ascertained that the cerebellar vermis *per se* is not formed through the fusion of the adjacent developing cerebellar hemispheres but it develops as a direct proliferation of the mesial primordium (**Fig. 6**). Experimental evidence shows us that granule cells, arising from the lateral upper rhombic lip migrate medially into the posterior cerebellum, whereas granule cells arising in the medial upper rhombic lip are confined to an anterior cerebellar distribution. Therefore, as the primordia are separate, the development of the posterior vermis is not dependent on that of the anterior vermis; by the 12^{th} to 13^{th} weeks of development, outward, lateral and rostral growth processes have reshaped the cerebellum to a transversely oriented bar of tissue overriding the fourth ventricle. Robinson in 2014, in an interesting editorial published on Ultrasound in Obstetrics and Gynaecology has pointed out that all these experimental evidences may have an important clinical relevance, since they may help in better understanding and diagnosing the so called "inferior vermis hypoplasia" (see subsequent paragraphs).

As the vermis grows caudally it invaginates into the rhombencephalic vesicle, and the posterior membranous area protrudes beneath the vermis into the overlying meninx primitiva. This evagination, first described in 1900, is known as Blake's pouch, and where Blake's pouch constricts to pass through the cerebellar vallecula (the normal space inferior to the vermis, superior to the nucleus gracilis and medial to the cerebellar hemispheres) it is known as Blake's metapore (**Fig. 6**). Even though Blake's pouch itself lies within the subarachnoid space of the developing cisterna magna, it is a direct extension of the fourth ventricle and, therefore, the fluid contained in Blake's pouch is intraventricular. Straight echoes (the cisterna magna septa), typically seen in the fetal cisterna magna at prenatal ultrasound scan, and most often described as bridging arachnoid septations, have recently been shown to represent the walls of Blake's pouch, which may now be considered a potential marker for normal development.

The future cisterna magna therefore forms in two compartments: a mesial compartment between the cisterna magna septa, which is derived from the rhombencephalic vesicle (Blake's pouch), and compartments lateral to the cisterna magna septa which develop through cavitation of the meninx primitiva overlying the surface of the brain, forming the subarachnoid space proper (**Fig. 6**). Blake's pouch usually, but not always, fenestrates to a variable degree down to the obex (the inferior recess of the fourth ventricle), which leads to communication between the mesial ventricular-derived compartment and the true subarachnoid space of the cisterna magna. Fenestration and disappearance of Blake's pouch, thus, leaves an opening at Blake's metapore which is known as the foramen of Magendie, allowing communication between the fourth ventricle and the cisterna magna. Thus, the foramen of Magendie does not demarcate the true junction between the ventricular system and subarachnoid space of the cisterna magna. A small communication beneath the vermis, between the fourth ventricle and the 'cisterna magna', often described in the literature on ultrasound and sometimes seen on mid-sagittal images, therefore represents the normal Blake's metapore. Ultrasonographic imaging the posterior fossa in the semicoronal plane may show this normal opening, but can give a false appearance of a vermian defect and, unfortunately, is often described wrongly

as “inferior vermis hypoplasia” (see subsequent paragraphs) (**Fig.7**). This error can be avoided by making sure that the cavum septi pellucidi is included in the image, thus ensuring that the scan plane is truly axial or modified-axial.

A 1.c Phylogeny of the cerebellum

‘*Ontogeny recapitulates phylogeny’,* or embryology repeats evolution. This important principle states that the development observed during embryology is like a ‘*time-lapse photography*’ rendition of the various steps taken during evolution; thus, structures that evolved first also develop first in the embryo, although the separate steps become somewhat merged.

The oldest part of the cerebellum, the archicerebellum, comprises the bilateral flocculi and the mesial nodulus, and is known as the flocculonodular lobe (**Fig. 8**). Functionally, this lobe, plus some of the adjacent uvula, comprise the vestibulocerebellum, which has connections with the vestibular nuclei (which, although situated within the brainstem, are considered surrogate deep cerebellar nuclei) and semicircular canals, receives visual information from the superior colliculi, and is involved in balance, position and tone. These functions appear early in evolution, are shared among all vertebrates and phylogenetically are first seen in fish and amphibians; consequently, they are the earliest to appear embryologically.

The next part of the cerebellum to appear is the paleocerebellum, which comprises the lobules of the anterior lobe of the vermis (lingula, centralis, culmen) (**Fig.9**) and, importantly, the more caudal lobules of the posterior lobe of the vermis (pyramis) and some of the adjacent uvula. The paleocerebellum, plus adjacent paravermian tissue in the cerebellar hemispheres, is known functionally as the spinocerebellum and, due to its connections with the spinocerebellar tracts and efferent connections via the deep cerebellar nuclei to the cerebral cortex, it is involved in proprioception and synergy of movement and locomotion. Phylogenetically, this is first seen in higher amphibians and, in relative terms, is largest in reptiles and birds.

The final part of the cerebellum to appear is the neocerebellum (also known as the cerebrocerebellum or pontocerebellum), which comprises the most rostral lobules of the posterior vermis (between the primary and pre-pyramidal fissures) (i.e. declive, folium, tuber) (**Fig.9**), plus the majority of the contiguous cerebellar hemispheres. Functionally, it is involved with motion intent, planning, precision, force and extent, and increasingly it is recognized to regulate cognitive and language functions. Phylogenetically, this is seen in mammals only and it is largest in humans; it is, therefore, the latest to appear both in evolution and embryologically. It contributes the most to the trans-cerebellar diameter, and thus is one of the most widely used markers for normal cerebellar development in the fetus**.**

A similar pattern of development is seen in the deep cerebellar nuclei, among which the phylogenetically older nuclei, the fastigial nuclei, are the most medial within the white matter and connect primarily with the archicerebellum, followed by the globose and emboliform nuclei, which are more lateral and connect primarily

with the paleocerebellum, and finally the dentate, the most lateral nuclei, which are connected primarily with the neocerebellum. It therefore appears that, from an evolutionary and embryological perspective, the cerebellum actually develops with the most rostral and most caudal parts appearing together, initially adjacent to each other, with the more phylogenetically recent structures subsequently developing between these older structures, akin to the opening of a flower in which the outer petals are the first to appear and the inner ones appear later. Thus, the more anterior and posterior lobules and the associated medial deep cerebellar nuclei appear first, and the more central lobules, hemispheres and associated most lateral deep cerebellar nuclei appear last.

A 1.d Some notes on the anatomy of the cerebellum and the posterior fossa

The cerebellar cortex is composed of 4 main types of neurons: granule cells, Purkinje cells and two types of inhibitory interneurons, the Golgi cells and the stellate/basket cells. The cortex receives three kinds of input: the mossy fibres (most afferent systems), the climbing fibres from the inferior olive, and diffusely organized monoaminergic and cholinergic fibres.

The cerebellum is organized as longitudinal zones of Purkinje cells (A-, B-, C– and D-zones), each projecting to its own cerebellar nucleus and receiving input from different parts of the inferior olive. A less well-studied zone is the X-zone between the A- and B-zones in the anterior vermis. The cerebellar nuclei also known as central or deep cerebellar nuclei are the medial nucleus fastigii, the intermediate nucleus globosus and the nucleus emboliformis (together also known as the nucleus interpositus), and the laterally situated, large nucleus dentatus . The vermis contains a medial zone (A- zone) , projecting to the nucleus fastigii, and a small B- zone that innervates the lateral vestibular nucleus of Deiters. The cerebellar hemispheres can be divided into intermediate and lateral zones. The intermediate zone consists of three C- zones, projecting to the nucleus emboliformis (C1 and C3) and the nucleus globosus (C2). The large lateral zone (D- zone) innervates the nucleus dentatus. The lobus flocculonodularis innervates the vestibular nuclei in mammals and birds. Purkinje cells of a zone project to a particular cerebellar or vestibular target nucleus. Zones can extend across one or more lobules; some span the entire rostrocaudal length of the cerebellum. The olivocerebellar projection is arranged in a similar way. Subnuclei of the inferior olive project to a single Purkinje-cell zone or to a pair of zones sharing the same target nucleus. These longitudinal zones are not evident on the outside of the cerebellum. However, a system of compartments in the white matter, which contains the axons of the Purkinje cells and the climbing fibres, can be visualized.

Afferent and efferent fibre connections of the cerebellum pass through the cerebellar peduncles. The pedunculus cerebellaris inferior or corpus restiforme contains cerebellar afferents: the tractus spinocerebellaris posterior and the fibrae cuneocerebellares from the spinal cord, trigeminocerebellar fibres from sensory trigeminal nuclei, olivocerebellar fibres and vestibulocerebellar fibres. The pedunculus cerebellaris medius or brachium pontis is formed by the massive pontocerebellar system. The pontine nuclei are innervated by the cerebral cortex via two

tracts: the frontopontine tract from the frontal lobe, the motor and premotor areas in particular, and the parietotemporo - occipitopontine tract, particularly arising in the somatosensory areas and the adjacent area. The pedunculus cerebellaris superior contains the tractus spinocerebellaris anterior and the main efferent system of the cerebellum, i.e. the brachium conjunctivum. The cerebellar nuclei are the output centres of the cerebellum. The targets of these nuclei differ considerably. The dentate and interposed nuclei mainly innervate the thalamus and the red nucleus, and control corticospinal and rubrospinal projections. The fastigial nucleus and the nucleus of Deiters control the reticulospinal and vestibulospinal projections. The subdivision of descending supraspinal pathways into lateral and medial systems is therefore also found in the cerebellar control system. The dentate nucleus also has important feedback loops to the cerebellum through the nucleus reticularis tegmentalis pontis and the dentato-rubro-olivary loop. Projections from the small-celled part of the red nucleus to the inferior olive pass via the central tegmental tract.

The cerebellum lies into one of the three distinct depressions of the floor of the cranial cavity: the posterior cranial fossa, which is the most posterior and deep of the three cranial fossae (**Fig. 10 a**). The posterior cranial fossa is comprised of three bones: the occipital bone and the two temporal bones. It is bounded as follows: anteriorly and medially it is bounded by the dorsum sellae of the sphenoid bone. This is a large superior projection of bone that arises from the body of the sphenoid. Anteriorly and laterally it is bounded by the superior border of the petrous part of the temporal bone, while posteriorly it is bounded by the internal surface of the squamous part of the occipital bone. The floor consists of the mastoid part of the temporal bone and the squamous, condylar and basilar parts of the occipital bone. There are several bony landmarks and foramina present in the posterior cranial fossa. The internal acoustic meatus is an oval opening in the posterior aspect of the petrous part of the temporal bone. It transmits the facial nerve, vestibulocochlear nerve and labrynthine artery. A large opening, the foramen magnum, lies centrally in the floor of the posterior cranial fossa. It transmits the medulla of the brain, meninges, vertebral arteries, spinal accessory nerve (ascending), dural veins and anterior and posterior spinal arteries. Anteriorly an incline, known as the clivus, connects the foramen magnum with the dorsum sellae. The jugular foramina are situated either side of the foramen magnum. Each transmits the glossopharyngeal nerve, vagus nerve, spinal accessory nerve (descending), internal jugular vein, inferior petrosal sinus, sigmoid sinus and meningeal branches of the ascending pharyngeal and occipital arteries. Immediately superior to the anterolateral margin of the foramen magnum is the hypoglossal canal. It transmits the hypoglossal nerve through the occipital bone. Behind the foramen magnum the squamous part of the occipital bone is marked in or near the median plane by a ridge of bone, called the internal occipital crest, which ends above and behind in an irregular elevation, named the internal occipital protuberance (**Fig. 10 b**). On each side of the protuberance a wide shallow groove curves laterally with a slight upward convexity to the postern-inferior angle of the parietal bone. It is produced by the transverse sinus, is usually deeper on the right side and at its lateral extremity is continuous with the groove for the sigmoid sinus. Below the groove for the transverse sinus the internal occipital crest divides the bone into two gently hollowed fossae, which

lodge the cerebellar hemispheres. The internal occipital crest corresponds to the lower, prominent division of the cruciate eminence of the occipital bone and it bifurcates near the foramen magnum, giving the attachment to the falx cerebelli (see later); in the attached margin of this falx is the occipital sinus, which is sometimes duplicated (**Fig. 11**). The internal occipital protuberance is related to the confluence of sinuses and is grooved on each side by the commencement of, the transverse sinus. The margins of the groove for the transverse sinus give attachment to the two layers of the tentorium cerebelli. Traced laterally the groove reaches the lowest part of the posterior inferior angle of the parietal bone, where it becomes continuous with the sigmoid groove. On each side of the internal occipital crest the bone is thin, and translucent, in marked contrast to the regions of the crest and of the internal occipital protuberance On the upper part of the internal occipital crest, a small depression is sometimes distinguishable; it is termed the vermian fossa since it is occupied by part of the vermis of the cerebellum.

The falx cerebelli (**Fig. 11**) is a small sickle shaped fold of dura mater, projecting forwards into the posterior cerebellar notch as well as projecting into the vallecula of the cerebellum between the two cerebellar hemispheres. The name comes from the Latin word falx meaning "*curved blade or scythe*" and cerebellum meaning "brain". Its base is attached, above, to the under and back part of the tentorium cerebelli; its posterior margin, to the lower division of the vertical crest on the inner surface of the occipital bone. The falx cerebelli generally lies somewhere between 2.8 and 4.5 cm in length and is approximately 1–2 mm thick. In its lower portion the falx cerebelli diminishes very rapidly in height and as it descends, it can divide into two smaller folds or diverging limbs, which are lost on the sides of the foramen magnum. Other variations such as duplication, triplication, absence, and fenestration are much less common. As dural venous sinuses are concurrent with the development of dural folds, duplication of the falx cerebelli is usually associated with duplicated occipital sinus.

A 1.e Developmental cerebellar Disorders with focus on midline malformations

Anatomically, cerebellar malformations may be classified into unilateral and bilateral abnormalities. Unilateral cerebellar malformations are most likely due to acquired insults, such as intracerebellar bleeding associated with prematurity. Depending on the part of the cerebellum involved, bilateral cerebellar malformations may be further classified into midline or vermis malformations, and malformations affecting both the vermis and the cerebellar hemispheres.

Agenesis or hypoplasia of the vermis may be found in a large number of malformations of the brain including the Dandy-Walker malformation (DWM) (see below) and syndromes with agenesis of the vermis as a constant feature, such as the Joubert syndrome and Walker-Warburg syndrome; a large group of syndromes in which absence of the vermis may occur, such as the Meckel-Gruber and Smith-Lemli-Opitz syndromes, and dysgenesis of the vermis in rare disorders, such as rhombencephalosynapsis, tectocerebellar dysraphia and Lhermitte-Duclos disease. Major malformations of the cerebellar midline structures are also found in the Chiari

malformations. The most common type, i.e. type II Chiari malformation, is almost always associated with a myelomeningocele, and is part of the neural tube defect spectrum. A high percentage of diagnosed dyslexic children show behavioural evidence of abnormal cerebellar function. Quantitative MRI studies showed an impaired growth of the vermis is detectable in idiopathic autism, as well as in autism associated with fragile X syndrome.

A developmental and genetic classification for all brain stem malformations, including those of the cerebellum, was published by Barkovich et al. in 2007 and 2009. Based on a large data base of experimental studies in mice and their own extensive clinical studies, they suggested four categories: (1) malformations secondary to anteroposterior and dorsoventral patterning; (2) malformations associated with later generalized developmental disorders affecting the brain stem and the cerebellum; (3) localized brain malformations affecting the brain stem and the cerebellum; and (4) combined hypoplasia and atrophy in putative prenatal-onset degenerative disorders.

Relatively to posterior fossa anomalies, from an exquisitely ultrasonographic point of view, it is possible to differentiate malformations into two broad categories: (1) cystic malformations, characterized by the presence of an apparent cerebrospinal fluid collection in the posterior fossa due to fourth ventricle/cisterna magna dilatation, or to true arachnoid loculations; and (2) non-cystic malformations, in which there is no apparent cerebrospinal fluid collection. To the cystic malformations belong the DWM, the Blake's pouch cyst, the mega cisterna magna and the vermian hypoplasia ("Dandy Walker variant").

The DWM (**Fig. 12**), named by Benda (1954) after the first descriptions of Dandy and Blackfan (1914) and Taggart and Walker (1942), is characterized by the following triad: (1) cystic dilatation of the fourth ventricle and an enlarged posterior fossa with upward displacement of the lateral sinuses, confluens sinuum and tentorium cerebelli, (2) varying degrees of vermian aplasia or hypoplasia, through which the 4th ventricle communicates with the cisterna magna; and (3) hydrocephalus. DWM has an estimated prevalence of approximately 1 per 30,000 births and is found in 4% to 12% of all cases of infantile hydrocephalus. Indeed, this latter sign, associated with a bulging occiput, is unusual at birth but is present by 3 months of age in about 75 % of patients. Early shunting of the cyst and hydrocephalus is advocated, because early management may give intellectual development a better chance and improve prognosis. Intellectual disability and seizures have been reported in up to 50 % of cases with a DWM. Most cases are sporadic. Associated brain malformations are present in up to 68 % of the cases, the most common of which is agenesis or hypogenesis of the corpus callosum. Other neural malformations include neuronal heterotopias, polymicrogyria, schizencephaly, occipital encephaloceles and lumbosacral meningoceles. Extra-neural malformations are found in about one third of the cases, particularly in familial ones, and include cleft lip and palate, cardiac malformations, urinary tract anomalies, polydactyly and syndactyly and minor facial dysmorphisms. The aetiology of DWM remains unknown. Probably, the malformation arises late in the embryonic period. Hypotheses include developmental arrest in the formation of the hindbrain, atresia of the fourth ventricular outlet foramina and delayed opening of the aperture of Magendie. The choroid plexus of the fourth ventricle arises

in the middle of the thin roof of the hindbrain. The area rostral to the plexus, i.e. the area membranacea superior of Weed, disappears during the formation of the vermis. Late in the embryonic period, the median aperture or foramen of Magendie arises in the area membranacea inferior, caudal to the plexus, and forms a connection between the fourth ventricle and the subarachnoid space. The lateral apertures or foramina of Luschka are formed in the fetal period. In one fifth of a large series of normal brains examined, the apertures of Luschka were not open, mostly bilaterally; therefore, atresia of the apertures of Luschka does not play a role in the aetiology of DWM. If the superior membranaceous area is not incorporated into the developing choroid plexus or if there is delayed opening of the aperture of Magendie, the roof of the fourth ventricle can balloon posteriorly to form a fourth ventricular cyst, identical to what is seen in DWM. Evidence that such a phenomenon may occur comes from a strain of mice with congenital hydrocephalus in which the superior membranaceous area remains, leading to a large cyst between the vermis and the choroid plexus. The formation of a large cyst in the posterior fossa impairs normal outgrowth of the vermis and corpus callosum.

Barkovich and others advocated the so called “Dandy- Walker complex” as a continuum of posterior fossa anomalies comprising DWM, the Dandy-Walker variant (that authors currently name “vermis hypoplasia”) and mega cisterna magna.

In the Dandy-Walker variant (“vermis hypoplasia”), the posterior fossa is variable enlarged; there is variable hypoplasia of the vermis, communication between the fourth ventricle and arachnoid space, and no hydrocephalus is present. The mega cisterna magna consists of an enlarged posterior fossa, secondary to an enlarged cisterna magna, but a normal vermis and fourth ventricle are found. For malformations of the posterior fossa with prominent cyst-like cerebrospinal fluid-containing spaces, that fail to fulfil all the criteria for the diagnosis DWM, such as the absence of hydrocephalus, Kollias and Ball in 1997 suggested the broad term vermian-cerebellar hypoplasia. Although true DWM and vermian-cerebellar hypoplasia are often associated with supratentorial and extraneural malformations, most of these cases cannot be classified according to well-defined syndromes (Kollias and Ball 1997) . Parisi and Dobyns (2003) introduced the term cerebellar vermis hypoplasia – dysplasia as an alternative for many cases of the Dandy-Walker variant and mega cisterna magna. However, here it is important to underline that, although the valuable efforts of the authors, there is still a considerable confusion in the literature regarding the terminology used when describing abnormalities of the cerebellum and of the vermis in particular.

Several families with cerebellar vermis hypoplasia-dysplasia follow X-linked inheritance. Mutations of the oligophrenin- 1 gene (OPHN1) at Xq12, previously associated with X-linked intellectual disability, have been identified in affected males for several clinically rather heterogeneous families with intellectual disability and vermis hypoplasia with a 50 % overall recurrence risk. The prognosis for individuals with this and related conditions is often worse than for classic DWM.

DWM has been frequently diagnosed prenatally, and has been reported as early as in the first trimester. The classic DWM is less commonly encountered than the Dandy-Walker variant. However, currently, prenatal imaging cannot reliably differentiate between true DWM and the wide spectrum of the "complex", including cerebellar vermis hypoplasia-dysplasia. Although the cisterna magna can be visualized in approximately 95 % of fetuses between 15 and 25 weeks of gestation, determination of pathology can be difficult in cases with mild dilatation. Caution is encouraged during the early second trimester prenatal ultrasound scan in making the diagnosis of partial vermian agenesis because the incompletely formed inferior cerebellar vermis may give the false impression of a vermian defect. This is especially common at prenatal ultrasound with a steep angle of section through the posterior fossa (**Fig.7**). A follow up scan is recommended if a defect of the vermis, especially the inferior vermis, is suspected. Criteria for an enlarged cisterna magna have not been firmly established thus far. An enlarged cisterna magna typically measures greater than 10 mm in anteroposterior dimension. However, this appearance is most commonly seen in normal foetuses, especially during the third trimester because the size of the cisterna magna varies slightly with the gestational age. When an enlarged cisterna magna is the only finding, especially during the third trimester, the overwhelming outcome is normal. However, an enlarged cisterna magna may be a primary clue to trisomy 18, although in this situation other subtle anomalies are often seen and the fetus is small for gestational age. Therefore, demonstration of an enlarged cisterna magna should stimulate a careful search for other anomalies, and this finding should be correlated with other risk factors. It is worth noting that in the large antenatal series reported in the literature, DWM is frequently over- and underdiagnosed compared to pathology. Whereas false-positive diagnoses are common, vermian defects can also be missed, especially in case of borderline cisterna magna. As with other cerebral malformation, intrauterine MRI can be useful in the assessment of DWM, particularly to evaluate the vermian defect as well as to identify associated anomalies, such as heterotopia.

Distinguishing inheritable syndromes from isolated cases of vermian-cerebellar hypoplasia is important for genetic counselling. Bordarier and Aicardi (1990) classified the genetically heritable syndromes with complex vermian- cerebellar hypoplasia into two groups: (1) those in which vermis aplasia is a constant feature, the most common entities being Joubert syndrome, Walker-Warburg syndrome and related cerebro-oculomuscular syndromes; and (2) those in which vermis aplasia is an occasional component, such as Meckel-Gruber syndrome, oro-facio-digital syndromes, Coffin-Siris syndrome, Smith-Lemli-Opitz syndrome and Ellis-van Creveld syndrome, all autosomal recessive traits. Vermian aplasia may also occur in X-linked disorders such as Aicardi syndrome. Most of these syndromes include severe intellectual disability and have a worse prognosis than isolated vermian-cerebellar hypoplasia or the DWM. Moreover, the risk of recurrence in siblings is high.

In Blake's pouch cyst (or 'persistent Blake's pouch') (**Fig. 13**) there is thought to be inadequate fenestration of both Blake's pouch and the foramina of Luschka, leading to imbalance of cerebrospinal fluid egress into the subarachnoid space of the cisterna magna, with consequent dilatation of the fourth ventricle. Although the pouch communicates freely with the fourth ventricle, there is a failure of communication between the pouch and the

perimedullary subarachnoid spaces. In most of the lower species, including dogs, Blake's pouch is a normal persistent structure, yet in these species the vermis grows even more caudally than it does in humans, thereby obliterating the mesial portion of Blake's metapore and dividing it into two lateral metapores. However, other than in humans, the foramina of Luschka are also larger and therefore the normal non-fenestration of Blake's pouch does not impede cerebrospinal fluid egress. In contrast, in humans, with smaller foramina of Luschka, non-fenestration of Blake's pouch causes it to enlarge and elevate/rotate the vermis away from the brainstem, but, because this causes a gap between the inferior vermis and the brainstem, this can lead to the false-positive diagnosis of '*inferior vermian hypoplasia'*. This theory of Blake's pouch cyst explains why historically there has been poor correlation of ultrasound and autopsy findings in apparent cystic malformations of the posterior fossa, because post-mortem the cyst deflates and the vermis de-rotates back into a normal position. This same scenario is seen in children and adults with Blake's pouch cyst, in whom there is no intrinsic vermian hypoplasia. Cerebrospinal fluid shunting or third ventriculostomy to decompress the ventricular system results in a return to normal appearance and clinical normality of these patients once the hydrocephalus has resolved. Isolated elevation/rotation of the vermis due to a persistent Blake's pouch does not necessarily indicate an adverse outcome. In one study, one third of cases of Blake's pouch cyst or mega cisterna magna underwent spontaneous resolution in utero and 90% of survivors with no associated anomalies had normal developmental outcome at 1–5 years, once the initial referral misdiagnosis of vermian hypoplasia had been excluded. In another large retrospective study of 19 cases of Blake's pouch cyst, associated anomalies were seen in eight. There were two neonatal deaths and eight terminations. Of nine survivors, one had trisomy 21, and the other eight were neurodevelopmentally normal, although obstructive hydrocephalus was seen in one. It has also been suggested in several cases in the literature that persistent Blake's pouch phenotype can be '*acquired*' if the balance of cerebrospinal fluid egress is upset by the presence of fetal intraventricular haemorrhage or fetal infection, which result in tetra-ventricular dilatation and enlargement of the 'cisterna magna' (i.e. enlargement of Blake's pouch contained within the cisterna magna), presumably through resultant debris within the ventricular system causing obstruction of the fenestrations in both the foramina of Luschka and Blake's pouch, in much the same way as can be demonstrated postnatally. However, it is important to recognize that, depending on the nature and timing of the insult, injury to the developing brain itself can also result from endotoxins, free radicals and inflammatory cytokines. Mega cisterna magna may, in fact, represent a mega Blake's pouch but with better cerebrospinal fluid egress such that the vermis is not elevated.

In the light of all these consideration, it appear evident that the prenatal assessment of a pathological posterior fossa is full of deceits: the pathophysiology of the abnormalities of the posterior fossa is complex, and it is still under debate; there is still a considerable confusion in the literature regarding the terminology used when describing abnormalities of the cerebellum and of the vermis in particular; the sonographic appearance of normal cerebellar development can resemble partial vermian agenesis during the early second trimester. This may give the false impression of a vermian defect.

A 2. Aim of the researches

More than 100 years ago, in 1898, Joseph A. Blake read a paper in occasion of a meeting of the Association of American Anatomists on the development of the fourth ventricle. His opening words were: "*My investigations on this subject were prompted by the contradictory opinions and lack of absolute knowledge concerning the nature of the communications between the cavity of the fourth ventricle and the subarachnoid space (Blake, 1900)*".

As pointed out in the introduction section, despite the numerous studies and advances in imaging, including the introduction of ultrasound and magnetic resonance, our knowledge on cerebellar development beyond the embryologic period remains limited, precluding in many cases clear differentiation between normal and pathological conditions. Although the imaging of the fetal posterior fossa represents an integral part of sonographic screening for fetal anomalies, Carroll et al. in 2000 found a lack of correlation in 57% (8 out of 14 fetuses) when comparing the results of the fetal ultrasound examinations, in which a cerebellar anomaly was diagnosed, to the results of autopsies on the aborted fetuses. Similar results were recently obtained in a larger study of 44 fetuses with an ultrasound diagnosis of DWM; the ultrasound examination failed to correctly diagnose DWM in 26 patients, as reported by Phillips et al. in 2006.

The introduction of MRI as a complementary method of diagnosis has shown that a correct diagnosis of some conditions included in the "Dandy-Walker complex", i.e. inferior vermian hypoplasia is difficult even with this technique with a false positive rate of 32%, as pointed out by Limperopoulos et al. in 2006. Recent knowledge in neurophysiology has shown that the cerebellar vermis is a fundamental midline structure which is involved not only in proprioception and synergy of movements, but also in language, behaviour and cognitive development; inferior vermian hypoplasia has been associated with many mental retardation syndromes and with autism; therefore, fetal medicine experts should be aware and extremely careful when making diagnosis of vermian pathologies in utero. Potential pitfalls also exist in the diagnosis of "benign" conditions such as persistence of Blake's pouch cyst or an isolated enlarged cisterna magna, with a number of mis-, over- and underdiagnoses. In other words, differential diagnosis is very challenging, since it can range from benign asymptomatic conditions to severe malformations associated with neurologic impairment.

In most of posterior fossa abnormalities, a wide communication between the fourth ventricle and the posterior fossa with a reduced size of the vermis are the common ground. However, in accordance with a recent classification reported by Robinson in 2009, the upward rotation of the vermis has been suggested as clue finding in the differential diagnosis.

Unfortunately, both sonographic and radiologic evaluation of this critical finding are usually subjective and no reference charts for normal and abnormal cases have been provided to date. Although the recent attention to vermian biometry by two- and three- dimensional approach, as well as some attempts to measure the angles between

vermis and the other posterior fossa structures, i.e. brainstem and tentorium proposed by Ghi et al. (2012), an accurate categorization of the fetal upward rotation/hypoplasia of the vermis remains a challenge.

Many pitfalls in the prenatal diagnosis of these conditions may be due to the fact that the standard antenatal ultrasonographic evaluation of these structures is limited to the axial plane and does not provide the assessment of cerebellar vermis size and integrity, which are thought to address the differential diagnosis of a wide range of pathologic conditions, including both minor and major anomalies. Furthermore, in the second and in the third trimester, a scanning angle too steep may create the impression of a vermian defect.

A window for assessing cerebellar vermis true size, integrity and relationship with other nearby brain structures can be provided by the mid-sagittal view of the fetal brain, as recently shown by authors. Indeed, the midsagittal plane offers a special view of the vermis as well as of the other midline structures of the brain and of the posterior fossa. This scan gives the advantage of the best evaluation of the relations of the vermis, considering also the morphogenesis of these structures, thanks to the antero-posterior view.

The purposes of this research line were:

Study a: to provide measurements of the cerebellar vermis circumference in normal fetuses during routine prenatal two-dimensional ultrasound examination, through the mid-sagittal plane, throughout pregnancy, in order to: (a) provide 2-dimensional (2D-US) nomograms of the cerebellar VC based on a large number of normal fetuses; (b) evaluate the reproducibility of these measurements between different operators (senior vs. junior); (c) evaluate the correlation among 2D and 3D-US measurements.

Study b: (a) to test a new method to assess the normal rotation of the cerebellar vermis over the brainstem using a novel measurements, the Vermian-Cresta angle (VCA) by transabdominal three-dimensional multiplanar ultrasonography in normal foetuses throughout pregnancy; (b) to provide three-dimensional ultrasonographic nomograms of the 3 cerebellar vermis diameters and volume based on a large number of normal fetuses; (c) to evaluate the reproducibility of these measurements between different operators (senior vs junior); and 4) provide a reference model in order to address differential diagnosis of PF abnormalities.

Study c: to test the feasibility of the VCA at intrauterine MRI in foetuses with normal brain throughout pregnancy (b) to evaluate the reproducibility of these measurements between different operators (senior vs. junior); (c) to evaluate the correlation among three-dimensional prenatal ultrasound scan and MRI measurements.

Study d: (a) to measure the VCA in foetuses with an abnormal posterior fossa; (b) to evaluate the role of the VCA in the differential diagnosis of upward rotation of the fetal cerebellar vermis; (c) to propose a novel classification system for the midline anomalies of the posterior fossa, based on the combination among the VCA and the other parameters of the posterior fossa.

Study e: to present a case series of a very rare condition associated with the agenesis or with the severe hypoplasia of the vermis, the romboencephalosynapsis, in which were not possible the measurement of the vermian biometries nor of the VCA.

A 3. Clinical studies

A 3.a Fetal cerebellar vermis circumference measured by two-dimensional ultrasound scan: reference range, feasibility and reproducibility.

Materials and methods

We performed a prospective cross-sectional study of sonographic imaging of the fetal cerebellar vermis between April 2014 and April 2015 at the private Centre "*Diagnostica ecografica prenatale Aniello Di Meglio srl*", Naples, Italy. Included were low-risk pregnant women with well-established dates [determined by a well-defined last menstrual period and confirmed by measurement of the crown-rump length on first-trimester ultrasound], and singleton, non-anomalous fetuses. All participants had a negative history for systemic diseases, as well as intact fetal membranes, normal amniotic fluid volume, and were not in labour at the time of inclusion in the study. Indications for ultrasound examination were assessment of either fetal anatomy or fetal growth.

Gestational age ranged between 14 and 36 weeks. Fractions of weeks were computed to the nearest week, with fractions of ≤4 days and >5 days assigned to the lower and higher weeks, respectively.

All deliveries occurred after 37 completed weeks. The neonates were healthy, and no infants had evidence of growth disturbances (fetal growth restriction or macrosomia). All women in the study delivered in 4 referral hospitals and underwent examination by an attending pediatrician.

As in cross-sectional studies, each fetus was considered only once. The study was approved by our Institutional Review Board and all women gave written informed consent to participate in the study.

The ultrasound machine used for two-dimensional ultrasound scan were standard Aloka (Aloka Co., Ltd, Tokyo, Japan) and Voluson E10 (GE Healthcare Ultrasound, Milwaukee, WI, USA) equipped with a curved linear array transabdominal transducer (2–5 MHz) as well as with a transvaginal 4–8 MHz probe.

The fetal vermis was examined in the mid-sagittal plane, with demonstration of the corpus callosum, the cervical spine and the cisterna magna. Freeze-frame ultrasound capabilities and electronic on-screen calipers were used for the measurements of the vermis circumference (VC). Colour Doppler imaging was not utilized.

The transvaginal approach was reserved for when the mid-sagittal view of the fetal brain could not be obtained by the transabdominal route due to fetal position.

Every measurement was taken online during the 20–40 min allocated for the routine scan and detected twice with the mean calculated.

In 33 fetuses each measurement was repeated twice by 2 blinded examiners (C.S. and M.S.) in order to assess the reproducibility of the measurements. The 2 operators were identified as n.1 (senior, i. e. more than 5 years of experience and expertise with prenatal ultrasound) and n.2 (junior, i.e. less than 5 years of experience with

prenatal ultrasound), and all measurements were numbered as 1 when performed by the senior or 2 for the junior operator.

In 24 fetuses a mid-sagittal view of the fetal head was also obtained by three-dimensional reconstructed planes in order to allow comparisons with measurements obtained by two-dimensional ultrasound scan.

Transabdominal three-dimensional volume acquisitions were performed on the same ultrasound machine used for two-dimensional ultrasound scans, equipped with a 4–8 MHz transabdominal probe, using the technique previously reported by other authors.

Brain volumes were acquired starting with the obtainment of a trans-cerebellar axial view of the fetal brain during fetal rest and maternal rest using a transabdominal acquisition angle of 45–60° depending on the GA.

Statistical analysis was performed with Graph-Pad Prism version 5.00 for Windows, (Graph-Pad Software, San Diego CA) and SPSS statistical software (version 19.0; SPSS Inc., Chicago, IL, USA).

To generate the VC reference intervals, only cases between 18 and 33 weeks of gestation were included in the analysis. The reference ranges for the VC were constructed using the method previously described by Royston and Wright. Polynomial regression analysis was performed to identify the regression curves that best fitted the mean and standard deviation (SD) of the VC as a function of gestational age. The standard deviation scores (Z scores) were calculated using the formula: observed VC measurement – mean VC/SD. To assess the model fit, the Gaussian distribution of the Z scores was checked using the Kolmogorov-Smirnov test. 10th and 90th percentiles for the cross-sectional VC throughout gestation were obtained as previously described using the formulas: mean ± 1.645 SD, and mean ± 1.28 SD, respectively.

The agreement between 2D and 3D measurements, transabdominal and transvaginal scans, as well as the inter-observer variability were assessed by interclass correlation coefficients (ICC). Bland-Altman plots were used too. Agreement was considered slight with ICC $\leq$ 0.2, fair with 0.2 $\leq$ ICC $\leq$ 0.4, moderate with 0.4 $\leq$ ICC $\leq$ 0.6, substantial with 0.6 $\leq$ ICC $\leq$ 0.8, and almost perfect with ICC $\geq$ 0.8.

Statistical significance was considered achieved when P was less than 0.05.

Results

Consecutive pregnant women meeting the eligibility criteria (n=397) were initially enrolled in the study. An adequate vermis measurement was obtained in 89.9% of these cases (n=357), using either the transabdominal (n=325) or the transvaginal (n=32) route.

In the excluded 40 cases, a mid-sagittal view of the fetal brain on two-dimensional ultrasound scan could not be obtained mainly due to unfavourable fetal position or excessive fetal movement.

Ten of the included pregnant women were lost at follow-up. Thus, 347 cases were ultimately considered for our analysis.

Fig. 14 a and **b** demonstrate a mid-sagittal view of the fetal head obtained by transabdominal two-dimensional ultrasound scan and three-dimensional reconstructed planes, respectively, showing the VC and adjacent anatomical landmarks at 20 and 24 weeks of GA, respectively, with electronic calipers denoting measurements.

Table 1 shows the clinical characteristics of the study population including perinatal outcome data.

To generate the VC reference intervals, 328 fetuses, ranging from 18 to 33 weeks, were utilized. The regression equation for the mean VC (y) according to gestational age (x) was: $y=-12.21+2.447x$ and for the standard deviation (y'), it was $y'=1.348+0.1302x$. **Fig. 15** and **Table 2** show the VC observed measurements and the fitted 10^{th}, 50^{th}, and 90^{th} percentiles for gestational age.

A high degree of consistency was observed between two-dimensional ultrasound scan and three-dimensional ultrasound measurements of the cerebellar vermis in the series of 24 fetuses studied with both techniques (interclass correlation coefficient (ICC)=0.846 95% confidence interval (CI) 0.679–0.930), as well as between transvaginal and transabdominal scans in the series of 32 cases approached trans-vaginally (interclass correlation coefficient (ICC)=0.874 95% confidence interval (CI) 0.746–0.976).

When the inter-observer variability was assessed for measurements obtained on 2D-US in the series of 33 fetuses, the ICC was 0.890 and its 95% confidence interval was 0.989–0.945.

Bland-Altman plots show the mean differences and 95% limits of agreement between 2D and 3D (mean difference=−0.604 95% CI −1.499–0.292) (**Fig. 16 a**) as well as the mean difference of inter-observer agreement (mean difference=0.948 95% CI −0.046–1.943) (**Fig. 16 b**).

A 3.b The vermian-cresta angle: a new method to assess fetal vermis position within the posterior fossa using three - dimensional ultrasound

Materials and Methods

We performed a prospective cross-sectional study of sonographic imaging of the fetal posterior fossa between May 2015 and October 2016 at the Department of Obstetrics and Gynaecology of the University of Bern, Switzerland. Included were low-risk pregnant women with well-established dates [determined by a well-defined last menstrual period and confirmed by measurement of crown-rump length at first trimester ultrasound], and singleton, non-anomalous fetuses. All participants were healthy women, with intact fetal membranes, normal amniotic fluid volume, and were not in labour at the time of inclusion in the study. Indications for ultrasound examination were assessment of either fetal anatomy screening or fetal growth.

All deliveries occurred after 37 completed weeks, neonates were healthy, and no infants had evidence of growth disturbances (fetal growth restriction or macrosomia). All study women delivered in referral hospitals and underwent routine examination by an attending paediatrician before demission.

As in cross-sectional studies, each fetus was considered only once. The study was approved by the Institutional Review Board of the participating centres.

The ultrasound machine used for measurements were Voluson E10 or E8 (GE Healthcare Ultrasound, Milwaukee, WI, USA) equipped with a curved electronic matrix 4D (eM6C) trans-abdominal transducer (2–6 MHz).

After routine examination of the fetal brain by two-dimensional sonography, three-dimensional volumes were acquired in a trans-cerebellar axial view during fetal and maternal rest using a trans-abdominal acquisition angle of 55° to 65° depending on the gestational age. The two-dimensional image was previously optimized as much as possible. The planes A, B and C of the acquired multiplanar images always corresponded to the axial, coronal and sagittal planes of the posterior fossa, respectively. The planes B (*falx cerebri vertical*) and C (*falx cerebri horizontal*) were adjusted to achieve an optimal midsagittal view of the brain in the A-plane, with the reference dot positioned in the middle of the vermis and vertical position of the cervical spine. On the magnified A plane, the calculation of the vermian-cresta angle (VCA) was carried out. Two landmarks were used for the measurements:

• the nodulus vermis, at the level of the fastigial peak of the 4th ventricle, and

• the internal occipital crest, visible posterior to the cerebellar vermis as a hyperechoic line at the level of the attachment on the falx cerebella.

Based on these landmarks, the following posterior fossa measurements were taken:

1. Vermian biometries:

• the supero-inferior vermian diameter [SDD], the distance between the superior and inferior borders of the vermis, which is anatomically related to the distance between the vermian culmen and uvula,

• the anteroposterior vermian diameter [APD], the distance between the fastigial peak of the fourth ventricle and the most posterior vermian edge, which corresponds to the tuber,

• the horizontal vermian diameter [HD], the distance between the two lateral borders of the vermis between the cerebellar hemispheres, measured in the coronal plane,

• vermian volume, calculated on the basis of the three orthogonal diameters.

2. VCA, defined by the convergence of two lines: the first, tangent to the internal occipital crest; the second, tangent to the nodulus vermis.

All measurements were obtained, using the 'Dist. 2 Point' and angle measurement tool of the ultrasound machine, by placement of the callipers on the outer echogenic borders of the structures studied. Visualization of PF contours was enhanced by activation of the thin-slice (1–2 mm) volume contrast imaging (VCI) mode.

Fig. 17 demonstrate a mid-sagittal and a mid-coronal view of the fetal head obtained by trans-abdominal three-dimensional reconstructed planes, respectively, showing the VCA and adjacent anatomical landmarks at 20 weeks of gestational age.

All study measurements were performed by a single expert observer (L.R.). Each of the five parameters were measured three times in each examination, for assessing intra-observer variation, and the mean of the three values were used for the study analysis. Inter-observer variation was tested in a subgroup of 26 arbitrarily selected fetuses which were assessed by a second blinded observer (M.S.) using 4D view (eM6C). In these cases, the two operators were identified as n.1 (senior, i.e. more than 5 years of skill and expertise with prenatal ultrasound) and n.2 (junior, i.e. less than 5 years of skill with prenatal ultrasound), and all measurements were numbered as 1 or 2, when performed by the senior and the junior operator, respectively.

In no case a transvaginal approach was used. Every measurement was taken online during the 20-40 min allocated for the routine scan.

Statistical analysis was performed with Graph-Pad Prism version 5.00 for Windows, (Graph-Pad Software, San Diego CA) and SPSS statistical software (version 19.0; SPSS Inc., Chicago, IL, USA). Correlations of the vermian diameters, and volume as well as VCA with gestational age were searched with Spearman rank test.

To generate reference intervals of the VCA only cases between 18 and 33 weeks of gestation were included in the analysis, as previously reported **study A 3.a**. The reference ranges for the VCA were constructed using the method previously described by Royston and Wright. Briefly, polynomial regression analysis was performed to identify the regression curves that best fitted the mean and standard deviation (SD) of the VCA as a function of gestational age. The standard deviation scores (Z scores) were calculated using the formula: observed VCA – mean VCA/SD. To assess the model fit, the Gaussian distribution of the Z scores was checked using the Kolmogorov-Smirnov test. 10th, and 90th centiles for the cross-sectional measurements throughout gestation were obtained as previously described using the formulas: mean±1.28SD, respectively. Inter-observer variability for the VCA, was assessed by interclass correlation coefficients (ICC), as reported in **study A 3.a**. Bland-Altman plots were used too. Statistical significance was considered achieved when P was less than .05.

Results

Consecutive pregnant women meeting eligibility criteria (n=140) were initially enrolled for the study. An adequate vermis measurement was obtained in all of these using the trans-abdominal route. Eleven of the included pregnant women were lost at follow-up. Thus, 129 cases were finally considered for our analysis.

Table 3 shows clinical characteristic of the study population, including perinatal outcome data.

The various Vermian biometries such as SDD, APD, HD and volume showed a significant correlation with gestational age (APD: r= .82, p < .0001; SDD: r= .83, p < .0001; HD: r= .71, p < .0001; volume: r= .85, p < .0001; respectively) (**Fig. 18**).

No correlation was found between VCA and gestational age (r=.15; p=.13). Mean ± SD VCA was 64.49°±11.45. Mean (y) and SD (y′) for VCA per gestational age (x) were: y= 63.35 + .04468 x, and y′=10.08 - .03976, respectively. **Figure 19** and **Table 4** shows the observed measurements and the fitted 10^{th}, 50^{th}, and 90^{th} centiles for gestational age for VCA, respectively.

When inter-observer variability for VCA was assessed in the series of 26 fetuses, ICC was 0.95 and its 95% confidence interval was 0.874-0.981 (p < .001).

Bland-Altman plot shows the mean difference of inter-observer agreement (mean difference=3.06 95% CI (-1.07-7.19) (**Fig. 20**).

A 3.c The vermian-cresta angle: a new method to assess fetal vermis position within the posterior fossa using MRI

Materials and methods

A retrospective study of all the intrauterine MRIs performed between January 2008 and January 2016 at the Department of Diagnostic and Interventional Neuroradiology, University of Bern, Switzerland, was conducted by searching the fetal imaging databases. MR imaging examinations were performed due to increased risk of suspected cerebral pathology, including suspected infectious fetopathy, suspected sonographic cerebral abnormality, positive family history, a previous pregnancy with abnormalities, decreased fetal movements, polyhydramnios, and extracranial anomalies such as club foot, cleft lip, and/or palate. Only those cases in which the suspicious of cerebral anomalies was not confirmed at MRI and there was no evidence of intracranial abnormalities at birth were included. The other inclusion criteria were the following: singleton pregnancy, good dating, normal obstetric course (no evidence of intrauterine growth restriction or macrosomia or pregnancy-related hypertensive disorders or gestational diabetes mellitus), absence of maternal disease (healthy women without any background illness such as hypercoagulability state, hypertension, diabetes, or other systemic disease), birth weight within the 10^{th} to the 90^{th} percentiles, clinically normal fetus at birth (normal Apgar scores at birth, normal neonate physical examination findings).

MRI exams were performed with a Siemens Magnetom Sonata or Avanto 1.5 T system (Siemens Medical Systems, Erlangen, Germany) using a four-channel body phased array coil combined with channels from the spine array coil adjacent to the fetus. Depending on patient comfort, patients were positioned supine or on the left lateral side. Intravenous contrast or sedative premedication were not used.

The standard protocol included T1-weighted fast-low angle shot (FLASH; TR = 85 ms, TE = 4.76 ms, flip angle = 70 degrees), T2-weighted half-Fourier acquired single-shot turbo-spin echo (HASTE; TR = 1,260 ms, TE = 84 ms), T1-weighted inversion recovery (TR = 9,470 ms, TE = 17 ms) and T2 weighted true fast imaging with steady procession (FISP, TR = 4.3 ms, TE = 1.86 ms; all three gradients refocused) sequences with a slice thickness of 3 mm and one acquisition. For all sequences, the field of view (320–400 mm) and acquisition matrix (256–448 mm) were adapted to the size of the mother to gain an in-plane resolution of 1.25×1.25 mm or less. In all patients, axial and coronal images were acquired by HASTE sequences, which were evaluated for the purposes of this study. The number of slices varied according to slice orientation and size of the fetus. Mean scanning duration was about 40 minutes. For the detection of posterior fossa anomalies, contiguous orthogonal slices in the axial, coronal and sagittal plane with a slice thickness of 3 mm were included.

The VCA was measured as described in **study A 3.b**, by tracing two lines: the first, tangent to the internal occipital crest; the second, tangent to the nodulus vermis. All the measurements were performed by a single operator. See **Fig. 21**. To evaluate the reproducibility of measurements, an arbitrary sample of 18 fetuses was evaluated twice by the first operator and then by a second operator. Each operator was unaware of the results obtained by the other. In these cases, the two operators were identified as n.1 (senior, i.e. more than 5 years of skill and expertise with prenatal ultrasound) and n.2 (junior, i.e. less than 5 years of skill with prenatal ultrasound), and all measurements were numbered as 1 or 2, when performed by the senior and the junior operator, respectively, as reported in **study A 3.a and A 3.b**.

All the MRI measurement were compared with the nomograms obtained at prenatal three-dimensional ultrasound scan in **study A 3.b**, in order to assess the agreement between the 2 imaging modalities.

Statistical analysis was performed with Graph-Pad Prism version 5.00 for Windows, (Graph-Pad Software, San Diego CA) and SPSS statistical software (version 19.0; SPSS Inc., Chicago, IL, USA). Correlations of the VCA with gestational age were searched with Spearman rank test as reported in **study 3.b.**

Comparison with the measurement of the VCA obtained in **study 3.B** were performed using the paired Student's t-test by gestational ages, after checking the normality of the distribution (one sample Kolmogoron–Smirnov test).

Inter-observer variability for the VCA, was assessed by interclass correlation coefficients (ICC) as reported in **study 3.A**. Bland-Altman plots were used too. Statistical significance was considered achieved when P was less than .05.

Results

Eighty-one cases were selected from the prenatal imaging database, which were suitable for our analysis. An adequate measurement of the VCA was obtained in all of these cases.

Table 5 shows clinical characteristic of the study population, including perinatal outcome data.

In accordance with **study A 3.b**, no correlation was found between VCA and gestational age (r=.19; p=.12). Mean ± SD of VCA was 68.46±10.29.

When we compared MRI measurements with those performed at three-dimensional ultrasound scan, paired Student T-test by gestational age showed that MRI and ultrasonographic measurements were similar, without any significant difference in this respect (p=.11)

When inter-observer variability for VCA was assessed in the series of 18 fetuses, ICC was 0.85 and its 95% confidence interval was 0.656-0.933 (p < .001).

Bland-Altman plot shows the mean difference of inter-observer agreement (mean difference=-0.49 95% CI (-2.72-1.73) (**Fig. 22**).

A 3.d The VCA may allow accurate categorization of fetal upward rotation of cerebellar vermis

Materials and methods

A retrospective study of all the intrauterine MRIs in fetuses with an abnormal posterior fossa, performed between January 2008 and January 2016 at the Department of Diagnostic and Interventional Neuroradiology, University of Bern, Switzerland, was conducted by searching the fetal imaging databases. The cases included patients from a screening population referring to the Department of Obstetrics and Gynaecology of the University of Bern, comprising about 4,500 pregnant women examined per year. Unfortunately, three-dimensional ultrasound volumes and two-dimensional digital images demonstrating a mid-sagittal view of the brain were not available for an "*a posteriori*" analysis.

Measurements were obtained from the midsagittal views of the fetal brain as described in **study A 3.b**. Inclusion criteria were availability of MRI digital images of good quality as well as detailed postnatal data. All measurements were performed by the same operator (M.S.). The following clinical data were recorded: gestational age, fetal sex, associated anomalies, maternal age, singleton or multiple gestation, fetal karyotype (if available), gestational age at birth and mode of birth; postnatally neonatal examination including neurosonography; and, in case of intrauterine or neonatal death or pregnancy termination, pathology reports.

All MRI exams were performed as reported in **study A 3.c**.

Statistical analysis was performed by calculating means and SDs. Groups were compared with the control group reported in **study A 3.b** using the one-way analysis of variance (ANOVA) with the Bonferroni adjustment. Box-and-whisker plots were used too.

Results

During the study period, complete records from 30 fetuses with inclusion criteria were available with posterior fossa abnormalities (5 with Blake's pouch cyst, 12 with DWM, 3 with vermian hypoplasia, 10 with mega cisterna magna). **Table 6** shows clinical characteristic of the study population, including perinatal outcome data.

The VCA was significantly changed in the DWM (p=<.001) and Blake's pouch cyst (p=<.001) subgroups of anomalies, the angle increasing with the severity of the condition (**Fig. 23**), while it did not change in cases of vermian hypoplasia (p=.84) as well as in cases of mega cisterna magna (p=.95). Box-and-whisker plots of distribution of VCA in controls and pathological cases is shown in **Fig. 24**.

By combining these data with the other available parameters of the posterior fossa, a possible categorization of the major abnormalities of the posterior fossa is proposed (**Table 7**).

A 3.e When the midline structures of the posterior fossa are missing: the special cases of rhomboencephalosynapsis

Materials and methods

The material consisted of 3 fetus examined at the gestational age of 24, 25 and 27 weeks by prenatal ultrasound scan at the private Centre "*Diagnostica ecografica prenatale Aniello Di Meglio s.r.l*", in Naples, Italy. All of them underwent brain MRI at the Department of Radiologic, Oncologic and Pathologic Sciences at La Sapienza University, in Rome, Italy.

Results

Case 1

A 33-year-old woman, gravida 2, para 0 (previous miscarriage during the second trimester), was referred to our Centre because a 23-week gestational age ultrasound scan had revealed a tri-ventricular ventriculomegaly. The karyotype from amniocentesis was normal (46XX). Our 24-week transabdominal ultrasound scan confirmed these findings and revealed an abnormal posterior fossa, with absent visualization of the vermis, fusion of the cerebellar hemispheres with a reduction of the trans-cerebellar diameter below the fifth centile, without demonstration of any communication between the fourth ventricle and the cisterna magna. A 25-week prenatal MR imaging scan was performed at 1.5 T using the following technique: multiplanar 3- to 4-mm thick, single-shot fast spin echo, T2 weighted sections (repetition time/echo time = 3000/90 milliseconds, field of view = 340 mm, matrix = 256 3 192). MRI showed agenesis of the cerebellar vermis, dorsal fusion of the cerebellar hemispheres, and clear reduction of the cerebellar transverse diameter (below the fifth percentile). These features, together with the ''keyhole'' shape appearance of the fourth ventricle, were consistent with those already well known from postnatal MRI studies of rhomboencephalosynapsis. A tri-ventricular ventriculomegaly (19-mm atrial width) was also evident (**Fig. 25**). The septum pellucidum and corpus callosum were visible. The brain parenchyma appeared normal. The patient decided for termination without fetal autopsies and then was lost to follow-up.

Case 2

A 31-year-old woman, gravida 3, para 2 (her previous pregnancies was uneventful, with normal-term deliveries), presented at our Centre at 25-weeks of gestational age, because a previous scan at 24 weeks had revealed a renal disease. At our ultrasound scan the fetal kidneys were symmetrically enlarged（right, 5.3×4.0 cm; left, 4.3×3.7 cm）and highly echogenic, leading to the absence of the corticomedullary differentiation. When we scanned the brain, an abnormal posterior fossa was evident, with absent visualization of the vermis, and fusion of the cerebellar hemispheres. No other brain anomalies were detected. Investigating family history of congenital malformations, the woman revealed that the first daughter of 3 years old had been diagnosed postnatally with ventriculomegaly and has cognitive impairment as well as a coloboma of the optic nerve. The karyotype of this daughter is normal. In the current pregnancy, the karyotype was normal too (46XY). At 26 weeks of gestational age, a prenatal MRI examination was performed with the same scanning technique as in the first case. MRI showed agenesis of the cerebellar vermis, dorsal fusion of the cerebellar hemispheres, which appeared without the normal cerebellar sulci, and a reduction of the fourth ventricle (**Fig. 26**). These signs were compatible with rhomboencephalosynapsis. The parents decided to terminate the pregnancy at another institution.

Case 3

A 42-year-old woman, gravida 1, para 0, was referred to our Centre at 26 weeks of gestational age because of a vaginal bleeding. When we scanned the fetal brain, an abnormal posterior fossa was evident, with absent visualization of the vermis, fusion of the cerebellar hemispheres with a reduction of the trans-cerebellar diameter below the fifth centiles, without demonstration of any communication between the fourth ventricle and the cisterna magna (**Fig. 27**). No other cerebral and extra-cerebral fetal anomalies were detected A 27-week gestational-age prenatal MRI scan was performed with the same scanning technique as in the other cases. It revealed cerebellar transverse diameter reduction (22 mm, below the fifth percentile), agenesis of the vermis, and dorsal fusion of the cerebellar hemispheres, consistent with rhomboencephalosynapsis. At 32 weeks GA, a preterm vaginal delivery occurred, which resulted in a stillborn female baby. The woman did not authorize autopsies.

A 4. Discussion

The classification of cerebellar malformations is controversial; no widely-accepted agreement has been reached, despite many attempts by neuroradiologists, geneticists, and neuropathologists. In particular, as far as the conditions associated with a defective vermis are concerned, there is no general consensus as to their categorization. In addition, cerebellar hemispheric and vermian malformations have been described but are poorly understood. Thus, the prognosis of patients with most cerebellar malformations is uncertain. Finally, it is often difficult to distinguish clearly, in an infant with signs and symptoms relating to the posterior fossa, between cerebellar or vermian atrophy, hypoplasia, or malformation. In the fetus, the situation is understandably even more confused, due to difficulties in the prenatal assessment of posterior fossa, both by ultrasound scan and by MRI.

However, based on a morphologic ultrasonographic approach, it is at least possible to differentiate posterior fossa anomalies into two broad categories: (1) cystic malformations, characterized by the presence of an apparent cerebrospinal fluid collection in the posterior fossa due to fourth ventricle/cisterna magna dilatation, or to true arachnoid loculations; and (2) non-cystic malformations, in which there is no apparent cerebrospinal fluid collection. To the cystic malformations belong the DWM, the Blake's pouch cyst, the mega cisterna magna and the vermian hypoplasia ("Dandy Walker variant").

It has been suggested that the DWM be considered in the group of mesenchymal-neuroepithelial signalling defects, since several cerebellar growth factors are derived from the overlying leptomeninges. In this light, abnormalities of the cerebellar leptomeninges may result in abnormalities of the cerebellum itself, as well as abnormalities of the surrounding cerebrospinal fluid spaces. This is the basis of development of the DWM: it requires abnormal development of the cerebellum itself and of the overlying leptomeninges. At prenatal ultrasound scan, on the axial trans-cerebellar view, a triangular or square-shaped open fourth ventricle apparently communicating with cistern magna can be seen, with an expansion of the posterior cranial fossa. To assess the presence, integrity, and position of the vermis, as well as the position of the torcular/tentorium, a mid-sagittal view is required. On this view, a small, upwardly rotated vermis, causing a superior displacement of the torcular/tentorium, with a normal or abnormal configuration (absence of fastigium and/or fissures) may be present. While an abnormal configuration usually indicates partial agenesis, a small vermis with a normal configuration indicates hypoplasia. However, the distinction between these two entities remain difficult. The DWM should be differentiated from other anomalies of the posterior fossa. As already pointed out, a median view of the fetal head is mandatory for an accurate assessment of the position and features of the vermis and of the characteristics of the cerebrospinal fluid collection of the posterior fossa (fourth ventricle and cisterna magna). The presence of an apparent communication between the fourth ventricle and cisterna magna (open fourth ventricle) associated with a normal vermis is indicative of a Blake's pouch cyst. In this case, the rotation of the vermis is usually less

pronounced. The presence of an apparent communication between the fourth ventricle and cisterna magna (open fourth ventricle) associated with the hypoplastic vermis, normally inserted tentorium/torcular, and no expanded posterior fossa is indicative of vermian hypoplasia. In this case, the rotation of the vermis, when present, is usually mild. In case of mega cisterna magna, the cisterna magna is large, but the cerebellum is intact and the fourth ventricle is closed. Several malformations have been reported to be associated with DWM. The most commonly associated anomalies are other anomalies of the central nervous system (in 50%–60% of cases), including midline anomalies (corpus callosum agenesis, holoprosencephaly, etc.). An association with facial clefts and other extra-brain anomalies (especially congenital heart disease and urinary anomalies) has been described, often in the context of genetic syndromes. The risk of chromosomal anomalies is high, with up to 35% of cases being associated with aneuploidy, mainly trisomies 18 and 13, as well as the risk of non- chromosomal syndromes, including the Walker–Warburg syndrome (eye anomalies + lissencephaly, midline anomalies, microcephaly, and cephalocele); Meckel–Gruber syndrome (encephalocele + polydactyly + polycystic kidneys); Aicardi syndrome (corpus callosum agenesis + vertebral defects); Neu–Laxova syndrome (lissencephaly + microcephaly + proptosis + diffuse joint contractures + subcutaneous tissue edema + intrauterine growth retardation). Due to the high risk of chromosomal anomalies, fetal karyotyping is mandatory when a DWM is suspecte. In addition, a thorough anatomic scan should be performed by an expert because of the high risk of association with other brain and extra-brain malformations. Serial ultrasonographic monitoring is also warranted, to verify the possible onset of severe hydrocephalus. Delivery should take place in a tertiary referral centre, in order to allow a definitive diagnosis and an adequate neonatal management. Postnatally, although there is obviously no treatment for the primary vermian lesion, the virtually ubiquitous secondary obstructive hydrocephalus may be treated with a cysto-peritoneal shunt. Indeed, the DWM is associated with late-onset hydrocephalus in more than 50% of cases. If hydrocephalus develops, whether in utero or in the neonatal period, there is an overall mortality rate of over 60%, with most survivors having a low intelligence quotient. When hydrocephaly is not associated, it has been suggested that the neurologic outcome is mainly related to the appearance of the cerebellar vermis: when the small vermis has a normal configuration, a normal development has been reported in more than 50% of cases. Conversely, when the vermis is abnormally lobulated and/or there are associated cerebral anomalies, the prognosis is poor.

The Blake's pouch is a normal, transient embryological structure, representing an evagination of the posterior membranous area, one of the two components of the rhombencephalic roof (the other being the anterior membranous area), that initially does not communicate with the surrounding subarachnoid spaces. Subsequent spontaneous perforation of the pouch, by the 10^{th} gestational week, forms the foramen of Magendie. The term Blake's pouch cyst was originally introduced in the contest of an infantile pediatric neuroradiology to indicate a type of obstructive hydrocephalus secondary to failure of formation of the foramen of Magendie and Luschka, resulting in a compressive cyst of the posterior fossa displacing superiorly the cerebellar vermis. More recently, the term has been used in fetal imaging studies to indicate cases with a posterior fossa cyst displacing superiorly an

intact cerebellar vermis, typically in association with a normal ventricular system and a normal size of the posterior fossa. This finding has been interpreted as failed or delayed regression of the Blake's pouch. The entity described in the original neonatal studies likely differs from the one later described in fetal studies, because the latter typically has a normal outcome and appears to be rarely associated with ventriculomegaly. Sonographically, on the axial trans-cerebellar view, Blake's pouch cyst is characterized by an hourglass opening (buttock sign) apparently communicating with the cisterna magna. On a mid-sagittal view of the fetal head, a normal but usually moderately upward-rotated vermis is evident, with the tentorium and torcular that are in normal position. There may also be visualization of the Blake's pouch cyst roof within the cisterna magna and a more translucent echogenicity of the cyst content in comparison with the cisterna magna fluid. As mentioned above, in the case of apparent communication between the fourth ventricle and the cisterna magna (open fourth ventricle), on an axial trans-cerebellar view, such as in the case of Blake's pouch cyst, a median plane of the fetal head is mandatory for an accurate assessment of the position and features of the vermis. The presence of a normal vermis rules out the possibility of a DWM and vermian hypoplasia. In addition, instead of DWM, in case of Blake's pouch cyst the rotation of vermis is less pronounced. As reported above, in case of mega cisterna magna, the cisterna magna is large but the fourth ventricle is closed. About one third of Blake's pouch cysts detected antenatally are associated with other anomalies, including chromosomal aberrations (in most cases trisomy 21). The risk of chromosomal anomalies or non-chromosomal syndromes is significant, especially when associated with other anomalies. Thus, fetal karyotyping is mandatory, especially in cases associated with other anomalies. In addition, a thorough anatomic scan should be performed by an expert because of the high risk of association with other brain and extra-brain malformations. Postnatally, in the rare cases associated with ventriculomegaly, the secondary obstructive hydrocephalus may be treated with a cysto-peritoneal shunt. However, when the BPC is an isolated finding and the karyotype is normal, the outcome is usually good. Furthermore, intrauterine remission occurs in a significant number of cases, and a normal developmental outcome is reported in nearly 100% of cases.

Mega cisterna magna is defined as a cisterna magna larger than 10 mm. It is characterized by an intact vermis, an enlarged cisterna magna, and a normal-sized fourth ventricle. It has been suggested that the enlargement of the cisterna magna may be secondary to a distension of the BP, which, however, does not displace the cerebellar vermis superiorly. On the axial trans-cerebellar view, a cerebrospinal fluid collection is seen in the posterior fossa. The vermis is normal, the fourth ventricle is closed, and the torcular and the tentorium are in normal position. This benign condition should be differentiated from other anomalies of the posterior fossa, especially arachnoid cysts. In fact, posterior fossa can mimic mega cisterna magna, but mass effect with asymmetric distortion of the cerebellum is usually associated. Al already reported, the presence of a normal vermis rules out the possibility of a DWM and isolated vermian hypoplasia, while the presence of a closed fourth ventricle and of a non-rotated vermis, rules out the possibility of a BPC. A significant number of associated anomalies have been reported, especially supra-tentorial anomalies (i.e., periventricular heterotopia).

The risk of chromosomal anomalies and non- chromosomal syndrome, when associated with other anomalies, it is significant. Therefore, fetal karyotyping is mandatory, especially in cases associated with other anomalies. In addition, a thorough anatomic scan should be performed by an expert because of the high risk of association with other malformations. Postnatally, no treatment is required. In the absence of associated anomalies, the prognosis is good. The vast majority of cases had normal development. Cases associated with abnormal cerebral findings (i.e., periventricular heterotopias) were found to have neurologic sequelae, often mild, in about one-third of cases.

Vermian hypoplasia, previously\sometimes referred to as Dandy–Walker variant, is characterized by an isolated small vermis, usually upwardly rotated. It has been suggested that the term hypoplasia should be limited to cases in which the vermis is small but has a normal morphology (all the lobules are present); conversely, the term partial agenesis should be used in those cases in which a part is absent. However, it can be difficult to differentiate, by ultrasound, between vermian agenesis and hypoplasia. In addition, hypoplasia or agenesis may affect any part of the vermis. The part of the vermis affected depends on the nature and timing of the insult. Some authors retain that the partial vermian agenesis involves the lower part of this structure, so they named this anomaly as "inferior vermis hypoplasia". Nevertheless, as recently pointed out by Robinson in 2014, recent researches showed that that the development of the vermis is more in a ventro-dorsal direction rather than in a cranio- caudal direction. Thus, the referral to any "inferior" part should be avoided or used with caution. On axial trans-cerebellar view, in presence of vermian hypoplasia, an open fourth ventricle apparently communicating with the cisterna magna is seen, while the posterior cranial fossa is not expanded. On the mid-sagittal view of the head, the small and sometimes upwardly rotated vermis can be seen. Tentorium and torcular are positioned normally. The hypoplastic vermis should be differentiated from other posterior fossa anomalies characterized by an open fourth ventricle. The presence of a communication between the fourth ventricle (open fourth ventricle) and cisterna magna associated with a normal vermis is indicative of Blake's pouch cyst. In this case, the rotation of the vermis is mild. The presence of a communication between the fourth ventricle (open fourth ventricle) and cisterna magna associated with a hypoplastic vermis, superiorly displaced tentorium/torcular, and expanded posterior fossa is indicative of DWM. In this cases the rotation of the vermis is usually broad.

Also in cases of vermian hypoplasia, numerous malformations have been reported to be associated, with a high risk of chromosomal and non- chromosomal syndromes, especially if associated with other anomalies. In particular, Joubert syndrome is a very severe albeit rare condition featuring vermian hypoplasia in association with dysgenesis of the isthmic portion of the brainstem at the pontomesencefalic junction, a deep posterior interpeduncolar fossa with thick elongated superior cerebellar peduncles. The diagnosis can be made on MRI only, and the typical aspect of the abnormal superior cerebellar peduncles is referred to as "*molar tooth sign*", evident on axial MRI slices of the brain. Symptoms range from general hypotonia with a froglike posturing, hyperpnea/apnea, ataxia. Colobomas, nystagmus and strabismus are associated. In case of vermian hypoplasia fetal karyotyping is

mandatory, because of the high risk of genetic syndromes. In addition, a thorough anatomic scan should be performed by an expert because of the high risk of association with other malformations. There is obviously no treatment of the primary vermian lesion. Vermian hypoplasia is frequently a part of multiple anomalies and genetic syndromes. When isolated, it may be asymptomatic but precise risk figures are not available.

In the light of all these considerations, it is possible to affirm that the differential diagnosis of the main cystic posterior fossa anomalies is based on the assessment of 2 main parameters, as well as on the combination of these parameters with the other detectable findings of the posterior fossa. These 2 main parameters are (a) the vermian size and morphology and (b) the position of the vermis, while the other detectable findings of the posterior fossa are: the size and appearance of cisterna magna, the position of tentorium and torcular, the relation between the fourth ventricle and cisterna magna, the presence of cisterna magna septa, the choroid plexus position, etc. All these additional parameters gain an increasing clinical significance when they are integrated with the 2 main parameters. This is the rationale of this research line, that investigated throughout the different gestational ages, in physiological and pathological cases, by different prenatal diagnostic imaging techniques i.e. two-dimensional ultrasound, three-dimensional ultrasound, MRI, the vermian size and morphology and the position of the vermis.

At current, the standard ultrasonographic antenatal evaluation of the cerebellum is limited to the axial plane, which does not provide a window to provide cerebellar vermis biometry as well as the relationship with the other structures of the posterior fossa. This can be obtained only performing a midsagittal view of the fetal brain. However, although interest in the ultrasonographic study of the posterior fossa is increasing, only few authors assess vermis biometry in clinical practice, and data regarding the normal biometry and position of the cerebellar vermis are still minimal. Therefore, a wrong/missed diagnosis of vermis abnormality, in particular when it is segmental, is still probable in ultrasonographic evaluation.

The **study A 3.a** is based on the need for a major increase in the use of two-dimensional ultrasound measurements of the cerebellar vermis in order to evaluate the feasibility and reproducibility of vermian biometry in clinical practice. The choice to start our measurements from the 18th week of pregnancy, in this first study but also in the subsequent ones, is due to the fact that the cerebellar vermis can appear not fully developed prior to this week, as explained in the introduction section. Our data, in accordance with previous papers, confirm that the cerebellar vermis grows in a linear fashion throughout gestation and the growth pattern correlates well with gestational age. To our knowledge, only a few papers have measured VC for assessing vermian growth throughout gestation. Our nomograms constructed by two-dimensional ultrasound correlated well with those previously reported by Malinger in 2001 and by Lei in 2015. We could not correlate our nomograms with those provided in other papers, since they focused on vermian diameter and area but not on VC. In this first study, we focused exclusively on VC because this parameter is rarely reported in the literature compared with vermis diameter. Furthermore, we believe that the assessment of the circumference can provide precise information about the

morpho-biometry of the vermis, is easy to perform and may provide more guarantee of agreement between different operators. To our knowledge, **study A 3.a** includes the largest series (n=328) ever published for the assessment of cerebellar vermis growth throughout gestation in a two-dimensional ultrasonographic transabdominal manner. The series of Zalel of 2002 included a small number of patients, while the series of Malinger of 2001 focused exclusively on the two-dimensional ultrasonographic transvaginal approach. Despite the large number of fetuses included in this our first analysis, we observed an inhomogeneous distribution of cases among the different gestational weeks, with most of the measurements performed before 24 weeks. This may be due to the fact that the major number of controls in normal pregnancies is scheduled in the second trimester and should be considered as a limit of this study. We did not observe any gender difference in the measurement of the VC. To our knowledge, this data is in accordance with previous papers which do not mention gender differences in their measurements. In this first study, we performed most of the ultrasonographic scans using the transabdominal approach. Indeed, we preferred the routine transabdominal rather than the transvaginal route, since the latter may be less immediate and more time-consuming, as well as less tolerated by pregnant women. However, in 32 cases a transvaginal probe was necessary for obtaining an adequate vermis view due to fetal position. We observed high agreement between values when transvaginal measurements were compared with transabdominal ones at the respective gestational age. These latter data encourage us to continue to prefer the transabdominal route when possible. In this first study, we focused on obtaining the mid-sagittal plane via two-dimensional rather than three-dimensional ultrasound scan. Indeed, our *a-priori* intention was to enhance and promote the assessment of vermis biometry among the most possible number of different centres, even when three-dimensional technology is not accessible. Furthermore, we reported good reproducibility between two-dimensional and three-dimensional measurements. These data are in agreement with other reports and suggest that two-dimensional measurements can be as adequate and accurate as three-dimensional measurements for the intrauterine study of some structures of the fetal brain.

The **study 3 A. b** wides the investigations of the previous study, providing 4 different vermian biometric data from a large cohort of foetuses from 18 to 33 weeks of gestation, this time assessed by three-dimensional imaging modality. So far, although various nomograms have been developed by sonography and MR imaging, including Vinals et al. 2005, Rizzo et al. 2012, and Lei 2015 with the aid of 3D technology, only few studies have provided data regarding 4 vermian parameters (SDD, APD, HD and volume) together. Another special feature of our second study is that we used not only the mid-sagittal plane as in **study 3 A. a**, but also the midcoronal plane. Indeed, we believe that the choice to take the measurements not only at the level of the midsagittal plane, but also integrating this view with the further information obtained by the coronal section of the posterior fossa, may be of a special help in detecting the size and the shape of the whole vermis, including the lower part, that often remain un-visualized at prenatal ultrasound examinations. Indeed, the coronal view that we need in order to correctly identify our crest reveals the inferior part of the posterior fossa and automatically directs the attention of the operator to the lower part of the vermis, which can thus be properly studied.

Our biometric data, in accordance with the **study 3 A. a**, as well as with the literature, confirm that the cerebellar vermis grows in a linear fashion throughout gestation and the growth pattern correlates well with gestational age.

In **study 3 A. b** for the first time we measured the VCA throughout prenatal life. The VCA is a simple measurement, which can be easily taken with three-dimensional reconstructed planes. Thanks to the three-dimensional technology, it is possible a thorough view of the posterior fossa, particularly at the level of the mid-sagittal and the coronal plane, which allows a proper identification and visualizations of the landmarks of posterior fossa, the vermis as well as of both the sides of the VCA.

In the occipital bone, the lower division of the cruciate eminence is prominent, and is named the internal occipital crest; it bifurcates near the foramen magnum and gives attachment to the falx cerebelli. In the upper part of the adult internal occipital crest, a small depression is sometimes distinguishable; it is termed the vermian fossa since it is occupied by part of the vermis of the cerebellum. During foetal life at prenatal ultrasound scan, the upper part of the internal occipital crest is easily visible in the midsagittal view of the posterior fossa as a hyperechogenic straight line, just behind the vermis. In the coronal view of the posterior fossa, the upper part of the internal occipital crest appears as a straight hyperechogenic median line between the bilateral insertion of the falx cerebelli.

With the visualization at the same time of the midsagittal and the coronal view of the PF, it is easy to identify the crest and thus trace the first side of the VCA, while the other side is drowned tangentially to the ventral contour of the cerebellar vermis and correspond to the fastigium of the vermis, a reference point already used by other authors, as Volpe in 2012. Thus, the evaluation of the VCA may be of help in assessing the foetal PF and gives an objective measurement of the normal position and rotation of the cerebellar vermis in relation to the medial occipital crest.

In our opinion, the choice of considering the medial occipital crest as a reference point of our angle is a strength of our study. Indeed, while other landmarks proposed by authors are often difficult to be visualized due to the low or variable echogenicity, or to shadowing phenomena, the osseous nature of our reference lets it to be always clearly visualized. Paladini in 2006 proposed a combination of three angles, the tentoro-vermian, the tentoro-clivus and clivo-vermian angles, for assessing the position of the vermis. However, tracing these angles may be tricky due to the characteristic echogenicity of these structures which often appear with soft edges, not properly defined and requires a trained eye in order to avoid mistakes. Ghi in 2012 proposed the assessment of the position of the vermis in relation to the brainstem, measuring the brainstem–vermis and brainstem–tentorium angles. However, the shadowing of the medulla oblongata often encountered when trying to proper visualize the landmarks makes the evaluation of these angles often tricky and time -consuming. In our study, the choice of a landmark that is posterior to the posterior fossa in the midsagittal view of the foetal hindbrain avoids any shadowing phenomena, with a good visualization. Another advantage of the choice of the internal occipital crest is that this

landmark is always displayable, independently of the gestational age. Indeed, this structure, although close to the posterior fossa, is an osseous structure external to the brain's soft tissues. On the contrary, any landmark inside the brain is more prone to become progressively more difficult to be visualized with the advancement of the pregnancy.

On the basis of our results, measuring this angle on static volume ultrasound appears feasible and reproducible. Indeed, the inter-observer agreement for both seems good, with high intra-class correlation coefficient (ICC) and small 95%CI. This is of interest, since we tested the inter-observer variability between a senior and a junior operator as also in **studies A 3.a and A 3.c**. To the best of our knowledge, this is the first time that the inter-observer variability has been tested between differently-skilled operators relatively to the posterior fossa assessment. The good reliability of measurements taken between the 2 examiners in all these studies may have useful implications in clinical practice. Our measurements may be looked at as a reliable reference when assessing the anatomy of the posterior fossa, in particular at mid-trimester scan.

Even more interesting, is that the VCA measurements performed at three-dimensional prenatal ultrasound are consistent with those performed at MRI, as reported in our **study A 3.c.** The complementary role of fetal MRI in evaluating the ultrasonographic suspected abnormalities with higher spatial resolution and tissue contrast is now well documented, and concerns about a cerebellar malformation is one of the main referral reasons for clinical MR examination. However, despite the recurrent use of the so called "*diametral*" MRI measurements (i.e. trans-cerebellar diameter and vermis dimensions), the complex structure of the posterior fossa requires a deeper analysis to improve the developmental descriptions. Modern advances in imaging sequences and post-acquisition processing techniques now allow for fetal MR data to be utilized for measurements "*a posteriori*", that enable to re-analyse cases performing new measurements and elaborating new observations. To our knowledge, only a few MRI studies have reported their findings for normal cerebellar growth over varying gestational age ranges, and even less studies have reported methods to objectively quantify the position of the cerebellar vermis during pregnancy in fetuses with normal posterior fossa. The choice to assess the VCA also at MRI has multiple reasons. First, we wanted to test this measurement, with an imaging modality that is widely spreading in the field of prenatal medicine. By the way, a recent paper of Griffith published on Lancet in 2016, reported that intrauterine MRI improved diagnostic accuracy and confidence for the fetal brain abnormalities and lead to management changes in a high proportion of cases. This finding, along with the high patient acceptability, led the authors to propose that any fetus with a suspected brain abnormality on ultrasound should have MRI to better inform counselling and management decision. Second, we wanted to assess the feasibility of this measurement, as well as its easiness to perform, since the other available MRI studies, reporting on the measurement of the position of the vermis, proposed angles difficult to enhance and trace. As an example, Vatansever in 2013 proposed the measurement of a number of angles, i.e. the ponto-cerebellar gap width, the fourth ventricle angle, the primary fissure angle, the tegmento-vermian angle, which may be tricky to identify, due to the need of a big magnification of the image, to the special MRI appearance of these structures with soft edges, not properly defined and to the requirement of a trained eye in order to avoid

mistakes. For tracing our angle, we used in most of cases high-quality T2-weighted MRI images. Indeed, description of pathoanatomy relies in most cases on high-quality T2-weighted contrast, allowing an equal assessment of the brain surface and parenchyma.

Curiously, our study shows that the VCA remains stable during the observed gestational age period. Indeed, the measurements obtained at any gestational week appear fairly constant with a narrow interval of values. We believe this is interesting and unexpected, for more than one reason. First, a special feature of our angle is that it consists of a "static" side – the "crest" side – and a "dynamic" side – the "vermian" side. While the "crest" side remains stable, due to its bony structure, we expected the "vermian" side to slowly change with the advancement of the pregnancy, due to the progressive adaptation of the vermis in the vermian fossa. This is even more true, considering the dynamic and changing fashion of the posterior fossa, and in particular of its midline structures during prenatal life (see introduction section). Indeed, the embryologic development of the PF, and thus of the cerebellum and the vermis includes several phases in which each structure continuously modifies shape, size and relations with the other developing organs. While within the 7^{th} weeks after conception the corpus cerebelli rapidly bulges as a "V" shaped structure, so outlining downwards the fourth ventricle and the plexus choroideus, the medial portion starts to develop later in prenatal life. During the third month of development, growth of the midline component accelerates and begins to fill the gap between the limbs of the V, thereby forming the vermis, as a zipper-like closure of the primordial limbs. This structure is not fully developed before 18 weeks of pregnancy, when Blake's pouch completes is fenestration. Indeed, Blake's pouch, also known as the rudimental fourth ventricular tela choroidea, is a normal transient structure during embryological development which regresses, usually by 12 weeks of gestation, when it starts fenestrating to form the foramen of Magendie. Second, in accordance with Lei (2015), we believe that the fact that we found a parameter that is constant, is helpful in the elimination of the effect of gestational age in evaluating the posterior fossa. For example, the parameter identified in this study can be expected to be most helpful in identifying the risk of posterior fossa anomalies in patients whose dates of conception are not known. This could allow assessment of fetal vermis position, and thus classification of patients as high or low risk at any point during the second trimester, thereby facilitating clinical decisions.

The fact that our angle remained stable during the physiological development of the posterior fossa represented the basis for our **study A 3.d**, in which we used of the VCA in pathological cases. Indeed, we hypothesized that, in case of failure of the normal embryological development of the vermis, which in turn leads to an abnormal size and rotation of the vermis, our angle would have been affected and thus useful to quantify objectively the degree and severity of an abnormal rotation. Furthermore, we hypothesized that combining the VCA with the vermis biometry (diameters and volume) may be helpful in detecting or in ruling out both the major and pathological conditions involved in the differential diagnosis of the abnormal posterior fossa, including the DWM, vermian hypoplasia, as well as the persistence of the Blake's pouch. Our results confirmed our a-priori hypothesis, suggesting that measurement of the VCA discriminates accurately posterior fossa fluid collections associated with

upward rotation of the cerebellum, including DWM, Blake pouch cyst, vermian hypoplasia and mega cisterna magna. As already discussed, distinguishing these entities is important, because of their different prognoses: a Blake's pouch cyst is a risk factor for anatomic and chromosomal anomalies but when isolated is probably a normal variant, while DWM and vermian hypoplasia are true malformations frequently associated with abnormal neurodevelopment. The differential diagnosis depends upon visualization of vermis size and position, as well the size and appearance of cisterna magna, the position of tentorium and torcular, the relation between the fourth ventricle and cisterna magna, the presence of cisterna magna septa, the choroid plexus position. All these findings can be demonstrated in utero with sonography and/or MRI, but, as already discussed, they are subjective and even in expert hands may be difficult to interpret, particularly early in gestation. In our series, the VCA discriminated accurately this group of anomalies. The VCA was increased in the study group compared with controls, in particular was significantly increased in cases of DWM and Blake pouch cyst, increasing with the severity of the condition. Interestingly, it remained stable in cases of mega cisterna magna and vermian hypoplasia, independently of the severity of the condition in these cases.

We acknowledge the limitations of our study. The number of abnormal cases was relatively small and they were investigated retrospectively. Further experience is certainly needed. Nevertheless, the spread of measurements between normal and abnormal cases and among the different categories of abnormalities suggest that the VCA may prove important in the differential diagnosis of fetal posterior fossa cystic anomalies, at least when used in combination with all the other existing criteria, as we proposed in **table 7**.

Our last **study 3 A. e** is quite different from the others, reporting a case series of a very special and rare condition that does not belong to the cystic malformation of the posterior fossa (it belongs to the non-cystic malformations), and thus is not detectable with the criteria proposed in the other studies. The decision to add this study is based on two reasons: first, because we believe the rhomboencephalosynapsis is a so rare condition, that every case causally encountered in the clinical practice should be mentioned in the research update activity and should be object of special study; second, to encourage further research in the assessment of the pathological posterior fossa since, despite the new studies and ideas, some conditions remain under-studied and poorly understood. Rhomboencephalosynapsis was first described by Obersteiner from the post-mortem examination of a 28-year-old man who committed suicide. Since the first description, more than 40 cases have been reported, most of which were diagnosed by MR imaging. This condition is characterized by vermian agenesis associated with fusion of the cerebellar hemispheres, peduncles, and dentate nuclei. Kinking of the brainstem is often present. On the axial trans-cerebellar view, the vermis is absent and the hypoplastic cerebellar hemispheres are fused on the midline. The cerebellum has a rhomboid shape due to the absence of the vermis. The posterior fossa is small and associated supra-tentorial abnormalities—absent septum pellucidum, abnormal gyration, and hydrocephalus—may be present. Supra-tentorial anomalies including hydrocephaly are often present. From the embryologic view, rhomboencephalosynapsis results from failure in vermian differentiation of the more rostral part of the midline

primordium; the fused cerebellar hemispheres may be explained by the fact that the cerebellar primordium is unpaired, according to the theory that the cerebellar primordium arises from the tuberculum cerebelli. The risk of chromosomal anomalies is low, while the risk of non-chromosomal anomalies is relatively high. A thorough anatomic scan should be performed by an expert because of the high risk of association with other CNS anomalies. The prognosis is commonly poor, with most affected patients dying in childhood.

Our report shows that prenatal ultrasound scan and MRI are able to depict rhomboencephalosynapsis and associated brain anomalies in the fetus accurately. This is important because this condition may be also an isolated malformation that can be difficult to be detected. In our study, 2 out of 3 cases showed no other brain anomalies but the rhomboencephalosynapsis (in case 2 a renal anomaly was present). The other few cases of an isolated rhomboencephalosynapsis reported in the literature showed significant neurologic symptoms such as irritability, poor balance, head rolling, abnormal eye movement, spasticity, dysarthria, strabismus, mild truncal ataxia, self-mutilation, and obsessive-compulsive disorder4 are also reported in these cases. Isolated cases have also been associated with developmental delay and severe mental retardation. Unfortunately, all our cases ended with either an abortion (case 1 and 2) or a preterm delivery of a stillborn fetus (case 3). We based our diagnosis on prenatal ultrasound scan, and confirmation of diagnosis was performed by MRI; however, it was not possible to have post-natal data. Alterations in aqueductal patency, together with midbrain tegmentum dysplasia, have been reported in postnatal studies. Early aqueductal obstruction during fetal life could explain some of the supra-tentorial anomalies such as the hydrocephalus and the extreme corpus callosum thinning or interruption. In our cases, prenatal MRI could not establish whether the aqueduct of Silvius was patent or not with certainty. The cause of this condition is unknown. The results of chromosomal analyses performed in previous cases were normal except for an interstitial deletion of chromosome 2q.1 In our report, cases 1 and 2 had a normal karyotype. No information are available about case 3. No teratogenic factors have been recorded in our case series. Rhombencephalosynapsis seems to be sporadic, without any instance of familial recurrence. The possibility of autosomal recessive inheritance was reported in only 1 case. In case 2 of our series, it has not been confirmed any relation between the condition of the fetus and that of the first daughter of the woman. From our limited series, we cannot provide any quantitative data about possible differences in the detection rate of these malformations between prenatal ultrasound and prenatal MR imaging; however, it is likely that the latter will be more accurate, especially with respect to standard ultrasonographic examinations not guided by a priori information.

A 5. References

A.J. Robinson. Editorial. Inferior vermian hypoplasia – preconception, misconception. Ultrasound Obstet Gynecol 2014; 43: 123–136.

Aicardi J. Diseases of the nervous system in childhood, 2nd edn. 1998; Cambridge University Press, Cambridge Alder J, Cho NK, Hatten ME. Embryonic precursor cells from the rhombic lip are specified to a cerebellar granule neuron identity. Neuron 1996; 17:389–399

Alexander L (1931) Die Anatomie der Seitentaschen der vierten Hirnkammer. Z Anat 95:531–707

Altman J, Bayer SA (a) Prenatal development of the cerebellar system in the rat. I. Cytogenesis and histogenesis of the deep cerebellar nuclei and the cortex of the cerebellum. J Comp Neurol 1978; 179:23–48

Altman J, Bayer SA (b) Prenatal development of the cerebellar system in the rat. II. Cytogenesis and histogenesis of the inferior olive, pontine gray, and the precerebellar reticular nuclei. J Comp Neurol 1978; 179:49–76

Altman J, Bayer SA. Embryonic development of the rat cerebellum. I. Delineation of the cerebellar primordium and early cell movements. J Comp Neurol 1985; 231:1–26

American Institute of Ultrasound in Medicine. AIUM practice guidelines for the performance of an antepartum obstetric ultrasound examination J Ultrasound Med 2010;29:157–166.

Barkovich AJ. Pediatric neuroimaging, 2000; 3rd edn. Lippincott, Philadelphia

Barkovich AJ, Kjos BO, Norman D, Edwards MS. Revised classification of posterior fossa cysts and cyst-like malformations based on the results of multiplanar MR imaging. AJNR Am J Neuroradiol 1989; 10:977–988

Barkovich AJ, Millen KJ, Dobyns WB. A developmental and genetic classification for midbrain-hindbrain malformations. Brain 2009; 132: 3199–230. 29.

Barkovich AJ, Millen KJ, Dobyns WD. A developmental classification of malformations of the brainstem. 2007; Ann Neurol 62:625–639

Barkovich AJ. Developmental disorders of the midbrain and hindbrain. Front Neuroanat 2012; 6: 7. 38. Barkovich AJ, Kjos BO. Revised classification of posterior fossa cysts and cystlike malformations based on the results of multiplanar MR imaging. AJR 1989; 153: 1289–300. 39.

Barth PG. Pontocerebellar hypoplasias. An overview of a group of inherited neurodegenerative disorders with fetal onset. Brain Dev 1993; 15:411–422

Barzegar M., Malaki M., Sadegi-Hokmabadi E. Joubert syndrome with variable features:presentation of two cases. Iran J Child Neurol 2013; 7: 43-6

Basson MA., Wingate RJ. Congenital hypoplasia of the cerebellum: developmental causes and behavioral consequences. Front Neuroanat. 2013; 3: 1-16

Bayer SA, Altman J, Russo RJ, Zhang X. Embryology 1995. In: Duckett S (ed) Pediatric neuropathology. Williams & Wilkins, Baltimore, pp 54–107

Benda CE. The Dandy-Walker syndrome or the so-called atresia of the foramen of Magendie. J Neuropathol Exp Neurol 1954; 13:14–29

Bergmann C, Zerres K, Senderek J, et al. Oligophrenin 1 (OPHN1) gene mutation causes syndromic X-linked mental retardation with epilepsy, rostral ventricular enlargement and cerebellar hypoplasia. Brain 2003; 126:1537–1544

Boltshauser E. Cerebellum – small brain but large confusion: a review of selected cerebellar malformations and disruptionAm J Med Genet A. 2004; 126A(Suppl):376–385

Boltshauser E, Schmahmann JD (eds) . Cerebellar disorders in children. Mac Keith, 2012, London

Bonnevie K, Brodal A. Hereditary hydrocephalus in the house mouse: IV. The development of the cerebellar anomalies during foetal life with notes on the normal development of the mouse cerebellum. Skr Norske Vid Akad I Math-Naturv Kl 1946; 4:1–60

Bordarier C, Aicardi J. Dandy–Walker syndrome and agenesis of the cerebellar vermis: diagnostic problems and genetic counselling. Dev Med Child Neurol 1990; 32: 285–94

Bourrat F, Sotelo C. Migratory pathways and selective aggregation of the lateral reticular neurons in the rat embryo: a horseradish in vitro study, with special reference to migratory pathways of the precerebellar nuclei. J Comp Neurol 1990; 294:1–13

Carroli SG., Porter H., Abdel-Fattah S et al. Correlation of prenatal ultrasound diagnosis and pathological findings in fetal brain anomalies. Ultrasound Obstet Gynecol. 2000; 16: 149-153.

Costa C, Hauw J-J. Pathology of the cerebellum, brain stem, and spinal cord. In: Duckett S (ed) Pediatric neuropathology 1995. Williams & Wilkins, Baltimore, pp 217–238

Courchesne E, Yeung-Courchesne R, Press GA, Hesselink JR, Jernigan TL. Hypoplasia of cerebellar vermis lobules VI and VII in autism. N Engl J Med 1988;318:1349–1354.

D'Antonio F., Khalil A., Garel C. et al. Systematic review and meta-analysis of isolated posterior fossa malformations on prenatal imaging (part 2): neurodevelopmental outcome. Ultrasound Obstet Gynecol 2016; 48: 28–37

Dekain LH., Kanel H., El-Bashir HO. Joubert syndrome labeled as hypotonic cerebral palsy. Neurosciences (Riyadh) 2014;19: 233-5

Englund C, Kowalcyk T, Daza RAM, Dagan A, Lau C, Rose MF, Hevner RF. Unipolar brush cells of the cerebellum are produced in the rhombic lip and migrate through developing white matter. J Neurosci 2006; 26:9184–9195

Espinosa JS, Luo L. Timing neurogenesis and differentiation: insights from quantitatie clonal analyses of cerebellar granule cells. J Neurosci 2008; 28:2301–2312

Gandolfi Colleoni G, Contro E, Carletti A, et al. Prenatal diagnosis and outcome of fetal posterior fossa fluid collections. Ultrasound Obstet Gynecol 2012; 39: 625–31. 35.

Garel C, Fallet-Bianco C, Guibaud L. The fetal cerebellum: development and common malformations. J Child Neurol 2011; 26: 1483–92. 30.

Garel C. Posterior fossa malformations: main features and limits in prenatal diagnosis. Pediatr Radiol 2010; 40:1038–1045

Ghi T., Contro E., De Musso F. et al. Normal morphometry of fetal posterior fossa at midtrimester: brainstem–tentorium angle and brainstem–vermis angle. Prenatal Diagnosis 2012, 32, 440–443

Ginath S., Lerman-Sagie T., Haratz Krajden K. et al. The fetal vermis, pons and brainstem: normal longitudinal development as shown by dedicated neurosonography. J Matern Fetal Neonatal Med. 2013; 26: 757-62.

Griffiths PD., Bradburn M.,Campbell MJ. Use of MRI in the diagnosis of fetal brain abnormalities in utero (MERIDIAN): a multicentre, prospective cohort study. The Lancet 2016 – 14 Dec 2016

Griffiths PD., Reeves M., Morris J., Larroche JC. Atlas of fetal and neonatal Brain MR imaging. Elsevier, 2009

Guibaud L, des Portes V. Plea for an anatomical approach to abnormalities of the posterior fossa in prenatal diagnosis. Ultrasound Obstet Gynecol 2006; 27: 477–82. 31.

Hart HN, Malamud N, Ellis WG. The Dandy-Walker syndrome. A clinicopathological study based on 28 cases. Neurology 1972: 22:771–780

Hashimoto M, Mikoshiba K. Mediolateral compartmentalization of the cerebellum is determined on the “birth date” of Purkinje cells. 2003 J Neurosci 23:11342–11351

Hatten ME, Heintz N. Mechanisms of neural patterning and specifi cation in the developing cerebellum. 1995 Annu Rev Neurosci 18:385–408

Herrup K. Role of the staggerer gene in determining cell number in the cerebellar cortex. I. Granule cell death is an indirect consequence of staggerer gene action. Brain Res 1983; 11:267–274

Herrup K, Mullen RJ (a) Regional variation and absence of large neurons in the cerebellum of the staggerer mouse. Brain Res 1979; 172:1–12

Herrup K, Mullen RJ (b) Staggerer chimeras: Intrinsic nature of Purkinje cell defects and implications for cerebellar development. Brain Res 1979; 178:443–457

Hess DT, Voogd J. Chemoarchitectonic zonation of the monkey cerebellum. Brain Res 1986; 369:383–387

Hochstetter F. (1929). Beiträge zur Entwicklungsgeschichte des menschlichen Gehirns, II. Teil, 3. Lieferung: Die Entwicklung des Mittel- und Rautenhirns. Deuticke, Vienna

Hong SE, Shugari YY, Huang DT, Al Shahwan S, Grant PE, Hourihane JO et al. Autosomal recessive lissencephaly with cerebellar hypoplasia is associated with human RELN mutations. Nat Genet 2000; 26:93–96

Hori A. Normale und pathologische Entwicklung des Nervensystems. In: Peiffer J, Schröder JM, Paulus W (eds) 2002 Neuropathologie. Morphologische Diagnostik der Krankheiten des Nervensystems und der Skelettmuskulatur, 3rd edn. Springer, Berlin/Heidelberg/New York, pp 21–61

Hori A, Peiffer J, Pfeiffer RA, Iizuka R. Cerebello-cortical heterotopia in dentate nucleus, and other microdysgeneses in trisomy D1 (Patau) syndrome. Brain Dev 1980; 2:345–352

Hoshino M, Nakamura S, Mori K, Kawauchi T, Terao M, Nishimura YV et al Ptf1a, a bHLH transcriptional gene, defi nes GABAergic neuronal fates in cerebellum. Neuron 2005;.47:201–213

International Society of Ultrasound in Obstetrics & Gynecology Education Committee. Sonographic examination of the fetal central nervous system: Guidelines for performing the basic examination and the fetal neurosonogram. Ultrasound Obstet Gynecol 2007; 29:109–116.

Ishak GE, Dempsey JC, Shaw DWW, Tully H, Adam MP, Sanchez- Lara PA et al. Rhombencephalosynapsis: a hindbrain malformation associated with incomplete separation of midbrain and forebrain, hydrocephalus and a broad spectrum of severity. Brain 2012; 135:1370–1386

Joubert MEJ, Eisenring JJ, Robb JP, Andermann F. Familial agenesis of the cerebellar vermis. A syndrome of episodic hyperpnea, abnormal eye movements, ataxia and retardation. Neurology 1969; 19: 813– 25

Juric-Sekhar G, Adkins J, Doherty D, Hevner RF. Joubert syndrome: brain and spinal cord malformations in genotyped cases and implications for neurodevelopmental functions of primary cilia. 2012 Acta Neuropathol (Berl) 123:695–709

Kapur RP., Mahony BS, Finch L et al. Normal and abnormal anatomy of the cerebellar vermis in midgestational human fetuses. Birth Defects Res A Clin Mol Teratol. 2009; 85: 700-9.

Katorza E., Bertucci E., Perlmann S. et al. Development of the Fetal Vermis: New Biometry Reference Data and Comparison of 3 Diagnostic Modalities–3D Ultrasound, 2D Ultrasound, and MRI maging. AJNR Am J Neuroradiol 2016; 37:1359–66

Kaufmann WE, Cooper K, Mostofsky SH, Capone GT, Kates WR, Newschaffer CJ et al. Specificity of cerebellar vermian abnormalities in autism: a quantitative magnetic resonance imaging study. J Child Neurol2003; 18:463–470

Lei T, Xie HN, Zhu YX, Zheng J, Zhang F, Feng JL. Date-independent parameters: an innovative method to assess fetal cerebellar vermis. Cerebellum. 2015 Jun;14(3):231-9.

Leibovitz Z., Shkolnik C., Krajden Haratz K et al. Assessment of fetal midbrain and hindbrain in mid-sagittal cranial plane by three-dimensional multiplanar sonography. Part 2: application of nomograms to fetuses with posterior fossa malformations. Ultrasound Obstet Gynecol 2014; 44: 581–587

Lemire RJ, Loeser JD, Leech RW, Alvord EC. Normal and abnormal development of the human nervous system. 1975; Harper & Row, Hagerstown

Limperoupoulos C., Robertson LR, Estroff JA et al. Diagnosis of inferior vermian hypoplasia by fetal MRI: potential pitfalls and neurodevelopmental outcome. Am J Obstet Gynecol. 2006 April ; 194(4): 1070–1076.

Liu F, Zhang Z, Liu X, Teng G, Meng H, Yu T et al. Development of the human fetal cerebellum in the second trimester: a post mortem magnetic resonance imaging evaluation. J Anat 2011; 219:582–588

Luciani L (1891) Il cervelletto: nuovi studi di fisiologia normale e pathological. Firenze : Le Monnier.

Malacarne MVG (1776) Nuova esposizione della vera struttura del cervelletto umano. Torino: Briolo.

Malacarne MVG (1791) Sulla neuro-encefalotomia. Lettere anatomico-fisiologiche di Vincenzo Malacarne e Carlo Bonnet, s.i.t. Pavia.

Malinger G, Lev D, Lerman-Sagie T. The fetal cerebellum. Pitfalls in diagnosis and management. Prenat Diagn 2009; 29: 372–80. 40. Klein O, Pierre-Kahn A, Boddaert N, et al. Dandy-Walker malformation: prenatal diagnosis and prognosis. Childs Nerv Syst 2003; 19: 484–9. 41.

Malinger G., Ginath S., Sagie-Lerman T et al. the fetal cerebellar vermis: normal development as shown by transvaginal ultrasound. Prenatal Diagnosis 2001; 21:687-692.

Malinger G., Lev D., Lerman-Sagie T. The fetal cerebellum. Pitfalls in diagnosis and management. Prenat Diagn 2009; 29: 372–380.

Malpighi M (1665) De cerebro epistola. Bologna: Benati.

Maria BL, Boltshauser E, Palmer SC, Tran TX. Clinical features and revised diagnostic criteria in Joubert syndrome. J Child Neurol 1999; 14:583–591

Maria BL, Quisling RG, Rosainz LC, et al. Molar tooth sign in Joubert syndrome: clinical, radiologic, and pathologic signifi cance. J Child Neurol 1999; 14:368–376

Mariani J, Crepel F, Mikoshiba K, et al.. Anatomical, physiological and biochemical studies of the cerebellum from reeler mutant mouse. Phil Trans R Soc Lond 1977; 281:1–28

Millen KJ, Gleeson JG. Cerebellar development and disease. 2008 Curr Opin Neurobiol 18:12–19

Moreau de la Sarthe JI (1805) Oeuvres de Vicq-d'Azyr: recueillies et publieìes avec des notes et un discours sur sa vie et ses ouvrages par Jacq L Moreau (de la Sarthe) L [Band 6 and atlas]. Paris: Duprat-Duverger.

Nyberg DA, Mahony BS, Hegge FN, Hickok D, Luthy DA, Kapur R. Enlarged cisterna magna and the Dandy-Walker malformations: factors associated with chromosome abnormalities. Obstet Gynecol 1991; 77:436–442

Paladini D., Quarantelli M., Pastore G. et al. Abnormal or delayed development of the posterior membranous area of the brain: anatomy, ultrasound diagnosis, natural history and outcome of Blake's pouch cyst in the fetus. Ultrasound Obstet Gynecol 2012; 39: 279–287

Paladini D., Volpe P. Posterior fossa and vermian morphometry in the characterization of fetal cerebellar abnormalities: a prospective three-dimensional ultrasound study. Ultrasound Obstet Gynecol 2006; 27: 482–489

Paladini D., Volpe P. Ultrasound of congenital fetal anomalies. CRC Press, 2014.

Parisi MA, Dobyns WB. Human malformations of the midbrain and hindbrain: review and proposed classification scheme. Mol Genet Metab 2003; 80:36–53

Parisi MA. Clinical and molecular features of Joubert syndrome and related disorders. Am J Med Genet C Semin Med Genet 2009; 151C: 326–40. 32. Tortori-Donati P, Rossi A, Biancheri R. Brain malformations. In: Tortori-Donati, ed. Pediatric Neuroradiology. Berlin: SpringerVerlag; 2005, 121–98. 33.

Pascual-Castroviejo I, Pascual-Pascual SI, Gutierrez-Molina M, Urich H, Katsetos. Cerebellar hypoplasia with heterotopic Purkinje cells in the molecular layer and preservation of the granule layers associated with severe encephalopathy. A new entity? 2003 Neuropediatrics 34:160–164

Pascual-Castroviejo I, Velez A, Pascual-Pascual S-I, Roche MC, Villarejo F. Dandy-Walker malformation: an analysis of 38 cases. Childs Nerv Syst 1991; 7:88–97

Pasquier L, Marcorelles P, Loget F, Pelluard F, Carles D, Perez M-J et al. Rhombencephalosynapsis and related anomalies: a neuropathological study of 40 fetal cases. Acta Neuropathol (Berl) 2009; 117:185–200

Patel S, Barkovich AJ. Analysis and classification of cerebellar malformations. AJNR Am J Neuroradiol 2002; 23: 1074–1087

Pilu G., Visentin A., Valeri B. The Dandy-Walker complex and fetal sonography. Ultrasound Obstet. Gynecol. 2000; 16: 115-7.

Poretti A., Boltshauser E., Doherty D. Cerebellar hypoplasia: differential diagnosis and diagnostic approach. Am J Med Genet Semin Med Genet 2014; 166C: 211-26

Prayer D. Fetal MRI. Springer 2011.

Purkinje J (1838) Die XV Versammlung deutscher Naturforscher und Aerzte zu Prag im September 1837. Sitzungen der Fachabtheilungen. V. Anatomie Ueber die scheinbar kanalikolöse Beschaffenheit der elementaren Nervencylinder. pp 582–583. In: Isis von oken.

Rakic P, Sidman RL. Histogenesis of cortical layers in human cerebellum, particularly the lamina dissecans. J Comp Neurol 1970; 139:473–500

Ramaeckers VT. Cerebellar malformations. In: Klockgether T (ed) Handbook of ataxia disorders. 2000 Dekker, New York, pp 115–150

Ramaeckers VT, Heimann G, Reul J, Thron A, Jaeken J. Genetic disorders and cerebellar structural abnormalities in childhood. Brain 1997; 120:1739–1751

Ramon y Cajal S (1894) The Croonian Lecture. La fine structure des centres nerveux. Proc R Soc Lond 55:444–467.

Rapoport M, van Reekum R, Mayberg H. The role of the cerebellum in cognition and behavior: A selective review. J Neuropsychiatry Clin Neurosci 2000;12:193–198.

Ray RS, Dymecki SM. Rautenlippe Redux – toward a unified view of the precerebellar rhombic lip. Curr Opin Cell Biol 2009; 21:741–747

Reil JC (1807-1808) Fragmente über die Bildung des kleinen Gehirns im Menschen. Arch Physiol 8:1–58.

Rezai Z, Yoon CH. Abnormal rate of granule cell migration in the cerebellum of "weaver" mutant mice. Dev Biol 1972; 29:17–26

Rhinn M, Brand M. The midbrain-hindbrain boundary organizer. Curr Opin Neurobiol 2001; 11:34–42

Rizzo G., Pietrolucci M.E., Mammarella S., et al. Assessment of cerebellar vermis biometry at 18-32 weeks of gestation by three-dimensional ultrasound examination. The Journal of Maternal-Fetal and Neonatal Medicine, 2012; 25 (5): 519-522

Robinson A.J. Inferior vermian hypoplasia – preconception, misconception. Ultrasound Obstet Gynecol 2014; 43: 123-136.

Robinson AJ, Goldstein R. The cisterna magna septa: vestigial remnants of Blake's pouch and a potential new marker for normal development of the rhombencephalon. J Ultrasound Med 2007; 26: 83–95. 34.

Rolando L (1809) Saggio sopra le vera struttura del cervello dell'uomo e degli animali e sopra le funzioni del sistema nervoso. Sassari: Stamperia da S.S.R.M.

Royston P, Wright EM. How to construct 'normal ranges' for fetal variables. Ultrasound Obstet Gynecol. 1998 Jan;11(1):30-8.

Salomon LJ, Alfirevic Z, Berghella V, Bilardo C, Hernandez-Handrade E, Johnsen SL, Kalache K, Leung KY, Malinger G, Munoz H, Prefumo F, Toi A, Lee W. Practice guidelines for performance of the routine mid-trimester fetal ultrasound scan Ultrasound Obstet Gynecol 2010;37:116–120.

Schmahmann JD. Disorders of the cerebellum: ataxia, dysmetria of thought, and the cerebellar cognitive affective syndrome. J Neuropsychiatry Clin Neurosci 2004; 16:367–378

Schumacher GH. Teratology in cultural documents and today. Ann Anat 2004; 186:539–546

Schwann T (1839) Mikroskopische Untersuchungen über die U¨ bereinstimmung in der Struktur und dem Wachstum der Thiere und Pflanzen. Berlin: Reimer.

Scott TG (1963) A unique pattern of localization within the cerebellum. Nature 200:793.

Sgaier SK., Millet S., Villaneuva MP et al. Morphogenetic and cellular movements that shape the mouse cerebellum; insight from genetic fate mapping. Neuron 2005; 45: 27-40

Sherer DM., Sokolovski M., Dalloul M., et al. Nomograms of the axial fetal cerebellar hemisphere circumference and area throughout gestation. Ultrasound Obstet Gynecol 2007; 29:32-37.

Shevell M, Majnemer A. Clinical features of developmental disability associated with cerebellar hypoplasia. Pediatr Neurol 1996;15: 337–339.

Sidman RL, Rakic P. Development of the human central nervous system. In: Haymaker W, Adams RD (eds) Histology and histopathology of the nervous system. 1982 Thomas, Springfield, pp 3–145

Sillitoe RV, Joyner AL. Morphology, molecular codes, and circuitry produce the three-dimensional complexity of the cerebellum. Annu Rev Cell Dev Biol 2007; 23:549–577

Snider RS, Stowell A. Receiving areas of the tactile, auditory and visual systems in the cerebellum. J Neurophysiol 1944; 7:331–357.

Sotelo C. Dendritic abnormalities of Purkinje cells in cerebellum of neurological mutant mice (weaver and staggerer). Adv Neurol 1975; 12:335–351

Sotelo C. Anatomical, physiological and biochemical studies of the cerebellum from mutant mice. II. Morphological study of cerebellar cortical neurons and circuits in the weaver mouse. Brain Res 1975; 94:19–44

Sotelo C. Cellular and genetic regulation of the development of the cerebellar system. Prog Neurobiol 2004; 72:295–339

Strata P., Voogd J. Cerebellum. Hystory. Neuroscience 2009;162: 549–559

Sugihara I, Shinoda Y. Molecular, topographic, and functional organization of the cerebellar cortex: a study with combined aldolase C and olivocerebellar labeling. J Neurosci 2004; 24:8771–8785.

Swisher DA, Wilson DB. Cerebellar histogenesis in the Lurcher (Lc) mutant mouse. J Comp Neurol 1977; 173:205–218

Taber Pierce E. Histogenesis of the deep cerebellar nuclei in the mouse: an autoradiographic study. Brain Res 1975; 95:503–518

Taggart JK, Walker AE. Congenital atresia of the foramens of Luschka and Magendie. Arch Neurol Psychiatry 1942; 48:583–612

ten Donkelaar HJ, Lammens M. Development of the human cerebellum and its disorders. Clin Perinatol 2009; 36:513–530

ten Donkelaar HJ., Lammens M, Hori A. Clinical Neuroembryology. Springer 2014.

Tennstedt H. Kleinhirnaplasie beim erwachsenen. Zblatt Allg Pathol 1965; 107:301–304.

Thompson RF, Steinmetz JE. The role of the cerebellum in classical conditioning of discrete behavioral responses. Neuroscience 2009; 162:732–755.

Tissir F, Giffinet A. Reelin and brain development. Nat Rev Neurosci 2003; 4:496–505

Toelle SP, Yalcinkaya C, Kocer N, Deonna T, Overweg-Plandsoen WCG, Bast T et al. Rhombencephalosynapsis: clinical fi ndings and neuroimaging in 9 children. Neuropediatrics 2002; 33:209–214

Tonni G., Grisolia G., Sepulveda W. Second trimester fetal neurosonography: reconstructing cerebral midline anatomy and anomalies using a novel three-dimensional ultrasound technique. Prenatal Diagnosis. 2014; 34: 75-83.

Tortori-Donati P, Fondelli MP, Rossi A, et al. Cystic malformations of the posterior cranial fossa originating from a defect of the posterior membranous area. Megacisterna magna and persisting Blake's pouch: two separate entities. Childs Nerv Syst 1996; 12: 303–8. 42.

Truwitt CL, Barkovich AJ, Shanahan R, Maroldo TV. MR imaging of rhombencephalosynapsis.. J Comput Assist Tomogr 1991; 17:211–214

Utsunomiya H, Takano K, Ogasawara T, Hashimoto T, Fukushoma T, Okazaki M. Rhombencephalosynapsis: cerebellar embryogenesis. AJNR Am J Neuroradiol 1998; 19:547–549

Valentin GG (1836) Ueber die Verlauf und den letzten Enden der Nerven. Nova Acta Acad Leopoldina 18:51–240, 531–543.

Varolio C (1573) De nervis opticis nonnulisque aliis prater communem opinionem in humano capite observatis epistole. Padova: Metti.

Vatansever D, Kyriakopoulou V., Allsop JM et al. Multidimensional Analysis of Fetal Posterior Fossa in Health and Disease. Cerebellum. 2013; 12:632–644

Vesalius A (1543) De humani corporis fabrica libris septem. Basel: Oporini.

Vieussens T (1684) Neurographia universalis. Lyons: CerteAckerman SL, Kozak LP, Przyborski SA, Rund LA, Boyer BB, Knowles BB. The mouse rostral cerebellar malformation gene encodes an UNC-5-like protein. Nature 1997; 386:838–842

Viñals F, Muñoz M, Naveas R, et al. The fetal cerebellar vermis: anatomy and biometric assessment using volume contrast imaging in the C-plane (VCI-C). Ultrasound Obstet Gynecol. 2005; Nov;26(6):622-7.

Volpe P, Contro E, De Musso F, et al. The brainstem-vermis and brainstem-tentorium angles allow accurate categorization of fetal upward rotation of the cerebellar vermis. Ultrasound Obstet Gynecol 2012; 39: 632–5. 36.

Volpe P., Contro E., De Musso F., et al. Brainstem–vermis and brainstem–tentorium angles allow accurate categorization of fetal upward rotation of cerebellar vermis. Ultrasound Obstet Gynecol 2012; 39: 632–635

Voogd J. The morphology of the cerebellum the last 25 years. Eur J Morphol 1992; 30:81–96

Voogd J. The cerebellum. In: Williams PL et al (eds) Gray's anatomy, 1995, 38th edn. Churchill Livingstone, Edinburgh, pp 1027–1064

Voogd J. The human cerebellum. J Chem Neuroanat 2003; 26:243–252

Voogd J, Jaarsma D, Marani E. The cerebellum: chemoarchitecture and anatomy. In: Swanson LW, Björklund A, Hökfelt T (eds) 1996 Handbook of chemical neuroanatomy, vol 12, Integrated systems of the CNS, Part III. Elsevier, Amsterdam, pp 1–369

Webb SJ, Sparks BF, Friedman SD, Shaw DW, Giedd J, Dawson G et al. Cerebellar vermal volumes and behavioral correlates in children with autism spectrum disorder. Psychiatry Res 2009; 172:61–67

Wingate RJT. The rhombic lip and early cerebellar development. Curr Opin Neurobiol 2001; 11:82–88

Zalel Y., Gilboa Y., Gabis L., et al. Rotation of the vermis as a cause of enlarged cisterna magna on prenatal imaging. Ultrasound Obstet Gynecol 2006; 27: 490–493

Zalel Y., Seidman D.S., Brandt N. et al. The development of the fetal vermis: an in utero sonographic evaluation. Ultrasound Obstet Gynecol 2002; 19:136-39

B) Secondary project: The developing cortex: the fetal fissures

B 1. Introduction

The adult human brain has a highly complex external morphology, and this is particularly true of the cerebral hemispheres. Someone looking at the surface of the adult brain for the first time likely would be convinced by the apparent randomness of the convoluted surface. However, it becomes apparent that the gyri/sulci form patterns that are common among individuals and, although variations exist, a large number of recurring themes can be found. Before 16 weeks' gestational age the fetal human cerebral hemispheres are effectively smooth and featureless. In contrast, the overall degree of sulcation at birth is effectively the same as the adult pattern. The huge changes in the external morphology of the brain that occur between those two-time points are due to the development of the cerebral cortex and the massive numbers of neurons and glia that migrate there from the germinal matrices. The gyral convolutions produce a greater surface area per unit volume compared with the smooth, agyric cortex present in many other mammals. Indeed, the gyric human cerebral cortex is estimated to have three times the surface area as an agyric brain of the same volume. The major sulci of the brain tend to appear in an ordered and predictable sequence; however, the patterns are only approximations, and one should not expect to be able to define with any degree of accuracy the gestational age of a fetus based on the sulcal patterns. Biologic variation is one issue, and the mechanisms for estimating the dates of a pregnancy have wide margins of error. In addition, the possible significant differences in the degree of sulcation between the two hemispheres within the same individual are well documented.

The cerebral hemispheres are separated from each other in the midline by the median (great) longitudinal fissure and its contents: the pia and arachnoid mater with the intervening subarachnoid space that overlie both cerebral hemispheres, and two layers of dura mater that are fused for the most part as the falx cerebri. The inferior sagittal sinus is contained within the free inferior border of the falx, whereas superiorly the two leaves of dura separate to contain the superior sagittal sinus. The falx is attached to the crista galli anteriorly, where it is quite narrow, but it widens as it sweeps posteriorly and eventually attaches along the midline of the tentorium cerebelli. The drainage of venous blood in the sagittal sinuses normally is from anterior to posterior; therefore, the structure increases in size passing posteriorly to accommodate for increasing drainage from the cortical veins. The surfaces of the cerebral hemispheres show many convolutions consisting of cortical gyri separated by sulci of varying sizes. The cerebral cortex and associated white matter form four lobes in each hemisphere (frontal, temporal, parietal, occipital), and those lobes are (incompletely) defined by prominent, relatively constant sulci.

The major sulci responsible for lobar anatomy consist of the lateral (Sylvian) sulcus, central sulcus, and parieto-occipital sulcus. For the most part the lobar anatomy is best defined on the lateral surface of the brain by the lateral and central sulci.

The lateral (Sylvian) sulcus or Sylvian fissure is a deep fissure that is first identified on the inferior surface of the brain close to the anterior perforated substance but becomes most visible on the lateral surface where it separates the frontal and parietal lobes from the temporal lobe. The frontal lobe is separated completely from the temporal lobe, whereas the posterior aspects of the parietal and temporal lobes remain in continuity without a well-defined external border. The parts of the frontal, temporal, and parietal lobes that protrude into and surround the lateral fissure are called the opercula. The anatomy of the lateral sulcus on the lateral surface of the brain is complicated as it divides into three rami: anterior horizontal, anterior ascending, and posterior. These can be seen well on MRI that allows nonorthogonal plane reformation of volume data. The anterior horizontal ramus protrudes into the inferior frontal gyrus running horizontally and anteriorly. The anterior ascending ramus runs vertically into the same gyrus and defines the pars triangularis portion of the inferior frontal gyrus anterior to the ascending ramus and the pars opercularis posteriorly. The posterior ramus extends posteriorly and slightly superiorly for approximately 8 cm before dividing into the posterior ascending and posterior descending rami.

The insula is defined as the cortical surface in the depth of the lateral fissure and is considered to be the "fifth cortical lobe" by some researchers. The mature insula has a complicated surface structure, which is best appreciated on whole brain preparations when the opercula have been removed. The insula is pyramidal in shape, with its apex directed inferiorly and anteriorly. The apex is the only portion of the insula that is not bounded by the circular gyrus. The large central insular sulcus runs from the apex, superiorly and posteriorly to form larger anterior and smaller posterior surfaces. The posterior region usually is divided by a single sulcus to form two "gyri longi," whereas the anterior area is inconsistently divided into three or four "gyri brevi."

The central sulcus on the lateral aspect of the cerebral hemisphere barely extends onto the medial surface. It separates the frontal and parietal lobes, and the frontal lobe can be completely delineated by the lateral and central sulci on the lateral surface of the brain. It takes a curved course posteriorly at approximately 70° towards the lateral sulcus but does not contact it. The postcentral sulcus lies approximately 1.5 cm posterior to the central sulcus and runs parallel to it. The correct localization of the central sulcus is hugely important on cross-sectional imaging as it defines the primary motor cortex anteriorly and the primary sensorimotor cortex posteriorly. This can be difficult and is best achieved on axial imaging as described in the section on the cingulate sulcus.

The parieto-occipital sulcus is predominantly a feature of the posterior portion of the medial hemispheric surface, although it can extend onto the lateral surface for a short way in some cases. It runs inferiorly and slightly anteriorly, separating the precuneus of the parietal lobe and the cuneus of the occipital lobe before joining the

calcarine fissure. Note that a temporo-occipital sulcus exists on the inferior surface of the brain but has highly variable appearances.

Other sulci of importance for fetal imaging include: the superior and Inferior frontal sulci, the superior frontal gyrus cingulate, the sulcus superior and inferior, the temporal sulci, the calcarine sulcus and the collateral sulcus.

Differences are seen between the conspicuity of cortical sulci on post-mortem tissue sections and in utero MRI. Specifically, the current data indicates delineation of sulci at earlier gestational ages on tissue sections. As an example, the Sylvian fissure is well seen on histologic studies as early as 16 weeks' gestational age but usually is not clearly demarcated in all fetuses at 19 to 20 weeks' gestation. Garel's textbook presents cases at 22 to 23 weeks, and at that stage the lateral sulcus was seen in 100% of normal fetuses. It is not sufficient to know merely when the Sylvian fissure can first be located. The Sylvian fissure is an exceptionally complicated structure that continues to develop after birth, and an understanding of its normal sequence of development is important. When the Sylvian fissure first appears, it is merely an oblique indentation in the lateral aspect of the second-trimester hemisphere. Over time it deepens and develops secondary sulci on the insular cortex, and the opercula portions of the surrounding frontal, parietal, and temporal lobes completely cover the insula, as described previously. The insular sulci form late. Garel did not see any evidence of the insular sulci before 31 weeks, and those structures were present in only 10% of 31-week fetuses. Insular sulci were present in all 36-week gestational age fetuses.

Imaging of the fetal brain in the axial plane allows good assessment of developing opercularization. The anterior and posterior lips of the opercula are everted up to 20 weeks' gestational age, but rapid cortical/subcortical growth causes the lips to grow toward each other, a process that is quite advanced by 26 weeks' gestational age. Garel assessed this development by measuring the distance between the anterior and posterior opercula and found few cases where the inter-opercular distance was less than 10 mm before 29 weeks. The distance then gradually reduced so that at 36 weeks' gestation, for example, 80% of values were between 4 and 8 mm. However, the opercula did not close completely before birth in any of the cases, so this event appears to occur postnatally. Cortical malformations may disrupt this process, but under-opercularization without obvious structural abnormality is one of the "soft" neuroradiologic features seen with high frequency in children with developmental delay. The central and precentral sulci are early features on the lateral surface of the developing hemispheres, with the central sulcus appearing first. Both structures are best assessed on axial imaging of the fetal brain. Garel found that the central sulcus was seen in 20% of her cases at 22 to 23 weeks, in 75% of cases at 26 weeks, and in all cases thereafter. In contrast, the precentral sulcus was not shown by Garel before 26 weeks but was seen in 90% of 28-week fetuses and consistently after that time. The parieto-occipital sulcus is best appreciated on sagittal images of the fetus. It is visible after 22 weeks' gestational age in the vast majority of, if not all, fetuses.

B 2. Aim of the researches

As pointed out in the introduction section, the cerebral cortex develops significantly faster and it increases in size more rapidly than the adjacent white substance during fetal life. From a completely smooth surface during the first and the early second trimesters of pregnancy, the brain changes into a complex arrangement of fissures, sulci and gyri, which become increasingly evident during the course of the third trimester. These structures have a relatively constant location and morphology, and may serve as anatomical landmarks when studying cortical development. Furthermore, each fissure, sulcus and gyrus become visible at examinations at specific gestational ages, as confirmed by several prenatal and postnatal as well as post-mortem MRI studies.

Currently, the assessment of the developing fetal brain at prenatal ultrasound scan is still challenging also for experienced sonographers. Indeed, most of the fetal fissures, sulci and gyri become visible only during late pregnancy. Furthermore, migrational disorders may be subtle and may have a variety of ultrasonographic appearances that are generally not detectable until the third trimester or even some month after birth.

Therefore, recent efforts of neurosonographers have been focused at studying the first visible morphological changes of the developing fetal cortex in order to facilitate an earlier diagnosis of abnormal neuronal migration also with the aid of three-dimensional technology.

The Sylvian fissure and the insula lobe are among the most well-studied anatomical structure of the fetal brain and demonstrate a typical pattern of development throughout gestation. In early second trimester, the Sylvian fossa appears at prenatal two-dimensional ultrasound scan as a smooth-margined, shallow notch on the lateral side of the cerebral hemisphere. During the course of the subsequent weeks of pregnancy, the profile of this structure begins to change, showing further indentation with distinct angularity at the margins of the insula.

The prenatal study of the development of the Sylvian fissure and insula lobe may be helpful in improving the prenatal detection of migrational disorders, since they appear early in the second trimester and can be studied through a routine trans-thalamic axial scan of the fetal brain. However, despite the increasing number of studies on fetal cerebral development, only few papers, with a small number of patients, have provided objective standardization for the assessment of Sylvian fissure and insula lobe by routine two-dimensional ultrasound scan.

The aim of this study was to measure the Sylvian fissure and insula lobe in normal fetuses at two-dimensional-ultrasound, through the standard trans-thalamic plane, throughout pregnancy, in order to (a) construct normal reference ranges for the Sylvian fissure and insula lobe, based on a large number of normal fetuses; (b) develop a novel parameter for the assessment of the brain cortex development, obtained by the ratio defined as Sylvian fissure /(Sylvian fissure + insula lobe), that we named the insula ratio (IR); (c) to evaluate the reproducibility of these measurements between differently skilled operators.

B 3. Clinical study

B 3.a The fetal sylvian fissure and insula lobe throughout gestation: a cross sectional study.

Materials and methods

We conducted a multicentre prospective cross-sectional study focused on the sonographic evaluation of the fetal Sylvian fissure and insula lobe at the prenatal Centre "*Diagnostica ecografica prenatale Aniello Di Meglio s.r.l*", Naples, Italy, and at the Department of Obstetrics and Gynaecology of the University of Bern, Switzerland. Consecutive low-risk pregnant women with well-established gestational age determined by a reliable last menstrual period and confirmed by the measurement of crown-rump length at first trimester ultrasound scan between 11 and 14 weeks of gestation were asked to participate. Only singleton foetus without structural abnormalities, were included in our trial. Each woman was considered only once. All participants had a negative anamnesis for systemic diseases, intact fetal membranes, normal amniotic fluid volume, and were not in labour at the time of inclusion in the study. Indications for ultrasound examination were assessment either for screening sonography or fetal growth ascertainment.

Gestational age at inclusion ranged between 18 and 33 weeks. Fractions of weeks were computed to the nearest week, with fractions of ≤4 days and >5 days assigned to the lower and higher weeks, respectively.

All deliveries occurred after 37 completed weeks and no infants had evidence of growth disturbances (birthweight between 2500 and 4000 grams). All neonates underwent routine neonatological examination within the first 48 hours.

At enrolment, all women gave a written informed consent to participate to the study, which was approved by the Institutional Review Board of all participating centres.

The ultrasound machine used for two – dimensional ultrasound scan were Aloka (Aloka Co., Ltd, Tokyo, Japan) and GE Voluson E10 (GE Healthcare Ultrasound, Milwaukee, WI, USA) equipped with a curved linear array trans-abdominal transducer (2–5 MHz).

Besides standard fetal biometric parameters such as biparietal diameter (BPD), head circumference (HC), abdominal circumference (AC), and femur length (FL), we obtained the measurement of Sylvian fissure and insula lobe. For standardization purposes, all brain measurements were performed in the hemisphere that was distal to the transducer, regardless of fetal side, to prevent shadowing from the fetal skull bones. We assessed the biometry of Sylvian fissure and insula lobe as follows: first, we obtained a standard trans-thalamic axial plane of the fetal head, as used for measurement of the BPD and HC, in which the cerebral falx and the cavum septi pellucid can be visualized and the thalami are visible symmetrically. Care was taken to ensure that the midline of the brain was equidistant from both sides of the calvarium to ensure that the plane was not oblique. The biometries of Sylvian fissure and insula lobe were taken as reported: insula lobe was measured from the cerebral falx, drawing a

perpendicular line to the point of maximum prominence of the insular cortex. The depth of Sylvian fissure was measured drawing a line in continuation with the insular line (perpendicular to the midline), from the insular cortex towards the inner table of the parietal bone. The ratio between the Sylvian fissure and the sum of the Sylvian fissure and insula lobe was calculated and called "insula ratio" (IR) (**Fig. 28**)

The first 38 fetuses each measurement was repeated twice by two examiners (S.M. and D.M.A.) in order to assess the reproducibility of the measurements. The two operators were identified as n.1 (senior, i.e. more than 5 years of experience of prenatal ultrasound) and n.2 (junior, i.e. less than 5 years of skill with prenatal ultrasound), and all measurements were numbered as 1 or 2, when performed by the senior and the junior operator, respectively.

Statistical analysis was performed with the SPSS package (SPSS inc., Chicago, IL, USA) and with Graph Pad Prism version 5.00 for Windows (Graph Pad Software, San Diego CA, USA). Normal ranges for Sylvian fissure and insula lobe were constructed according to the method previously described by Royston and Wright in 1998. Gestational age dependency of the brain parameters was analysed using Spearman rank correlation. Polynomial regression analysis was performed to identify the regression curves that best fitted the mean and standard deviation (SD) as a function of gestational age. The standard deviation scores (Z-scores) were calculated using the formula: observed measurement – mean measurement/SD. To assess the model fit, the Gaussian distribution of the Z-scores was checked using the Kolmogorov–Smirnov test. The 5^{th} and 95^{th} centiles for Sylvian fissure, insula lobe, and IR throughout gestation were obtained as previously described using the formula: mean ± 1.645 SD (21-22). The inter-observer variability was assessed by interclass correlation coefficients (ICC) and Bland-Altman plots. Statistical significance was considered achieved when $P < 0.05$.

Results

During the study period, 343 patients met the inclusion criteria. Patient characteristics are displayed in **Tab. 8**. An adequate measurement of the Sylvian fissure and the insula lobe was obtained in all cases using the trans-abdominal route. Fourteen of the included women were lost for follow-up. Thus, 329 cases were finally considered for our analysis. A significant correlation was found between gestational age and Sylvian fissure ($r=0.79$; $p<0.0001$) as well as with insula lobe ($r=0.77$; $p<0.0001$). Similarly, the IR showed also a significant correlation with gestational age ($r=0.39$; $p<0.0001$).

The regression equation for the mean of the different measurements according to gestational age (x) were: SF (y) $y = -19.69 + 1.813x - 0.02422x2$, and for the SD (y′) was: $y' = -0.1557 + 0.04511x$. IL (z) $z = -3{,}060 + 0.8495x$ and for the SD (z′) was: $z' = -1.102$. IR (q) $q = -0.1593 + 0.03795x - 0.0006778x2$ and for the SD (q′) was: $q' = 0.2674$. **Fig. 29** shows the fitted 5^{th} , 50^{th} , and 95^{th} centiles for gestational age calculated as explained before, while **tab. 9** summarizes mean and SD per week in the interval between 18 and 33 weeks for Sylvian fissure, insula lobe and IR.

When inter-observer variability was assessed for measurements obtained on two-dimensional ultrasound in the series of the first 38 fetuses, ICC was 0.97 (95% CI: 0.94-0.98). In the Bland-Altman plots the mean difference of inter-observer agreement was 0.03 and 95% CI limits were -0.31 to -0.37 (**Fig. 30**).

B 4. Discussion

Any event that is able to alter neuronal proliferation, migration, or cortical organization can cause a cerebral cortex malformation. Neuroblast proliferation starts in the seventh week of gestation in the subependymal region around the walls of the lateral ventricle. This proliferation is particularly active between 13 and 26 weeks' gestation. After 26 weeks, the volume of the germinal zone rapidly decreases. Neuronal migration to the cerebral cortex starts around the eighth week and is completed by 20–24 weeks' gestation; glial cell migration continues until after birth. During this period, the neurons migrate from the germinal matrix within the periventricular zone, on radial glial guides, toward the pial surface. Waves of migrating neuroblasts lead to the formation of a superficial cortical plate separated from the deep germinal layer by an intermediate zone containing concentric migrating cells. The migration waves form an "inside-out" six-layered cortex, in which the first wave of migrating neuroblasts forms the deepest cortical layer, while the later waves constitute the most superficial layer. At the same time, the intermediate zone increases in width and forms the white matter.

Recently, it has been shown that not all cerebral cortical neurons are generated in the germinal zones of the dorsal telencephalon and migrate radially to the developing cortex; in fact, a not insignificant number of cortical interneurons are generated in the lateral, medial, and caudal ganglionic eminences and migrate tangentially into the cerebral cortex. In addition, recent reports have made it clear that radial glia are much more active participants in cortical development. Indeed, radial glia are neuronal and glial precursors as well as guides and may, as well, have a role in orchestrating the entire migration process. Myelination, in contrast, starts only after birth.

Gyration and sulcation occur during neuronal migration and continue until after birth. The main malformations of cortical development are classified into three basic groups, based on the stage at which the developmental process is likely disturbed. Group I (abnormal neuronal and glial proliferation/apoptosis) comprises microcephaly, megalencephaly, and cortical dysgenesis with abnormal cell proliferation. Group II (abnormal neuronal migration) includes various types of heterotopia and lissencephaly. Group III (abnormal postmigration development) includes polymicrogyria and schizencephaly, focal cortical dysplasia, and post migration microcephaly.

The development of the Sylvian fissure is one of the major brain maturational processes occurring in fetal life and an altered development of this fissure leads to the main malformations of cortical development. Using MRI, abnormalities in this process, leading to aberrant operculization, have been diagnosed increasingly in infants and children with developmental delay.

Although the maturational phases of the operculum have been defined by neuropathological evaluation of fetuses, relatively few papers have described the ultrasonographic imaging of normal operculization. Since the introduction of ultrasound for evaluation of the fetal brain, emphasis has been on the ventricular system and

surrounding structures, while the study of the cortex has been overlooked. This fact can be explained mainly by technical issues that have precluded visualization of the proximal hemispheric surface and by the rapid developmental changes in cortical milestones through pregnancy that are difficult to standardize and remember during real-time scanning.

The seminal study by Chen et al. in 1995 describing the normal topography of the cerebral operculum on MRI led to papers describing its abnormal formation and paved the way to the in-utero identification of related conditions. In 2008, Quarello et al. suggested a standardized approach to following fetal Sylvian fissure development and Guibaud et al. presented their experience with the prenatal diagnosis of abnormal development of this structure and correlate their imaging findings with neuropathological and postnatal data.

Quarello et al. defined six gross landmarks in the normal operculization process based first on the angle between the insula and the temporal lobe and then on the extent of overriding of the posterior half of the insula by the temporal lobe; these landmarks and the stages in between them were scored between 0 and 10. According to Malinger, this method, although described as being reproducible and reliable, is cumbersome, time-consuming and relatively difficult to apply in daily practice and is unnecessary during the performance of a routine examination. This opinion is strengthened by the fact that all cases with abnormal operculization described by Guibaud et al. were referred for associated findings, including ventriculomegaly, abnormal head circumference and other central nervous system and other anomalies. Dedicated neurosonography and MRI later defined the abnormal operculization and added information regarding the presence of malformations of cortical development, such as lissencephaly and polymicrogyria.

Chen et al. divided abnormal operculization into five types. Isolated abnormal operculization was found only among patients with Type 5 (normal-appearing insula with under developed operculum consistent with the developing operculum found after 32 weeks of gestation). This group included children with abnormal head circumference, metabolic diseases and trisomy 21 and children with non-specific developmental delay. The authors suggested that the abnormal operculization in some of these children could signify delayed maturation, similar to delayed myelination, that would improve with time with concomitant improvement of the developmental delay. Therefore, the initial evaluation, even in the hands of a sonographer without proficiency in neurosonography, would usually be sufficient to identify most at-risk fetuses, enabling referral for consultation at a fetal neurology clinic, where the scoring method previously described would be very useful for accurate definition of the brain anomaly.

Since Kuzniecky et al. first described congenital bilateral perisylvian syndrome in 1989, abnormal operculum formation has been considered almost synonymous with polymicrogyria. However, the paper by Guibaud et al. highlights the fact that most children with abnormal operculization will not have an associated malformation of cortical development (10 out of 15 cases). These results are consistent with the findings of Chen

et al.13, that only 14 out of 86 patients had a malformation of cortical development. In these 14 patients, the operculum was either unformed or abnormally formed.

In the light of these considerations, it appears evident that more papers assessing the cortical development in physiological and pathological cases, in particular by dedicated neurosonography, are still necessary to investigate this interesting issue. This was the rational of the choice of our study, that aimed at assessing the operculization process throughout gestation by the measurements of the Sylvian fissure and the insula lobe at two-dimensional prenatal ultrasound scan in physiological cases.

The sonographic measurement of the Sylvian fissure and the insula lobe was reproducible and easy to perform. Our findings showed that Sylvian fissure and insula lobe increase in depth in a linear fashion throughout gestation, and the growth pattern correlates well with gestational age. These data are in line with previously reported reference limits constructed by using two-dimensional and three-dimensional ultrasound scan. All these values can serve as a reference to all sonographers which evaluate the development of the fetal cortex.

To our knowledge, this is the first study that assess the ratio between the Sylvian fissure and the sum of the Sylvian fissure and the insula lobe throughout pregnancy. Interestingly, this ratio behaves as a polynomial regression in relation to gestational age, increasing till 26 week and then showing a plateau before starting to decrease.

This ratio may be a mirror of the embryological and anatomical development of the Sylvian fissure and the insula lobe, which changes not only in size but also in shape, with smooth curved margins at 20 weeks and a more indentated, trapezoidal and rectangular shape at 30 weeks; this change is in accordance with the opercularization process, that is asymmetrical. Indeed, unlike the posterior, the anterior opercula develops later in pregnancy (see introduction section), at the beginning of the third trimester and this can explain the plateau at 26 weeks followed by the slow drop of the insula ratio. Thus, our ratio may be an easy marker of the ongoing process of the development of the fetal cortex.

This study includes also the largest series ever published for the construction of Sylvian fissure and insula lobe nomograms throughout gestation in two-dimensional trans-abdominal manner. The only other series of Alonso et al. included only 15 pregnant women; other authors constructed fetal brain fissure reference curves using three-dimensional technology and without assessing the depth of the insula lobe.

Pistorius et al. in 2010 evaluated the development of selected fissures and elaborated a simple score in order to assess the grade of maturation of fetal cortex; however, they did not provide ultrasonographic nomograms for Sylvian fissure and insula lobe. Garel et al., as reported in the introduction section, investigated the timing of normal sulcation landmarks according to gestational age by using in utero MRI imaging, without providing any nomograms of for Sylvian fissure and insula lobe growth. Monteagudo et al. determined the feasibility of imaging specific sulci,

gyri and fissures and focused exclusively on the two-dimensional transvaginal approach, again without providing any reference range for Sylvian fissure and insula lobe.

The early recognition of the absence or abnormal appearance of a particular sulcus or fissure at the appropriate fetal age should be raise suspicion about the possibility of abnormal or delayed cortical development and is crucial for identifying an impaired neuronal migration manifesting with lissencephaly (smooth brain). Prenatal diagnosis of an affected fetus allows proper counselling and optimization of obstetric management as well as proper targeted further examinations.

Nevertheless, the current international guidelines on fetal anomaly screening ultrasound, although recommend the investigation of the trans-thalamic plane of the fetal brain, do not include the Sylvian fissure and insula lobe among the structures to be visualized or measured. In other words, as stated by Malinger "*the study of the cortex has lagged behind*". Our choice to assess the sylvian fissure and insula lobe was based on this consideration and we aim to promote an easy and practical measurement to be performed during the routine scan. Indeed, these structures can be easily identified on the standard trans-thalamic section which is universally used for measuring the BPD and the HC throughout pregnancy, since early sulcal development is best depicted on images obtained perpendicular to the expected course of the sulci.

The choice of starting our measurements from the 18^{th} weeks of pregnancy is due to the fact that Sylvian fissure and insula lobe becomes for the first time visible as a smooth, shallow depression on the lateral surface of the brain starting as early as 18 weeks gestation.

In our study, we did not observe any gender difference in the measurement of the Sylvian fissure and insula lobe. However, other authors observed a small (and maybe not clinically relevant) gender difference in the measurements of the Sylvian fissure, with females having smaller measurements than males.

To date, this is the first time that inter-observer reproducibility of Sylvian fissure and insula lobe measurements between a senior and a junior operator have been tested. Of interest is that the reliability of measurements taken between the two examiners, although differently skilled, was good as expressed by an interclass correlation coefficients (ICC) of 0.97. This last finding might support the hypothesis that these measurements are feasible and reproducible enough to be usable also by sonographers who do not have special training in neurosonography as well as applied in every clinical context in which diagnosis of migration disorders is required.

Our data support the use of routine trans-abdominal two-dimensional route to assess such anatomical structures and encourage even less experienced operators to perform these measurements. We believe that the assessment of fetal cortex development should be incorporated into practice and part of routine prenatal ultrasound screening. The reference ranges provided by our study may help facilitate the identification of cases with suspected

abnormal cortical development as well as help in providing the basis for proper management and counselling of this condition. Further studies, including also pathological cases, are needed to strengthen our findings.

B 5. References

Adachi Y, Poduri A, Kawaguch A, et al. Congenital microcephaly with a simplifiedgyral pattern: associated findingsand their significance AJNR 2011; 32: 1123–9. 45.

Afif A, Bouvier R, Buenerd A, Trouillas J. Development of the human fetal insular cortex: study of the gyration from 13 to28 weeks. Brain StructFunct 2007; 212: 335–346.

Alonso I., Borenstein M., Grant G., Narbona I., Azumendi G. Depth of Brain fissures in normal fetuses by prenatal ultrasound between 19 and 30 weeks of gestation. Ultrasound ObstetGynecol 2010; 36: 693-699.

Altman DG, Chitty LS. Chart of fetal size: 1. Methodology. Br J ObstetGynaecol 1994; 101: 29–34

Altman J, Bayer SA: Regional differences in the stratified transitional field and the honeycomb matrix of the developing human cerebral cortex. J Neurocytol 31:613–632, 2002. 9.

Alves C.M.S., Araujo E Junior, et al. Reference ranges for fetal Brain Fissures Development on 3-Dimensional Sonography in the Multiplanar Mode. J Ultrasound Med. 2013; 32: 269-77

Barkovich AJ, Guerrini R, Kuzniecky RI, et al. A developmental and genetic classification for malformations of cortical development: update 2012. Brain 2012; 135: 1348–69. 44.

Barkovich AJ, Kuzniecky RI, Dobyns WB, et al: A classification scheme for malformations of cortical development. Neuropediatrics 1996; 27:59–63,

Bayer SA, Altman J: Atlas of Human CNS Development: Volume 3—The Human Brain During the Second Trimester. Boca Raton, FL, CRC Press, 2005.

Bendersky M, Musolino P, Rugilo C, Shuster G, Sica R. Normal anatomy of the developing fetal brain. Ex vivo anatomical–magnetic resonance imaging correlation. J NeurolSci 2006; 250: 20–26.

Bendersky M, Tamer I, Van Der Velde J, et al.. Prenatal cerebral magnetic resonance imaging. J NeurolSci 2008; 275: 37–41.

Bernard C, Droulle P, Didier F, et al.. Aspects ´echografiques des silons c´er´ebraux `a la period ante et p´erinatale. J Radiol1988; 69: 521–532.Copyright 2010 ISUOG. Published by John Wiley & Sons, Ltd. Ultrasound ObstetGynecol 2010; 36: 693–699.

Bingham PM, Zimmerman RA, McDonald-McGinn D, et al. Enlarged Sylvian fissures in infants with interstitial deletion of chromosome 22q11. Am J Med Genet 1997; 74: 538–543.

Bland JM, Altman DG. Applying the right statistics: analyses of measurement studies. Ultrasound ObstetGynecol 2003; 22:85–93.

Chen C, Zimmerman R, Faro S, et al.. MR of cerebral operculum: abnormal opercularization in infants and children. AJNR Am J Neuroradiol 1996; 17: 1300–1311.

Chen C-Y, Zimmerman RA, Faro S, et al.. MR of the cerebral operculum: topographic identification and measurement of interopercular distances in healthy infants and children. AJNR Am J Neuroradiol 1995; 16: 1677–1687.

Chi JG, Dooling EC, Gilles FH. Gyral development of the human brain. Ann Neurol 1977; 1: 86–93.

Cohen-Sacher B, Lerman-Sagie T, Lev D, Malinger G. Sonographic developmental milestones of the fetal cerebral cortex: a longitudinal study. Ultrasound Obstet Gynecol. 2006; 27: 494–502.

Correa F, Lara C, Bellver J, Remohi J, Pellicer A, Serra V. Examination of the fetal brain by transabdominal three dimensional ultrasound: potential for routine neurosonographic studies. Ultrasound Obstet Gynecol. 2006; 27: 503–508.

Dobyns WB, Truwit CL: Lissencephaly and other malformations of cortical development: 1995 update. Neuropediatrics 1995; 26:132–147,

Dorovini-Zis K, Dolman CL. Gestational development of brain. Arch Pathol Lab Med 1977; 101: 192–195.

Droulle P, Gaillet J, Schweitzer M. Maturation of the fetal brain. Echoanatomy: normal development, limits and value of pathology. J Gynecol Obstet Biol Reprod 1984; 13: 228–236.

Feess-Higgins A, Larroche J-C (eds): Development of the Human Foetal Brain: An Anatomical Atlas. Paris, INSERM CNRS, 1987.

Fong KW, Ghai S, Toi A, et al. Prenatal ultrasound findings of lissencephaly associated with Miller-Dieker syndrome and comparison with pre- and postnatal magnetic resonance imaging. Ultrasound Obstet Gynecol 2004; 24: 716–23.

Garel C. MRI of the Fetal Brain. Berlin, Springer-Verlag, 2004. 7. Chi JG, Dooling EC, Gilles FH: Gyral development of the human brain. Ann Neurol 1977; 1:86–93,

Garel C, Chantrel E, Brisse H, Elmaleh M, Luton D, Oury JF, Sebag G, Hassan M.Fetal cerebral cortex: normal gestational landmarks identified using prenatal MR imaging. AJNR Am J Neuroradiol. 2001; 22:184-9.

Garel C. Development of the fetal brain – results. In: Garel C., ed. MRI of the fetal brain: normal development and cerebral pathologies. Berlin, Germany: Springer-Verlag, 2004; 35-86.

Ghai S, Fong K, Toi A, Chitayat D, Pantazi S, Blaser S. Prenatal US and MR imaging findings of lissencephaly: review of fetal cerebral sulcal development. Radiographics 2006; 26:389–406.

Ghai S., Fong KW, Toi A., Chitayat D., Pantazi S., Blaser S. Prenatal US and MR imaging findings of lissencephaly: review of fetal sulcal development. Radiographics 2006; 26:389-405

Griffith PD, Bradburn M, Campbell MJ et al. Use of MRI in the diagnosis of fetal brain abnormalities in utero (MERIDIAN): a multicentre, prospective cohort study. Lancet 2016; (16)31723-8.

Griffiths PD, Bolton P, Verity C: White matter abnormalities in tuberous sclerosis complex. Acta Radiol 1998; 39:482–486,

Guibaud L, Selleret L, Larroche JC, et al. Abnormal Sylvian fissure on prenatal cerebral imaging: significance and correlation with neuropathological and postnatal data. Ultrasound Obstet Gynecol 2008; 32: 50–60.

International Society of Ultrasound in Obstetrics and Gynaecology (ISUOG) guidelines. Sonographic examination of the fetal central nervous system: guidelines for performing the 'basic examination' and the 'fetal neurosonogram'. Ultrasound ObstetGynecol 2007; 29: 109–116.

Jissendi-Tchofo P, Kara S, Barkovich AJ. Midbrain–hindbrain involvement in lissencephalies. Neurology 2009; 72: 410–18. 46.

Kivilevitch Z, Achiron R, Zalel Y. Fetal brain asymmetry: in utero sonographic study of normal fetuses. Am J ObstetGynecol 2010; 202: 359.e1–e8.

Kostovic I, Judas M, Rados M, Hrabac P: Laminar organization of the human fetal cerebrum revealed by histochemical markers and MR imaging. Cereb Cortex 2002; 12:536–544,

Kostovic I, Rakic P: Developmental history of the transient subplate zone in the visual and somatosensory cortex of the macaque monkey and human brain. J Comp Neurol 1990; 297: 441–470,

Kuzniecky R, Andermann F, Guerrini R. Congenital bilateral perisylvian syndrome: study of 31 patients. The CBPS Multicenter Collaborative Study. Lancet 1993; 341: 608–612.

Kuzniecky R, Andermann F, Tampieri D, Melanson D, Olivier A, Leppik I. Bilateral central macrogyria: epilepsy, pseudobulbar palsy, and mental retardation–a recognizable neuronal migration disorder. Ann Neurol 1989; 25: 547–554. 15.

Larroche J. The development of the central nervous system during intrauterine life. In: Falkner F, ed. Human development. Philadelphia, Pa: Saunders, 1966; 257-260

Lerman-Sagie T, Malinger G. Opinion. Focus on the fetal Sylvian fissure. Ultrasound Obstet Gynecol 2008; 32:3–4

Levine D, Barnes P. Cortical maturation in normal and abnormal fetuses as assessed with prenatal MR imaging. Radiology 1999; 210: 751–758.

Malinger G, Kidron D, Schreiber L, et al. Prenatal diagnosis of malformations of cortical development by dedicated neurosonography. Ultrasound Obstet Gynecol 2007; 29 (2): 178-91

Malinger G. Focus on the Fetal Sylvian Fissure. Ultrasound Obstet Gynecol 2008;32:3-4.

Mittal P, Goncalves L, Kusanovic J, et al. Objective evaluation of Sylvian fissure development by multiplanar 3-dimensional ultrasonography.J Ultrasound Med 2007; 26: 347–353.

Monteagudo A, Timor-Tritsch I, Mayberry P. Three-dimensional transvaginal neurosonography of the fetal brain: 'navigating' in the volume scan. Ultrasound ObstetGynecol 2000; 16: 307–313.

Monteagudo A, Timor-Tritsch IE. Development of fetal gyri, sulci and fissures: a transvaginal sonographic study. Ultrasound Obstet Gynecol 1997; 9: 222–228.

Naidich TP, Brightbill TC: The pars marginalis I. A "bracket" sign for the central sulcus in axial plane CT and MRI. Int J Neuroradiol 1996; 2:3–19.

Naidich TP, Kang E, Fatterpekar G, et al: The insula: Anatomic study and MR imaging at 1.5 T. Am J Neuroradiol 2004; 25:222–232,

Naidich TP, Valavanis AG, Kubik S: Anatomic relationships along the low-middle convexity: Part 1—Normal specimens and MR imaging. Neurosurgery 1995; 36:517–531,

Pavone L, Corsello G, Pavone P, Iannetti P. Lissencephalic syndromes: brain and beyond. Front Biosci 2010; 2:85–95

Perkins L, Hughes E, Srinivasan L, et al. Exploring cortical subplate evolution using magnetic resonance imaging of the fetal brain. Dev Neurosci 2008; 30:211–220

Pistorius L.R., Stoutenbeek P., Groenendaal F., et al. Grade and symmetry of normal fetal cortical development: a longitudinal two- and three- dimensional ultrasound study. Ultrasound Obstet Gynecol 2010; 36: 700-708

Quarello E, Stirnemann J, Ville Y, Guibaud L. Assessment of fetal Sylvian fissure operculization between 22 and 32 weeks: a subjective approach. Ultrasound Obstet Gynecol 2008; 32: 44–49.

Rados M, Judas M, Kostovic I: In vitro MRI of brain development. Eur J Radiol 2006; 57:187–198.

Rizzo G., Pietrolucci M.E., Mammarella S., et al. Assessment of cerebellar vermis biometry at 18-32 weeks of gestation by three-dimensional ultrasound examination. The Journal of Maternal-Fetal and Neonatal Medicine, 2012; 25 (5): 519-522

Rolland Y, Adamsbaum C, Sellier N, Robain O, Ponsot G, Kalifa G. Opercular malformations: clinical and MRI features in 11 children. Pediatr Radiol 1995; 25: S2–S8.

Royston P, Wright EM. How to construct 'normal ranges' for fetal variables. UltrasoundObstetGynecol 1998; 11: 30–8

Royston P. Constructing time-specific reference ranges. Stat Med 1991; 10: 675-690

Siedler D, Filly R. Relative growth of the higher fetal brain structures. J Ultrasound Med 1987; 6: 573–576.

Stranding S (ed): Gray's Anatomy, 39th ed. Edinburgh, Elsevier, 2005.

Tatum WO, Coker SB, Ghobrial M, Abd-Allah S. The open opercular sign: diagnosis and significance. Ann Neurol 1989; 25: 196–199.

Toi A, Lister WS, Fong KW. How early are fetal cerebral sulci visible at prenatal ultrasound and what is the normal pattern of early fetal sulcal development? Ultrasound Obstet Gynecol 2004; 24: 706–715.

Van Der Knaap M.S., Valk J. Classification of congenital abnormalities of the CNS. AJNR Am J Neuroradiol. 1988; 9: 315-326

C) Ancillary project: A role for mesenchymal stem cell-derived exosomes in peripartum neuroregenerative therapy for encephalopathy of prematurity

C 1. Current research in this field

Perinatal brain injury is common in both developed and unprivileged Countries, affecting both term and preterm infants. Depending on the timing of injury and/or delivery, infants need to face with different challenges. In the preterm infant, the spectrum of injury suggests that the underlying pathophysiology is not due to a single lesion but consists of white and grey matter disturbances. Thus, a comprehensive multidimensional assessment of potential contributing factors such as maternal medical history, obstetric antecedents, intrapartum factors (including fetal heart rate monitoring results and issues related to the delivery itself), and placental pathology is recommended. In the term born infants, perinatal insults such as birth asphyxia or perinatal stroke affect 1 to 3 newborns out of 1000. In contrast, in preterm-born infants morbidity and mortality strongly relate to the gestational age. In about 1 % of singletons and 9 % of twin pregnancies, preterm birth before 32 weeks of gestation occurs, with a mortality rate ranging between 7.3 and 21.4 % at 30 days and 9.0 and 22.7 % at 1 year. Additionally, a large number of survivors suffer significant long-term disabilities including cerebral palsy, epilepsy, increased hyperactivity, and developmental disorders. For example, the risk to develop cerebral palsy is 30 times higher in infants born before 33 weeks of gestation compared to term-born infants. Moreover, injury in these infants is frequently exacerbated by fetal inflammation, that preferentially affects cerebral white matter resulting in periventricular leukomalacia and germinal matrix haemorrhage.

Currently, the only intervention known to reduce the burden of perinatal brain injury in the term population is hypothermia. Several large clinical trials confirmed that hypothermia in infants with neonatal hypoxic-ischemic encephalopathy is associated with a significant reduction in death and disability. However, 40–50 % of infants treated with hypothermia still die or develop significant neurological disability. In the preterm population, therapeutic options are lacking as hypothermia is contra-productive. Antenatal magnesium sulfate prior to birth at less than 30 weeks of gestation reduces cerebral palsy and combined cerebral palsy and mortality rate at 2 years of age. However, randomized control trials do not demonstrate long-term neurological benefits.

The principal pathogenic mechanism underlying neurological damage resulting from hypoxic-ischemic brain injury is the deprivation of the glucose and oxygen supply, which causes a primary energy failure and initiates a cascade of biochemical events leading to cell dysfunction and ultimately to cell death. Perinatal brain damage is an evolving process, which is comprised of two phases. A first phase consists of an early energetic failure, where the oxidative energy metabolism of cells decreases and it promotes necrotic death. This is followed by a second phase of cell death, a late energetic failure, which occurs during reperfusion and reoxygenation several hours after

the initial event and lasts for days. The pathophysiology of this late energetic failure initiates a cascade of biochemical events (**Fig. 31**), which involve nitric oxide synthases activation, the production of cytotoxic free radicals, inflammation, membrane dysfunction and apoptosis, among others.

Interestingly, inflammation is increasingly recognized as being a critical contributor to both normal development and injury outcome especially in the immature brain. Maternal infection/inflammation is not only a major risk for preterm birth but is linked to systemic fetal inflammatory response which, in turn, may elicit injury in the fetus. Perinatal inflammation modulates vulnerability to and development of brain injury and influences critical phases of myelination and cortical plasticity. Several studies suggest that inflammation may play a critical role in autism and schizophrenia. Together, brain development, myelination, vascularization, and apoptosis are strongly influenced by inflammatory responses in both physiologic and pathophysiologic conditions. Pivotal regulators of inflammatory responses in the brain are glial cells which orchestrate the release of pro- and anti-inflammatory cytokines. The regulation of the inflammatory responses in the newborn appears to be a link that may explain some of the common features of organ injury in preterm infants. The fetal inflammatory response to certain cues such as lipopolysaccharides (LPS) can be detected not only in the brain but also in remote tissues not directly exposed to LPS such as the spleen, liver, and mediastinal lymph nodes. Protective strategies to counteract the cascades leading to injury should therefore not focus on one organ or system but rather treat perinatally acquired injury globally, in which the immune system plays a key role.

Mesenchymal stem cells possess a regenerative potential. They were shown to modulate innate and adaptive immune responses, to have antiapoptotic effects, to decrease inflammation, and to enhance tissue repair, mostly through the release of paracrine factors. Stem cells are broadly defined as cells with self-renewing and differentiation capacity. Although stem cells derived from embryonic tissue were identified first, the clinical use is limited due to ethical concerns and tumorigenic potential. Clinical and animal stem cell-based studies to prevent or repair perinatally acquired injury have emerged during the recent years with mesenchymal stem cells being particularly promising. These cells are considered somatic stem cells as they originate from stem cell niches such as bone marrow, skin, adipose umbilical cord, and placental tissues. mesenchymal stem cells can be isolated from placental membranes and tissues, amniotic fluid, umbilical cord blood, and the umbilical cord connective tissues (Wharton's jelly). Although all of these cells are mesenchymal stem cells, all these subtypes are different relatively to clinical use, time of application, application route, availability, and ethical aspects. Mesenchymal stem cells-based therapies are an attractive strategy since the pathophysiology of perinatally acquired injury is heterogeneous and mesenchymal stem cells have the capacity to adapt to the microenvironment of injured organs. The strategy may be either or both replacement/restoration of lost tissue and/or protection/salvage of injured cells. In term infants at risk for hypoxic-ischemic injury or neonatal ischemic stroke, mesenchymal stem cells could exert a neuroprotective effect starting at the acute phase of injury. In these cases, the timing and presentation of the acute injury are usually well defined. Mesenchymal stem cells could provide trophic support and/or amelioration of the

inflammatory responses, leading to repair or reduced cell death. However, the different cell types, transplantation routes, and the timing need to be accounted for. Given the gold standard therapy of hypothermia for this kind of injury, mesenchymal stem cells have to proof additive/synergistic effects in order to be considered. In contrast, in the preterm population, the timing of the injury is often unclear and the pathophysiology is more complex. The clinical diagnosis of infants at risk is challenging as symptoms such as cerebral palsy are diagnosed in early childhood years. Thus, the injury may be considered chronic as extensive atrophy and gliosis of the white matter tract or dysfunction of lung architecture are present. Mesenchymal stem cells could modulate not only the inflammatory response after delivery but also the degree and magnitude of the injured white matter and epithelial cells as well. However, many questions such as altered pattern of growth factors and intercellular matrix proteins that could affect proliferation or differentiation of the desired cell types need to be addressed first.

The approach of mesenchymal stem cells as a therapy for perinatal injury is based on several crucial properties of mesenchymal stem cells, including delivery of the cells "homing" to the site of injury. Migration and homing to the tissue of injury is influenced by multiple factors including age, passage, and number of cells; culture conditions; and delivery method. The apparent migration and homing abilities of mesenchymal stem cells without tumorigenic potential were described by several groups and in different disease models. Experimental studies identified chemokines as major molecules responsible for cell homing with chemokine receptors CXCR3, CXCR4, and CXCR6 being particularly important. Further secretion of factors such as SDF-1α, which is a CXCR4 ligand, promotes migration of mesenchymal stem cells to the injury site. Interestingly, the phenotype of mesenchymal stem cells is an important criterion as well. Currently, mesenchymal stem cells characterization is based on a set of minimal criteria and they display a cell surface repertoire and gene expression pattern which differ among mesenchymal stem cells from various tissues of origin and culture conditions used. For example, Wharton's jelly-mesenchymal stem cells express a special assortment of cell surface markers, that make them able to differentiate more efficiently into neural progenitors compared to other subtypes of mesenchymal stem cells. In addition, the underlying clinical condition may also affect the phenotype of mesenchymal stem cells. Wharton's jelly – mesenchymal stem cell derived from umbilical cords collected after preeclamptic pregnancies seem to be more committed to neuroglial differentiation compared to cords from uncomplicated pregnancies.

While mesenchymal stem cells have a proven restorative capacity in response to injury cues, the question of potential protective mechanisms remains unclear. Most of the available data comes from adult neurodegenerative and lung diseases or in vitro studies. Studies identified the induction of cytokines, interleukins, and trophic factors predominately involved in neurogenesis, angiogenesis, hematopoiesis, and cardiovascular regeneration being crucial for the mostly paracrine effects. For example, Wharton's jelly- mesenchymal stem cells secretome triggers neuronal survival and differentiation in vitro and in vivo. Secreted factors such as VEGF-A, angiopoietin-1, FGF-I, HGF, FGF-II, BDNF, GDNF, and PDGF-AB were identified. Importantly, mesenchymal stem cells' secretome alters both adaptive and innate immune responses: inhibit autoreactive T cell responses in animal models of multiple

sclerosis and hypoxic-ischemic brain injury as well as inhibit B cell proliferation, neutrophil and monocyte function, and NK toxicity. Although these modulatory effects are partially understood, direct cell-to-cell contact and soluble factors are relevant. Additionally, mesenchymal stem cells effects expand beyond constitutive immune modulatory properties with the release of cytokines and growth factors such as VEGF, TGF-β1, TNF-α, IL-1, IL-6, and IFN-γ.

Mesenchymal stem cells' multipotency and self-renewal properties make them valid candidates for providing cell regeneration/replacement. Although, this strategy for repair carries risks such as tumorigenic potential, mesenchymal stem cells were successfully differentiated into various types of cells including cardiomyocytes, myocytes, and epidermal and endothelial cells. Although this line of investigation is particularly intriguing, mesenchymal stem cells' potential to replace injured cells is not proven and is a matter of constant debate. For example, intravenously injected mesenchymal stem cells improve myocardial infarction without permanent replacement of injured cells. In the lung, mesenchymal stem cells embolize causing endothelial damage and are cleared in a matter of hours. Taken together, the mesenchymal stem cells' low rate of in vivo engraftment and differentiation suggests that transplanted cells affect tissue injury and repair through paracrine factors. Whether the factors released by the mesenchymal stem cells or the cells themselves are more promising for the therapy of lung and brain injury in the newborn still remains an open question.

The translation "*from bench to bedside*" requires the most efficacious and safest approach. Thus, the question of cell based versus cell-free therapy needs to be addressed.

Given that the mesenchymal stem cells' therapeutic potential has been shown to be largely triggered via paracrine effects and not differentiation, recent studies focus on extracellular vehicles (EV). These are all types of vehicles present in the extracellular space, including shedding vesicles, apoptotic bodies, and exosomes. Exosomes (40–100 nm in diameter) are secreted by cells in a regulated fashion, possess the ability to transfer proteins and functional genetic materials such as messenger RNA (mRNA) and microRNAs, and are involved in cell-to-cell signalling and regulation. MicroRNAs are 17-24 nucleotides of small RNAs that do not code for proteins, but have effects on transcriptional regulation, chromatin structure, translation and posttranslational processing. They act by the repression or activation of mRNA transcripts of protein-coding genes via base-pairing with complementary sequences. miRNAs are essential for neuronal development, including neuronal stem/progenitor cell renewal, proliferation and differentiation, neuritogenesis and outgrowth, synapse formation and plasticity. Several miRNAs abundant in the brain have been identified to regulate neural progenitor cells development. Some promote neural progenitor cells self-renewal and block neuronal differentiation and maturation (miR-134, miR-137, miR-184), while others block self-renewal and promote the development into neurons (let-7, miR-9, miR-124). The neural stem cells' multistage differentiation into myelinating oligodendrocytes is controlled by various miRNAs. MicroRNAs have also been recognized as modulators of disease states like neuroinflammation or hypoxia-

ischemia. The conditional knockdown of the miR-processing enzyme Dicer in oligodendrocyte progenitor cells (OPC) in a perinatal hypoxia-ischemia brain lesion mouse model abolished the hypoxia-ischemia related increase of miR-138 and miR-338 and rescued the animals from white matter loss. Perinatal hypoxia-ischemia encephalopathy resulted in a decrease of miR-374a in the cord blood of affected neonates. A number of other miRNAs were differentially expressed after neonatal hypoxia-ischemia brain injury in rat models. miR-139-5p is downregulated after neonatal hypoxia-ischemia, leading to the promotion of neuronal apoptosis.

Not surprisingly, mesenchymal stem cells -derived EV are contributing to tissue repair in brain injury including stroke and Alzheimer's disease. The cell-free approach is very promising; however, it is still in its infancy. In fact, stem cells do not just secrete growth factors and/or cytokines but encourage the growth and even supplement (host) cells. Importantly, the stem cells' potential of immunomodulation and protection after injury seems to depend on the bidirectional communication between the injured host cells and the graft via the exchange of specific information.

As a result of their remarkable regenerative potential, mesenchymal stem cells are ideal candidates for clinical cell therapy. Mesenchymal stem cells are easily available, have a good safety profile and homing capacity, and importantly are relatively immune-privileged, allowing allogeneic transplantation. Not surprisingly, mesenchymal stem cells have been tested in clinical trials in several neurodegenerative diseases such as stroke, amyotrophic lateral sclerosis, multiple sclerosis, and spinal cord injury. Several clinical trials indicated no serious side effects or dose-limiting toxicity in acute respiratory distress syndrome and chronic obstructive pulmonary disease. Also safety and feasibility trials for cerebral palsy were successful. A recent double-blind randomized control study used allogeneic umbilical cord blood, in combination with erythropoietin, in children diagnosed with cerebral palsy showing motor and cognitive benefits. In contrast to previous studies, a large safety study used autologous umbilical cord blood directly after birth for infants at risk for hypoxic-ischemic encephalopathy. This approach differs significantly from previous studies as it aims mainly to prevent and not to replace affected cells. Cells were transplanted directly after birth and in combination with hypothermia. Authors concluded that the collection, preparation, and infusion of fresh autologous umbilical cord blood cells for use in infants with hypoxic-ischemic encephalopathy are feasible. Several other clinical trials for neonatal brain injury are currently listed as in progress or completed, and more results should become available in the near future (ClinicalTrials.gov Identifiers: NCT01832454, NCT01962233, NCT01988584, NCT01207869).

C 2. Previous results of our group

At the Laboratory of Prenatal Medicine of the University of Bern, Switzerland, mesenchymal stem cells were isolated from human placental tissues and characterized. Only in-vitro experiments are here reported. These cells showed the typical mesenchymal stem cells phenotype and differentiated into chondroblasts, osteoblasts, adipocytes, myocytes and neural lineages, including neurons and oligodendrocytes. These cells were also grown and differentiated on a chorion scaffold to use as a potential composite osteogenic graft for novel treatments for peripartal bone regeneration. Methods have been established methods for the isolation and expansion of mesenchymal stem cells from umbilical cord connective tissue (Wharton's jelly). Isolated cells were analysed for the cell surface expression of mesenchymal stem cells markers and absence of hematopoietic and major histocompatibility complex markers. Wharton's jelly- mesenchymal stem cells were differentiated from term and preterm births into rat hippocampal neuronal progenitor cells (rNPC) and into OPC.

To assess the neuroregenerative potential of Wharton's jelly- mesenchymal stem cells in vitro, co-cultures of these cells and rNPC were established. After 96h of co-colture, total mRNA and proteins of markers of astrocytes and oligodentrocytes (Gfap and Mbp, respectively) were significant increased. To confirm the paracrine effects of Wharton's jelly- mesenchymal stem cells on rNPC, conditioned medium from these cells was collected after 48h and cellular debris were removed; rNPC were cultured in serum-free medium for 24 h. Culture of rNSC with Wharton's jelly- mesenchymal stem cells - conditioned medium for 96h resulted in a marked increase of Gfap at the mRNA and the protein (flow cytometry, fluorescence-activated cell sorting, immunocytochemistry) level. Then, the expression of neurotrophic factors was analysed using a Human Neurotrophins and Receptors protein chain reaction (PCR) array in neurospheres induced from Wharton's jelly- mesenchymal stem cells. Neural differentiation resulted in the upregulation of neurotrophic factors including GDNF, PSPN, FRS3, UCN, MEF2C and TGFB1 and the downregulation of NTF3, BDNF and FOS. Wharton's jelly- mesenchymal stem cells released IL-6 and BDNF. The secretome of cultured Wharton's jelly- mesenchymal stem cells from term and pre-term birth was analysed using mass spectrometry.

Subsequently, exosomes from Wharton's jelly- mesenchymal stem cells were isolated using a serial (ultra) centrifugation protocol. The final pellet was re-suspended in phosphate-buffered saline (PBS) and either directly used for protein and RNA extraction or frozen at -80°C. The protein yield was determined by a bichinchoninic acid (BCA) assay. Exo-Check™ exosome antibody array was used to prove exosome identity. The miRNA cargo of the exosomes was quantified using the Human Neurological Development & Disease miScript miRNA PCR Array (MIHS-107Z). The miRNAs most abundantly expressed in the exosomes all have their role in neuroprotection (in the order of expression levels): miR-328-3p shows reduced expression upon glioma progression, miR-22-3p has a neuroprotective in cerebral ischemia-reperfusion injury, miR-489-3p targets myeloid differentiation primary

response gene 88 (Myd88) and Akt79 and maintains stem cell quiescence, miR-125b-5p was downregulated after hypoxic-hyschemic brain damage in neonatal rats and miR-409-3p in the Rett syndrome, miR-29a-3p has a role in neuronal survival (miR-29), is enriched in mature neurons and reduces neuronal vulnerability to ischemia and miR-29c-3p is involved in neuroprotection via the PKA/CREP pathway and is correlated with BDNF expression. Other highly expressed miRNAs included miR-24-3p, miR-148b-3p, miR-27a-3p, miR-26b-5b, miR-191-5p, miR-320a, miR-15b-5p, let-7i-5p, miR-7-5p, miR-19b-3p, miTR134-5p and miR-433-3p.

Taken together, these first results showed that the Wharton's jelly- mesenchymal stem cells - derived exosomes have the potential to serve as a neuroprotective therapeutic agent.

C 3. Current ongoing results

To verify if the Wharton's jelly- mesenchymal stem cells - derived exosomes might be used to deliver their cargo to neural cells in the brain, we used an in vitro co-culture model. The murine neuroblast cell line N2a (CCL-131; ATCC) as well as rNPC was seeded at 37'500 cells/cm^2 and grown overnight (DMEM, 10% FBS, 1 mM L-glutamine, 1% penicillin-streptomycin; Thermo Fisher Scientific). Exosomes were diluted in PBS (3 µg/µl), labelled with Dil (2 µg/ml, 37°C 5min, 4°C 15min, Thermo Fisher Scientific), washed with PBS and ultracentrifuged (100'000xg, 4°C) to remove excess Dil. The stained exosomes were resuspended in fresh PBS and added to N2a cultures. For immunocytochemistry (ICC) analysis, cell of Wharton's jelly- mesenchymal stem cells - derived exosomes after co-culture with an N2a/rNPC cell line were fixed in methanol and cell nuclei counterstained with 4',6-diamidino-2-phenylindole (DAPI). Analysis was done by conventional fluorescence and confocal microscopy (3D visualization by Imaris software). Furthermore, exosomal RNA fluorescently labelled with Exo-Red was detected in the cytoplasma of N2a cells and GFP-expressing hippocampal rNPC after 2 hours of co-culture (**Fig. 32**). We confirmed the uptake of Wharton's jelly- mesenchymal stem cells - derived exosomes in N2a cells as a model for neural progenitors.

To assess the Wharton's jelly- mesenchymal stem cells - derived exosomes's effect on specific neuroprotective outcomes, we tested their influence on the proliferation, differentiation and activation in in vitro conditions mimicking neonatal brain injury. At first, brain cell lines cultured in normoxia or with an oxygen glucose deprivation-reperfusion (OGD-R) model were compared. Secondly, Wharton's jelly- mesenchymal stem cells - derived exosomes were added to the cell lines on the onset of OGD (immediately before or later, see below) and compared with untreated OGD-stressed cells. The OGD-R model has been set up in our laboratory according to published protocols as follows: cells are expanded in their respective media. After reaching ~80% confluency (usually after 24h), the medium is replaced by glucose-free medium and the cells are incubated in hypoxia (1% O2 in a 95%N2/5% CO^2 gas mixture) for 2, 4, 6, 8 and 24h, respectively. Thereafter, the medium is replaced with standard expansion medium and cell cultures returned to normoxia. According to this protocol, both the first and the second phase of the hypoxic-ischemic brain injury can be mimicked. Exosomes are given at different time points, allowing a prevention – and – treatment model: 24h before OGD, 1h before OGD, as well as immediately after the OGD. Furthermore, exosomes are given at different concentrations: 0.1µg/ml and 1 µg/ml. Cell collection is set at two different time points: 24h after OGD and 48h after OGD (**Fig. 33**).

We used well established cell lines as models for neural cell lineages in the neonatal brain: for neuronal cells, we used neuroblastoma cell line N2a (CCL-131; ATCC) and rNPC. N2a cells were cultured as we described before. Differentiation of N2a cells was induced in serum-free medium containing 1 µM retinoic acid for 24h. Cell differentiation stages was monitored by immunocytochemical detection (ICC) of doublecortin (Dcx, immature

neurons) and NeuN or Map2 (mature neurons) and expressed as the amount of positive vs total number of cells. Cell viability, necrosis and apoptosis, as well the expression of markers of inflammation/apoptosis at RNA and protein level were the outcome measures for cellular damage. Cell viability was measured using the PrestoBlue® Cell Viability Reagent (Thermo Fisher Scientific), necrosis by measuring the LDH release (Colorimetric LDH Assay Kit; Abcam) and apoptosis with a terminal deoxynucleotidyl transferase dUTP nick end labeling (TUNEL) assay (Fluorescein In Situ Cell Death Detection Kit; Roche Diagnostics). Expression of markers of inflammation/apoptosis at RNA level was measured by real-time PCR, while expression of markers of inflammation/apoptosis at protein level was measured by Western Blot analysis.

We observed that Wharton's jelly- mesenchymal stem cells - derived exosomes protected N2a cells subjected to OGD-R injury by reducing apoptosis and increasing cell viability (**Fig. 34**). These protective effects were associated with the reduction of the expression of death-related markers at the level of RNA expression, such as cleaved caspase-3, as well as of inflammatory markers such as TLR-4 in treated compared with not-treated cells (**Fig. 35**). Wharton's jelly- mesenchymal stem cells - derived exosomes also enhanced the expression of some miRNAs involved in neuronal differentiation and in the modulation of the inflammatory response, such as Let 7a in treated - cells compared with not-treated cells (**Fig. 36**). All these effects seem to be dose- and time- dependent, being the highest concentration of exosomes, given 24h hours before OGD, the condition associated with the mostly significant changes of our markers (**Fig. 35-36**).

Taken together, our findings suggest that Wharton's jelly- mesenchymal stem cells - derived exosomes are able to boost neuroprotection and neuroregeneration in hypoxic-ischemic perinatal brain injury.

C 4. Next steps

Our next aim we will be to identify all the microRNAs responsible for the effect and identify the pathways involved in the mechanisms of exosome therapy. Candidates will be the 10 most abundantly expressed microRNA. Antisense oligonucleotides (antimiR) will be designed to inhibit the activity of the miRNAs in a loss-of-function study using the OGD-R model. Cell lines responsive to OGD-R will be plated in 24-well plates, grown to 60% confluency and transfected with miRNA inhibitors (miRIDIAN microRNA Hairpin Inhibitors, 2/10/50 nM; Dharmacon, GE Healthcare Life Sciences) using Lipofectamine 2000 (Thermo Fisher Sciences). The assays will be validated using positive (miR-16) and non-targeting negative (cel-miR-67; both Dharmacon) controls. OGD-R will be initiated 48h after transfection and outcomes determined as outlined previously. To confirm results of the loss-of-function study, a gain-of-function assay will be carried out for selected miRNA. The cell lines will be transfected with double-stranded RNA oligonucleotides designed to mimic the function of endogenous, mature microRNAs (miRIDIAN microRNA Mimics, Dharmacon). Positive (targeting endogenous Aldolase A) and negative (cel-miR-67 mimic, both Dharmacon) control mimics will be used to test for specificity.

Results on differential miRNA expression will be collected. miRNAs that have an impact on neuroprotective outcomes after OGD-R will be used to identify overlapping miRNA targets. Common putative miRNA targets will be identified in silico by screening miRNA target databases using the miRror 2.0 suite (http://www.mirrorsuite.cs.huji.ac.il.). Protein and reactome/pathway databases (Human Protein Reference Database: http://www.hprd.org/; REACTOME: http://www.reactome.org/; Kyoto Encyclopedia of Genes and Genomes, KEGG: http://www.genome.jp/kegg/; Pathway Interaction Database: http://pid.nci.nih.gov/) will then be screened for these putative targets to identify the mechanisms of exosome therapy. As an example, using the most abundantly expressed miRNA cargo of our WJ-MSC as an input, miRror 2.0 renders the BCL2-antagonist/killer 1 (BAK1) gene as a predicted target. BAK1 belongs to the BCL2 protein family and induces the release of cytochrome c and apoptosis (NCBI Gene ID 578). Therefore, WJ-MSC exosomes might be neuroprotective through the inactivation of BAK1-induced apoptosis via their miRNA cargo.

C 5. References

Aggarwal S, Pittenger MF. Human mesenchymal stem cells modulate allogeneic immune cell responses. Blood 2005; 105(4):1815–1822.

Bai L, Lennon DP, Caplan AI, et al. Hepatocyte growth factor mediates mesenchymal stem cell-induced recovery in multiple sclerosis models. Nat Neurosci 2012; 15(6):862–870.

Balasubramanian S, Thej C, Venugopal P, et al. Higher propensity of Wharton's jelly derived mesenchymal stromal cells towards neuronal lineage in comparison to those derived from adipose and bone marrow. Cell Biol Int 2013; 37(5):507–515.

Bianco P, Cao X, Frenette PS, et al. The meaning, the sense and the significance: translating the science of mesenchymal stem cells into medicine. Nat Med 2013; 19(1):35–42.

Brooke G, Tong H, Levesque JP, Atkinson K. Molecular trafficking mechanisms of multipotent mesenchymal stem cells derived from human bone marrow and placenta. Stem Cells Dev 2008; 17(5):929–940.

Brown GC, Neher JJ. Inflammatory neurodegeneration and mechanisms of microglial killing of neurons. Mol Neurobiol 2010 (2-3):242–247.

Bruno S, Deregibus MC, Camussi G. The secretome of mesenchymal stromal cells: role of extracellular vesicles in immunomodulation. Immunol Lett. 2015

Buntinx M, Moreels M, Vandenabeele F, et al. Cytokine-induced cell death in human oligodendroglial cell lines: I. Synergistic effects of IFN-gamma and TNFalpha on apoptosis. J Neurosci Res 2004; 76(6):834–845.

Cerio FC., Lara-Celador I., Alvarez A. et al. Neuroprotective therapies after perinatal hypoxic-ischemic brain injury. Brain Sci. 2013; Mar 5;3(1):191-214

Connick P, Kolappan M, Crawley C, et al. Autologous mesenchymal stem cells for the treatment of secondary progressive multiple sclerosis: an open-label phase 2a proof-of concept study. Lancet Neurol 2012; 11(2):150–156.

Constantin G, Marconi S, Rossi B, et al. Adipose-derived mesenchymal stem cells ameliorate chronic experimental autoimmune encephalomyelitis. Stem Cells 2009; 27(10):2624–2635.

Cotten CM, Murtha AP, Goldberg RN, et al. Feasibility of autologous cord blood cells for infants with hypoxic-ischemic encephalopathy. J Pediatr 2014; 164(5):973–979.

De Coppi P, Bartsch G Jr, Siddiqui MM et al. Isolation of amniotic stem cell lines with potential for therapy. Nat Biotechnol 2007; 25(1):100–106.

Di Nicola M, Carlo-Stella C, Magni M, et al. Human bone marrow stromal cells suppress T-lymphocyte proliferation induced by cellular or nonspecific mitogenic stimuli. Blood 2002; 99(10):3838–3843

Diez-Tejedor E, Gutierrez-Fernandez M, et al. Reparative therapy for acute ischemic stroke with allogeneic mesenchymal stem cells from adipose tissue: a safety assessment: a phase II randomized, double-blind, placebo-controlled, single-center, pilot clinical trial. J Stroke Cerebrovasc Dis 2014; 23(10):2694–2700

Dominici M, Le Blanc K, Mueller I, et al. Minimal criteria for defining multipotent mesenchymal stromal cells. The International Society for Cellular Therapy position statement. Cytotherapy 2006; 8(4):315–317.

Donega V, Nijboer CH, van Velthoven CT, et al. Assessment of long-term safety and efficacy of intranasal mesenchymal stem cell treatment for neonatal brain injury in the mouse. Pediatric research 2015

Doyle LW, Anderson PJ, Haslam R, Lee KJ, Crowther C, Australasian Collaborative Trial of Magnesium Sulphate Study G. School-age outcomes of very preterm infants after antenatal treatment with magnesium sulfate vs placebo. JAMA 2014; 312(11):1105–1113.

Dreyer JL. New insights into the roles of microRNAs in drug addiction and neuroplasticity. Genome Med 2010; 2(12):92.

Duffy MM, Ritter T, Ceredig R, Griffin MD. Mesenchymal stem cell effects on T-cell effector pathways. Stem Cell Res Ther 2011; 2(4):34. doi:10.1186/scrt75

Edwards AD, Brocklehurst P, Gunn AJ, et al. Neurological outcomes at 18 months of age after moderate hypothermia for perinatal hypoxic ischaemic encephalopathy: synthesis and meta-analysis of trial data. BMJ 2010340:c363.

Eklind S, Mallard C, Leverin AL, et al. Bacterial endotoxin sensitizes the immature brain to hypoxic-ischaemic injury. Eur J Neurosci 2001; 13(6):1101–1106

Erices A, Conget P, Minguell JJ. Mesenchymal progenitor cells in human umbilical cord blood. Br J Haematol 2000; 109(1):235–242

Favrais G, van de Looij Y, Fleiss B, et al. Systemic inflammation disrupts the developmental program of white matter. Ann Neurol 2011; 70(4):550–565.

Fong CY, Chak LL, Biswas A, et al. Human Wharton's jelly stem cells have unique transcriptome profiles compared to human embryonic stem cells and other mesenchymal stem cells. Stem Cell Rev 2011; 7(1):1–16.

Franquesa M, Hoogduijn MJ, Bestard O, Grinyo JM. Immunomodulatory effect of mesenchymal stem cells on B cells. Front Immunol 2012; 3:212.

Gao LR, Zhang NK, Ding QA et al. Common expression of stemness molecular markers and early cardiac transcription factors in human Wharton's jelly derived mesenchymal stem cells and embryonic stem cells. Cell Transplant 2013; 22(10):1883–1900.

Gerdoni E, Gallo B, Casazza S, et al. Mesenchymal stem cells effectively modulate pathogenic immune response in experimental autoimmune encephalomyelitis. Ann Neurol 200761(3):219–227.

Glenn JD, Whartenby KA. Mesenchymal stem cells: emerging mechanisms of immunomodulation and therapy. World J Stem Cells 2014; 6(5): 526–539.

Graham EM, Ruis KA, Hartman AL, Northington FJ, Fox HE. A systematic review of the role of intrapartum hypoxia-ischemia in the causation of neonatal encephalopathy. Am J Obstet Gynecol 2008; 199(6):587–595.

Gu W, Zhang F, Xue Q, et al. Transplantation of bone marrow mesenchymal stem cells reduces lesion volume and induces axonal regrowth of injured spinal cord. Neuropathology 2010; 30(3):205–217.

Hagberg H, Mallard C, Ferriero DM, et al. The role of inflammation in perinatal brain injury. Nat Rev Neurol 2015; 11(4):192–208.

Higgins RD, Raju T, Edwards AD, et al. Hypothermia and other treatment options for neonatal encephalopathy: an executive summary of the Eunice Kennedy Shriver NICHD workshop. J Pediatr 2011; 159(5):851–858.

Honmou O, Houkin K, Matsunaga T, et al. Intravenous administration of auto serum-expanded autologous mesenchymal stem cells in stroke. Brain 2011; 134(Pt 6):1790–1807.

Hsieh JY, Wang HW, Chang SJ, et al. Mesenchymal stem cells from human umbilical cord express preferentially secreted factors related to neuroprotection, neurogenesis, and angiogenesis. PLoS ONE 2013; 8(8):e72604.

Igura K, Zhang X, Takahashi K, et al.Isolation and characterization of mesenchymal progenitor cells from chorionic villi of human placenta. Cytotherapy 2004; 6(6):543–553

In 't Anker PS, Scherjon SA, Kleijburg-van der Keur C et al. Amniotic fluid as a novel source of mesenchymal stem cells for therapeutic transplantation. Blood 2003; 102(4):1548–1549.

In 't Anker PS, Scherjon SA, Kleijburg-van der Keur C, et al. Isolation of mesenchymal stem cells of fetal or maternal origin from human placenta. Stem Cells 2004; 22(7):1338–1345.

Ivanova-Todorova E, Bochev I, Mourdjeva M, et al. Adipose tissuederived mesenchymal stem cells are more potent suppressors of dendritic cells differentiation compared to bone marrow-derived mesenchymal stem cells. Immunol Lett 2009; 126(1-2):37–42.

Jaerve A, Muller HW. Chemokines in CNS injury and repair. Cell Tissue Res 2012; 349(1):229–248.

Jellema RK, Wolfs TG, Lima Passos V, et al. Mesenchymal stem cells induce T-cell tolerance and protect the preterm brain after global hypoxia-ischemia. PLoS ONE 2013; 8(8):e73031.

Joerger-Messerli M, Bruhlmann E, Bessire A, et al. Preeclampsia enhances neuroglial marker expression in umbilical cord Wharton's jelly-derived mesenchymal stem cells. J Matern Fetal Neonatal Med 2015; 28(4):464–469.

Katsuda T, Kosaka N, Takeshita F, Ochiya T. The therapeutic potential of mesenchymal stem cell-derived extracellular vesicles. Proteomics 2013; 13(10- 11):1637–1653.

Katsuda T, Tsuchiya R, Kosaka N, et al. Human adipose tissue-derived mesenchymal stem cells secrete functional neprilysin-bound exosomes. Sci Rep 2013; 3:1197.

Kim YJ, Yu JM, Joo HJ, et al. Role of CD9 in proliferation and proangiogenic action of human adipose-derived mesenchymal stem cells. Pflugers Arch 2007; 455(2):283–296.

Kuypers E, Willems MG, Jellema RK, et al. Responses of the spleen to intraamniotic lipopolysaccharide exposure in fetal sheep. Pediatr Res 2015; 77(1-1):29–35.

Lee JS, Hong JM, Moon GJ, et al. A long-term follow-up study of intravenous autologous mesenchymal stem cell transplantation in patients with ischemic stroke. Stem Cells 2010; 28(6):1099–1106.

Lee RH, Pulin AA, Seo MJ, et al. Intravenous hMSCs improve myocardial infarction in mice because cells embolized in lung are activated to secrete the anti-inflammatory protein TSG-6. Cell Stem Cell 2009; 5(1):54–63

Lee YH, Choi KV, Moon JH, et al. Safety and feasibility of countering neurological impairment by intravenous administration of autologous cord blood in cerebral palsy. J Transl Med 2012; 10: 58.

Leite C, Silva NT, Mendes S, et al. Differentiation of human umbilical cord matrix mesenchymal stem cells into neural-like progenitor cells and maturation into an oligodendroglial-like lineage. PLoS ONE 2014; 9(10):e111059.

Li D, Chai J, Shen C, et al. Human umbilical cord-derived mesenchymal stem cells differentiate into epidermal-like cells using a novel co-culture technique. Cytotechnology 2014; 66(4):699–708.

Llufriu S, Sepulveda M, Blanco Y, et al. Randomized placebocontrolled phase II trial of autologous mesenchymal stem cells in multiple sclerosis. PLoS ONE 2014; 9(12):e113936.

Ma L, Feng XY, Cui BL, et al. Human umbilical cord Wharton's Jelly-derived mesenchymal stem cells differentiation into nerve-like cells. Chin Med J (Engl) 2005; 118(23):1987–1993

Mancias-Guerra C, Marroquin-Escamilla AR, Gonzalez-Llano O, et al. Safety and tolerability of intrathecal delivery of autologous bone marrow nucleated cells in children with cerebral palsy: an open-label phase I trial. Cytotherapy 2014; 16(6):810–820.

Maneenil G, Kemp MW, Kannan PS, et al. Oral, nasal and pharyngeal exposure to lipopolysaccharide causes a fetal inflammatory response in sheep. PLoS ONE 2015; 10(3):e0119281.

Mariotti E, Mirabelli P, Abate G, et al. Comparative characteristics of mesenchymal stem cells from human bone marrow and placenta: CD10, CD49d, and CD56 make a difference. Stem Cells Dev 2008; 17(6):1039–1041.

Martinez-Lopez DG, Funderburg NT, Cerissi A, et al. Lipopolysaccharide and soluble CD14 in cord blood plasma are associated with prematurity and chorioamnionitis. Pediatr Res 2014; 75(1-1):67–74.

Mazzini L, Ferrero I, Luparello V, et al. Mesenchymal stem cell transplantation in amyotrophic lateral sclerosis: a phase I clinical trial. Exp Neurol 2010; 223(1):229–237.

Messerli M, Wagner A, Sager R, et al. Stem cells from umbilical cord Wharton's jelly from preterm birth have neuroglial differentiation potential. Reprod Sci 2013 (12):1455–1464.

Meyer U, Feldon J, Dammann O. Schizophrenia and autism: both shared and disorder-specific pathogenesis via perinatal inflammation? Pediatr Res 2011; 69(5 Pt 2):26R–33R.

Min K, Song J, Kang JY, et al. Umbilical cord blood therapy potentiated with erythropoietin for children with cerebral palsy: a double-blind, randomized, placebo-controlled trial. Stem Cells 2013; 31(3):581–591.

Moorefield EC, McKee EE, Solchaga L, et al. Cloned, CD117 selected human amniotic fluid stem cells are capable of modulating the immune response. PLoS ONE 2011; 6(10):e26535.

Mueller M., Wolfs TGA., Schoeberlein A., et al. Mesenchymal stem/stromal cells—a key mediator for regeneration after perinatal morbidity? Molecular and Cellular Pediatrics (2016) 3:6

Nartprayut K, U-Pratya Y, Kheolamai P, et al. Cardiomyocyte differentiation of perinatally derived mesenchymal stem cells. Mol Med Rep 2013; 7(5):1465–1469.

Numerato D, Fattore G, Tediosi F, et al. Mortality and length of stay of very low birth weight and very preterm infants: a EuroHOPE study. PLoS ONE 2015; 10(6):e013168

Pal R, Venkataramana NK, Bansal A, et al. Ex vivo-expanded autologous bone marrow-derived mesenchymal stromal cells in human spinal cord injury/ paraplegia: a pilot clinical study. Cytotherapy 2009; 11(7):897–911.

Park WS, Sung SI, Ahn SY, et al. Hypothermia augments neuroprotective activity of mesenchymal stem cells for neonatal hypoxic-ischemic encephalopathy. PLoS ONE 2015; 10(3): e0120893.

Phillips AW, Johnston MV, Fatemi A. The potential for cell-based therapy in perinatal brain injuries. Transl Stroke Res 2013; 4(2):137–148.

Pires AO, Neves-Carvalho A, Sousa N, Salgado AJ. The secretome of bone marrow and Wharton's jelly derived mesenchymal stem cells induces differentiation and neurite outgrowth in SH-SY5Y cells. Stem Cells Int 2014: 438352.

Pleasure D, Soulika A, Singh SK, et al. Inflammation in white matter: clinical and pathophysiological aspects. Ment Retard Dev Disabil Res Rev 2006; 12(2):141–146.

Ploemacher WJCRaRE. Primary murine MSC show highly efficient homing to the bone marrow but lose homing ability following culture. Leukemia 2003; 17(1):160–170

Prasad VK, Kurtzberg J. Umbilical cord blood transplantation for nonmalignant diseases. Bone Marrow Transplant 2009; 44(10):643–651.

Prasanna SJ, Gopalakrishnan D, Shankar SR, Vasandan AB. Proinflammatory cytokines, IFNgamma and TNFalpha, influence immune properties of human bone marrow and Wharton's jelly mesenchymal stem cells differentially. PLoS ONE 2010; 5(2):e9016.

Raffaghello L, Bianchi G, Bertolotto M. et al. Human mesenchymal stem cells inhibit neutrophil apoptosis: a model for neutrophil preservation in the bone marrow niche. Stem Cells 2008; 26(1):151–162.

Rahmat Z, Jose S, Ramasamy R, Vidyadaran S. Reciprocal interactions of mouse bone marrow-derived mesenchymal stem cells and BV2 microglia after lipopolysaccharide stimulation. Stem Cell Res Ther 2013; 4(1):12.

Ramalho-Santos M, Willenbring H. On the origin of the term "stem cell". Cell Stem Cell 1(1):35–38. Caplan AI (1991) Mesenchymal stem cells. J Orthop Res 2007; 9(5):641–650.

Ribeiro CA, Fraga JS, Graos M, et al. The secretome of stem cells isolated from the adipose tissue and Wharton's jelly acts differently on central nervous system derived cell populations. Stem Cell Res Ther 2012; 3(3):18.

Ribeiro CA, Salgado AJ, Fraga JS, et al. The secretome of bone marrow mesenchymal stem cells-conditioned media varies with time and drives a distinct effect on mature neurons and glial cells (primary cultures). J Tissue Eng Regen Med 2011; 5(8):668–672.

Robertson CM, Watt MJ, Yasui Y. Changes in the prevalence of cerebral palsy for children born very prematurely within a population-based program over 30 years. JAMA 2007; 297(24):2733–2740.

Roobrouck VD, Vanuytsel K, Verfaillie CM. Concise review: culture mediated changes in fate and/or potency of stem cells. Stem Cells 2011; 29(4): 583–589.

Schaaf JM, Mol BW, Abu-Hanna A, Ravelli AC. Trends in preterm birth: singleton and multiple pregnancies in the Netherlands, 2000-2007. BJOG 2011; 118(10):1196–1204.

Schoeberlein A, Mueller M, Reinhart U, et al. () Homing of placenta-derived mesenchymal stem cells after perinatal intracerebral transplantation in a rat model. Am J Obstet Gynecol 2011; 205(3): 277.

Shrivastava K, Chertoff M, Llovera G, et al. Short and long-term analysis and comparison of neurodegeneration and inflammatory cell response in the ipsilateral and contralateral hemisphere of the neonatal mouse brain after hypoxia/ischemia. Neurol Res Int 2012:781512.

Sofroniew MV. Astrocyte barriers to neurotoxic inflammation. Nat Rev Neurosci 2015; 16(5):249–263.

Sohni A, Verfaillie CM. Mesenchymal stem cells migration homing and tracking. Stem Cells Int 2013:130763.

Spaggiari GM, Capobianco A, Abdelrazik H et al. Mesenchymal stem cells inhibit natural killer-cell proliferation, cytotoxicity, and cytokine production: role of indoleamine 2,3-dioxygenase and prostaglandin E2. Blood 2008; 111(3):1327–1333.

Strackx E, Sparnaaij MA, Vlassaks E, et al. Lipopolysaccharide-induced chorioamnionitis causes acute inflammatory changes in the ovine central nervous system. CNS Neurol Disord Drug Targets 2015; 14(1):77–84

Subramanian A, Fong CY, Biswas A, Bongso A. Comparative characterization of cells from the various compartments of the human umbilical cord shows that the Wharton's jelly compartment provides the best source of clinically utilizable mesenchymal stem cells. PLoS ONE 2015; 10(6): e0127992.

Teixeira FG, Carvalho MM, Neves-Carvalho A, et al. Secretome of mesenchymal progenitors from the umbilical cord acts as modulator of neural/glial proliferation and differentiation. Stem Cell Rev 2015; 11(2):288–297.

Troyer DL, Weiss ML. Wharton's jelly-derived cells are a primitive stromal cell population. Stem Cells 2008; 26(3):591–599.

Uccelli A, Benvenuto F, Laroni A, Giunti D. Neuroprotective features of mesenchymal stem cells. Best Pract Res Clin Haematol 2011; 24(1):59–64.

Voulgari-Kokota A, Fairless R, Karamita M, et al. Mesenchymal stem cells protect CNS neurons against glutamate excitotoxicity by inhibiting glutamate receptor expression and function. Exp Neurol 2012; 236(1):161–170.

Wang HS, Hung SC, Peng ST, et al. Mesenchymal stem cells in the Wharton's jelly of the human umbilical cord. Stem Cells 2004; 22(7):1330–1337.

Wang JF, Wang LJ, Wu YF, et al. Mesenchymal stem/progenitor cells in human umbilical cord blood as support for ex vivo expansion of CD34(+) hematopoietic stem cells and for chondrogenic differentiation. Haematologica 2004; 89(7):837–844

Wang X, Cheng H, Hua R, et al. Effects of bone marrow mesenchymal stromal cells on gross motor function measure scores of children with cerebral palsy: a preliminary clinical study. Cytotherapy 2013; 15(12):1549–1562.

Weiss DJ, Casaburi R, Flannery R, et al.A placebo-controlled, randomized trial of mesenchymal stem cells in COPD. Chest 2013143(6):1590–1598.

Wu KH, Zhou B, Lu SH, et al. In vitro and in vivo differentiation of human umbilical cord derived stem cells into endothelial cells. J Cell Biochem 2007; 100(3):608–616.

Xin H, Li Y, Buller B, et al. Exosome-mediated transfer of miR-133b from multipotent mesenchymal stromal cells to neural cells contributes to neurite outgrowth. Stem Cells 2012; 30(7):1556–1564.

Yan ZJ, Hu YQ, Zhang HT, et al. Comparison of the neural differentiation potential of human mesenchymal stem cells from amniotic fluid and adult bone marrow. Cell Mol Neurobiol 2013; 33(4):465–475.

Yang DY, Sheu ML, Su HL, et al. Dual regeneration of muscle and nerve by intravenous administration of human amniotic fluid-derived mesenchymal stem cells regulated by stromal cell-derived factor-1alpha in a sciatic nerve injury model. J Neurosurg 2012; 116(6):1357–1367.

Yang WZ, Zhang Y, Wu F, et al. Safety evaluation of allogeneic umbilical cord blood mononuclear cell therapy for degenerative conditions. J Transl Med 2010; 8:75.

Zhang X, Wang H, Shi Y, et al. Role of bone marrow-derived mesenchymal stem cells in the prevention of hyperoxia-induced lung injury in newborn mice. Cell Biol In 2012; 36(6):589–594.

Outlook

The two clinical branches of this project have dealt with the modern, available diagnostic modalities to investigate the physiologic and the pathological developing brain. Indeed, the ability to visualize the fetal brain has undergone almost incredible development in the last few decades: the resolution of the ultrasonographic equipment has improved to the point that it is possible, among others, to visualize the early embryonic development of the central nervous system in vivo and to demonstrate details of structures such as the posterior fossa and the fetal developing fissures. Prenatal MRI has also developed at a rapid pace, from the "*tissue characterization information that complements the superior anatomic detail of US*" of the 1980s (McCarthy, 1985[1]) to arguably "*the optimal method for depicting the specific abnormalities that characterize each type of malformation of the brain in the fetus*" (Raybaud, 2003[2]). This raises the question: is MRI the optimal method and inherently superior to ultrasound for the assessment of the fetal brain, or is "*dedicated neurosonography equal to MRI in the diagnosis of fetal brain anomalies*"? Malinger et al. (2004[3]). The answer remains under debate.

When reviewing the available literature on the diagnostic value of ultrasound and MRI in fetal neuroimaging, it is difficult to determine when either modality would be appropriate, or when the two could best be combined to optimize the ability to diagnose a fetal central nervous system lesion. Many publications are hampered by an obvious bias by comparing a diagnosis made in primary care by ultrasound with a tertiary diagnosis by MRI, often after a long interval, with only few reports on a comparison between high quality ultrasound and high quality MRI.

Future development of these two clinical branches of this project looks at this issue. The availability of a tertiary care centre, with the possibility to combine ultrasound and MRI at the same level as well as with relative easiness and a short interval, will be the motivation and a support to go further. In particular, our outlook includes:

- to test the VCA, as well as the combination of this angle with all the available parameters of the posterior fossa, in a prospective-designed study with a big number of pathological cases;

- to analyse these cases first with three-dimensional ultrasound scan, then with MRI, and compare the findings among these two techniques in the same fetus;

- combining the synergic data provided by ultrasound and MRI, to analyse the relation between the internal occipital crest and the cerebellar falx and its eventual changes, both in physiological and pathological cases, at different gestational ages, also with the aid of the mid-coronal plane;

---

[1] McCarthy SM, Filly RA, Stark DD, Hricak H, Brant-Zawadzki MN, Callen PW, Higgins CB. Obstetrical magnetic resonance imaging: fetal anatomy. Radiology 1985; 154:427–432

[2] Raybaud C, Levrier O, Brunel H, Girard N, Farnarier P. MR imaging of fetal brain malformations. Childs Nerv Syst 2003; 19:455–470

[3] Malinger G, Ben Sira L, Lev D, Ben Aroya Z, Kidron D, Lerman-Sagie T. Fetal brain imaging: a comparison between magnetic resonance imaging and dedicated neurosonography. Ultrasound Obstet Gynecol 2004; 23:333–340

- to test the measurement of the Sylvian fissure and insula lobe with the MRI in physiological cases throughout gestation, as well as in pathological cases, in a prospective-designed manner, with a proper combination between ultrasound and MRI;

- based on the current literature, which reported association between ventral induction defects and a failure of neuronal migration, to investigate deeper the association between cortical development defects and posterior fossa anomalies;

- to investigate, by combining ultrasound and MRI, acquired brain lesions in the fetus, in particular hypoxic-ischemic brain injury, since we believe that in these cases the synergy between ultrasound and MRI may reach the best expression.

It is important to underline that imaging does not equate diagnosis. Many studies affirm the value of a multidisciplinary discussion and it would appear that this is where the real strength lies: not in the choice between ultrasound or MRI, but in using each modality to its maximum capability and arriving at a final diagnosis during a multidisciplinary discussion.

Regarding the third, pre-clinical, branch of this project, the next steps will include the treatment of perinatal brain injury in the rat model, after assessing the possible intracellular pathways involved in the mechanism of action of the Wharton's jelly – mesenchymal stem cells - exosomes in in-vitro experiments. Outcome evaluation will include histological changes, inflammatory response, systemic immune response, peripheral inflammatory response as well as neurofunctional outcomes. Interestingly, prenatal imaging would be useful also in this context. It would be of value to include, among the outcome measures of Wharton's jelly – mesenchymal stem cells – exosomes treatment after perinatal brain injury in the rat model, the in-vivo imaging of the brain with comparative anatomy investigations. Indeed, the currently available imaging tools in Neuroscience and Prenatal Medicine may represent a connecting bridge between pre-clinical and clinical studies in the pathophysiology of the developing brain, thus enhancing the translation "*from bench to bedside*".

The lack of effective interventions for many morbidities related to prematurity unlocks the potential of cell-based personalized treatments. Safe and effective clinical interventions are future perspectives bearing hope to improve the lifelong outcomes of the infants in our care.

Acknowledgements

This phD Thesis would not have been possible without the guidance and the help of many people who contributed and extended their valuable assistance in the preparation and completion of this research.

First of all, I would like to thank my Italian supervisor Professor Pasquale Martinelli, Ordinary Professor in Obstetrics & Gynaecology at University of Naples Federico II, who gave me the opportunity to target my research to the fascinating and challenging field of Prenatal Medicine; I am also grateful to Dr. Aniello Di Meglio and his precious collaborator Dr. Carmine Sica, who gave me the passion to Prenatal Ultrasound and constantly guided, supported and encouraged me in the first half of this three-year project in Naples.

I am full of gratitude to my Swiss supervisor Professor Daniel Surbek, Director of the Department of Obstetrics and Gynaecology of the University of Bern, who gave me the possibility to start a new professional experience in an amazing Country, and allowed me to interlace a fruitful collaboration with his valuable clinical and research equipe at the Prenatal Ultrasound Unit and at the Laboratory of Prenatal Medicine, respectively. In particular, the clinical part of this phD Thesis would not have been fully developed without the interest, enthusiastic guidance, inspiration, patience and steadfast encouragement of Professor Luigi Raio, Head of the Prenatal Ultrasound Unit. I would also like to express my deepest gratitude to Dr. PD Andreina Schoberlein, the Head of the Laboratory of Prenatal Medicine, for her kind and constant support to the pre-clinical part of this project. Besides, I would like to thank Dr. Bzron Opplinger and Dr. Marianne Jöerger - Messerli. They excellently introduced me in the laboratory techniques and provided dedicated guidance at any time. I am indebted to Professor Ronald Wiest, Director of the Department of Diagnostic and Interventional Neuroradiology, for his kind support to the MRI studies.

All of these people provided me excellent technical equipment and a pleasant working climate that made the development of this thesis not just possible, but a fulfilling and exciting time.

Tables

Characteristic	Value
Age, y	31 (range: 21–39)
Body mass index, kg/m^2	23.5±3.38
Gravidity	1.4±0.61
Parity	1.0±0.41
Birth weight, g	3084±503
Birth percentiles	45±12
Male/female ratio	0.59

Data are presented as mean±SD where applicable

Table 1. Clinical Characteristics of the Study Population Including Perinatal Outcome Data (study A 3.a).

GA	no. of cases	10th percentile	50th percentile	90th percentile
18	18	27.77	32.40	37.03
19	24	29.86	33.96	38.50
20	70	32.47	37.93	42.39
21	75	34.85	38.75	44.65
22–23	54	37.75	43.02	47.29
24–25	24	42.72	47.42	53.12
26–27	19	46.44	52.1	59.76
28–30	23	53.30	59.75	65.20
31–33	21	59.87	65.15	73.83

Table 2. Predicted cerebellar vermis circumference (VC) (mm) values by gestational age (weeks) (GA).

Characteristic	Value
Age, y	33 (range: 22–38)
Gestational age, w	26.3±4.6 (range: 17-35.5)
Body mass index, kg/m2	23.8 ± 3.79
Gravidity	2.6 ± 0.66
Parity	1.8 ± 0.41
Birth weight, g	3152 ± 633
Birth percentiles	47 ± 18
Male/female ratio	0.47

Data are presented as mean ± SD where applicable

Table 3. Clinical Characteristics of the Study Population Including Perinatal Outcome Data (study A 3.b).

GA (weeks)	No. of cases	10th percentile	50th percentile	90th percentile
18-19	17	51.97	64.15	76.34
20-21	15	52.18	64.27	76.35
22-23	25	52.35	64.36	76.36
24-25	19	52.52	64.44	76.37
26-27	13	52.69	64.53	76.38
28-29	15	52.85	64.62	76.39
30-31	13	53.02	64.71	76.40
32-33	12	53.19	64.80	76.41

Table 4. Predicted vermian-cresta angle (VCA) (°) values by gestational age (weeks) (GA).

Characteristic	Value
Age, y	34 (range: 28–38)
Gestational age, w	26.3±2.6 (range, 22-32).
Body mass index, kg/m2	24.2 ± 2.44
Gravidity	2.7 ± 0.9
Parity	2.2 ± 0.37
Birth weight, g	3301 ± 426
Birth percentiles	58 ± 14
Male/female ratio	0.55

Data are presented as mean ± SD where applicable

Table 5. Clinical Characteristics of the Study Population Including Perinatal Outcome Data (study A 3.c).

Characteristic	**Value**
Age, y	31 (range: 21–45)
Gestational age, w	24.3±2.6 (range, 19-28)
Body mass index, kg/m2	24.4 ± 2.2
Gravidity	2.1 ± 0.24
Parity	1.7 ± 0.55
Karyotype analysis	5 abnormal*/ 22 analysed
Associated malformations	N=15 (50%)**
Intrauterine fetal deaths	N=3 (10%)***
Termination of pregnancy	N=9 (30%)†
Male/female ratio	1.5

Data are presented as mean ± SD where applicable

*: 2 trisomies 18, 2 trisomies 13 and 1 chromosome-4-6 translocation. Four of five karyotypic anomalies were in fetuses with the final diagnosis of DWM; the fifth case was associated with a MCM.

**: cardiac (n=8), brain (n= 7), skeletal (n=8), renal (n=3) and gastrointestinal malformations (n=2).

***: 1 with DWM with no other malformations and a normal karyotype; 1 with VH and additional malformations; and 1 with confirmed DWM in trisomy 18

†: 5 with DWM, 2 with MCM and 2 with VH, both with additional malformations

Table 6. Clinical Characteristics of the Study Population Including Perinatal Outcome Data (study A 3.d). DWM, Dandy-Walker Malformation; VH, Vermian Hypoplasia; MCM, mega cisterna magna.

	Vermis				
Findings	***Vermian-Crest Angle (VCA)***	*Hypoplasia*	*Cisterna magna septa*	*Choroid plexus position*	*Diagnosis*
Enlarged Blake's pouch, enlarged posterior fossa, elevated torcula, (often hydrocephalus)	**Increased**	Yes: variable, may be severe	Invisible: apposed to side walls of cisterna magna	Inferior margin of Blake's pouch	Dandy–Walker malformation
Enlarged Blake's pouch, normal-sized posterior fossa, normal torcula	**Normal**	Yes: variable to intermediate	Invisible: apposed to side walls of cisterna magna	Inferior margin of Blake's pouch	Dandy–Walker variant or 'inferior vermian hypoplasia'
Enlarged Blake's pouch, normal-sized posterior fossa, normal torcula	**Mild increased**	No: may be misdiagnosed as 'inferior vermian hypoplasia'	Visible: bowed laterally	Superior margin of Blake's pouch	Blake's pouch cyst, a.k.a. persistent Blake's pouch
Enlarged Blake's pouch, enlarged posterior fossa	**Normal**	No	Visible: bowed laterally	Superior margin of Blake's pouch	Mega cisterna magna

Table 7. A proposal of categorization of the major posterior fossa malformations including the Vermian-Cresta angle (VCA) [modified from Robinson (2014)].

Characteristic	**Value**
Age, y	31 (range 21-39)
Body mass index, kg/m^2	24.5 ± 3.38
Gravidity	1.4± 0.61
Parity	1.0± 0.41
Birth weight, g	3084 ± 503
Birth centiles	45± 12
Males, %	37

- Data are presented as mean ± SD where applicable.

Table 8. Clinical characteristics of the study population, including perinatal outcome data.

Gestational Age (weeks)	Investigated Parameters	N patients	Mean (mm)	SD (mm)
18-19	Sylvian Fissure	43	5.72	1.07
	Insula Lobe		12.42	0.92
	Insula Ratio		0.31	0.04
20-21	Sylvian Fissure	120	7.25	1.36
	Insula Lobe		14.39	1.35
	Insula Ratio		0.33	0.04
22-23	Sylvian Fissure	39	8.65	1.23
	Insula Lobe		15.61	1.90
	Insula Ratio		0.36	0.05
24-25	Sylvian Fissure	27	10.53	1.58
	Insula Lobe		17.89	2.61
	Insula Ratio		0.37	0.04
26-27	Sylvian Fissure	28	12.10	1.49
	Insula Lobe		20.41	2.00
	Insula Ratio		0.37	0.03
28-29	Sylvian Fissure	20	11.37	1.14
	Insula Lobe		21.62	1.51
	Insula Ratio		0.34	0.03
30-31	Sylvian Fissure	25	12.75	1.57
	Insula Lobe		22.35	1.92
	Insula Ratio		0.36	0.04
32-33	Sylvian Fissure	20	13.88	2.06
	Insula Lobe		25.25	1.60
	Insula Ratio		0.35	0.04

Table 9. Mean and standard deviation (SD) for Sylvian fissure, insula lobe and insula ratio per gestational week.

Figures

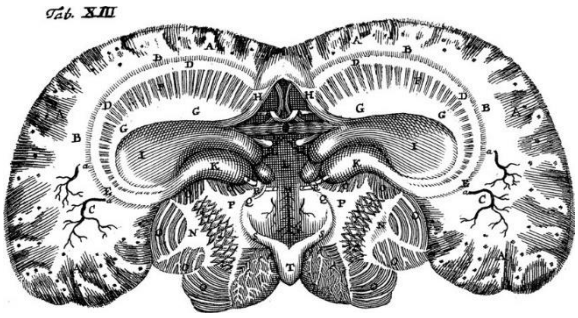

Fig. 1. Figure of a split brain and cerebellum from Vieussens (1684). The floor of the fourth ventricle is visible, the initial portion of the spinal cord is indicated by a T. The cerebellar halves are further dissected to show the corpus rhomboideum, indicated as an area with double hatching, located in the white matter between N and P. (modified from M. Glickstein et al. Neuroscience 162 (2009) 549–559).

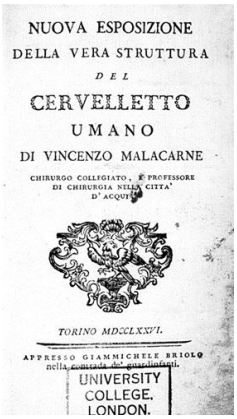
NUOVA ESPOSIZIONE
DELLA VERA STRUTTURA
DEL
CERVELLETTO
UMANO
DI VINCENZO MALACARNE
CHIRURGO COLLEGIATO, E PROFESSORE
DI CHIRURGIA NELLA CITTA'
D'ACQUI
TORINO MDCCLXXVI.
APPRESSO GIAMMICHELE BRIOLO
nella contrada de' guardinfanti.

Fig. 2. Title page of Malacarne's "Il cervelletto," the first book devoted entirely to the cerebellum (modified from M. Glickstein et al. Neuroscience 162 (2009) 549–559).

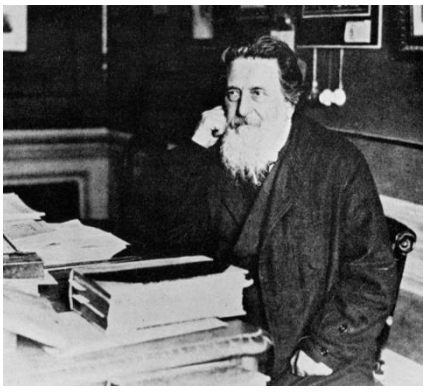

Fig. 3. Luigi Luciani; portrait.

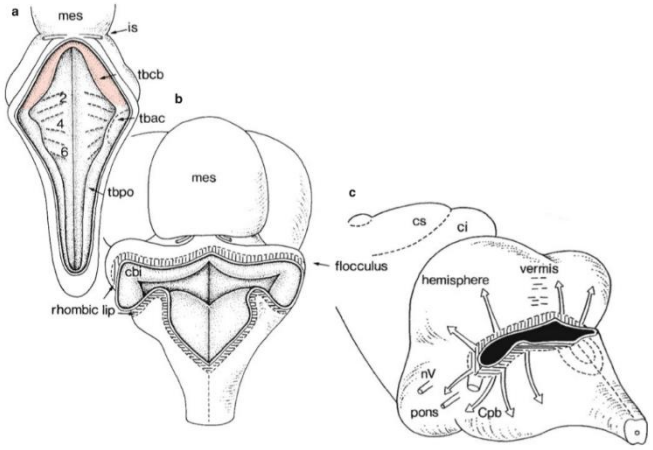

Fig. 4. Early development of the human cerebellum: (a) at approximately 4 weeks of development; (b) at the end of the embryonic period; (c) at 13 weeks of development. The V-shaped tuberculum cerebelli is shown in light red , and the upper and lower rhombic lips by vertical and horizontal hatching, respectively. In (c) arrows show the migration paths from the rhombic lips; cbi: internal cerebellar bulge, ci: colliculus inferior, Cpb: corpus pontobulbare, cs: colliculus superior, is: isthmus, mes; mesencephalon, nV: trigeminal nerve, tbac: tuberculum acusticum, tbcb: tuberculum cerebelli, tbpo: tuberculum ponto-olivare, 2, 4, 6 rhombomeres (modified from Hans J. ten Donkelaar, Martin Lammens, Akira Hori. Clinical Neuroembryology. Development and Developmental Disorders of the Human Central Nervous System. Springer 2014).

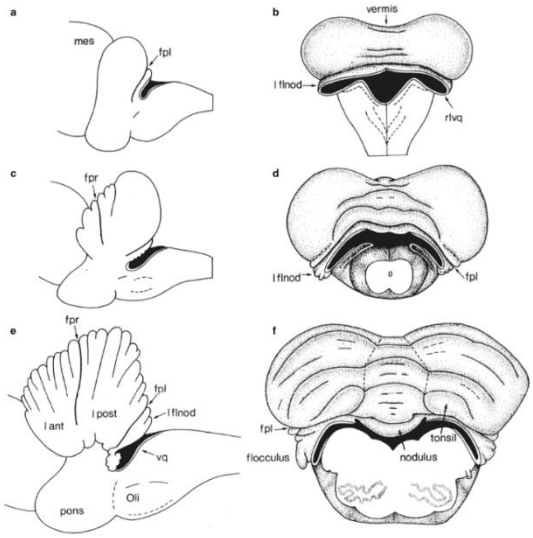

Fig. 5. Fetal development of the human cerebellum shown in lateral (on the left) and dorsal (on the right) views: (a , b) 13 weeks of development; (c, d) 4 months of development; (e, f) 5 months of development; fpl: fissura posterolateralis, fpr: fissura prima, l: ant lobus anterior, l fl nod: lobus fl occulonodularis, l post: lobus posterior, mes: mesencephalon, Oli: oliva inferior, rlvq: lateral recess of fourth ventricle, vq: ventriculus quartus (modified from Hans J. ten Donkelaar, Martin Lammens, Akira Hori. Clinical Neuroembryology. Development and Developmental Disorders of the Human Central Nervous System. Springer 2014).

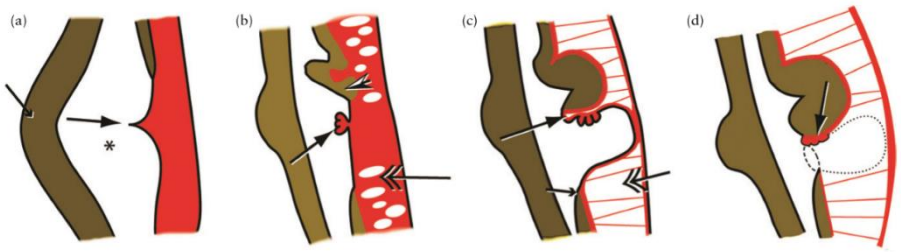

Fig. 6. (a) During formation of the dorsal pontine flexure (small arrow) a transverse crease (large arrow) forms in the roof of the rhombencephalic vesicle (*), dividing it into anterior (cranial) and posterior (caudal) membranous areas. (b) The vermis (arrowhead) develops from the rhombic lip at the superior margin of the anterior membranous area. Choroid plexus develops in the crease (arrow). Cavitation starts in the overlying meninx primitiva (double arrow) to form the subarachnoid space. (c) As the cerebellum grows inferiorly the posterior membranous area bulges out between the vermis (large arrow) and the nucleus gracilis (small arrow), forming Blake's pouch. The subarachnoid space remains trabeculated by pia-arachnoid septations (double arrow). (d) Blake's pouch fenestrates (dotted line) and the neck of Blake's pouch becomes the foramen of Magendie (dashed line). The choroid plexus (arrow) now appears to be in the cisterna magna (modified from Robinson AJ. Inferior vermian hypoplasia – preconception, misconception. Ultrasound Obstet Gynecol 2014; 43: 123–136).

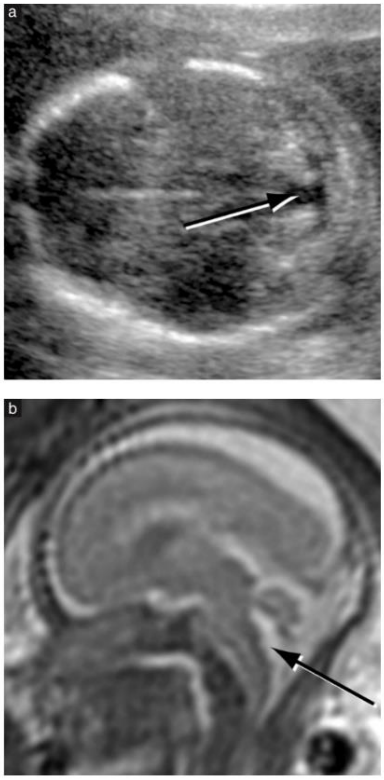

Fig. 7. (a) Modified axial sonogram at 19 gestational weeks demonstrates a small gap inferior to the vermis and between the cerebellar hemispheres (arrow) which represents the foramen of Magendie. (b) Sagittal magnetic resonance image in same fetus at 21 weeks, after referral for 'inferior vermian hypoplasia', demonstrating small gap inferior to the vermis (arrow) in keeping with the foramen of Magendie. Follow-up imaging and outcome were normal. (modified from Robinson AJ. Inferior vermian hypoplasia – preconception, misconception. Ultrasound Obstet Gynecol 2014; 43: 123–136).

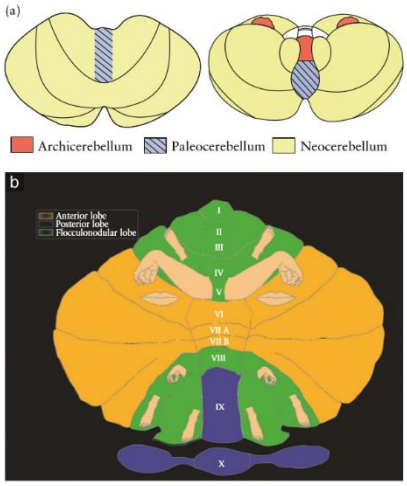

Fig. 8. (a) Phylogenetic origins of the cerebellum. Phylogenetically, the archicerebellum is oldest and is only seen in fish and lower amphibians. The paleocerebellum is newer, is seen in higher amphibians and is larger in reptiles and birds. The neocerebellum is the most recent phylogenetically, is only found in mammals and is largest in humans. Note that the central lobules of the vermis are of neocerebellar origin. Superior (left) and inferior (right) views are shown. (b) Phylogenetically older functions which are common to more species map further away from the 'equator' than do newer functions which are seen in fewer species. A general correlation with evolutionary steps is seen, i.e. bipedality before manual dexterity before oromotor skills and associated cognitive and language skills, which developed last. (modified from Robinson AJ. Inferior vermian hypoplasia – preconception, misconception. Ultrasound Obstet Gynecol 2014; 43: 123–136).

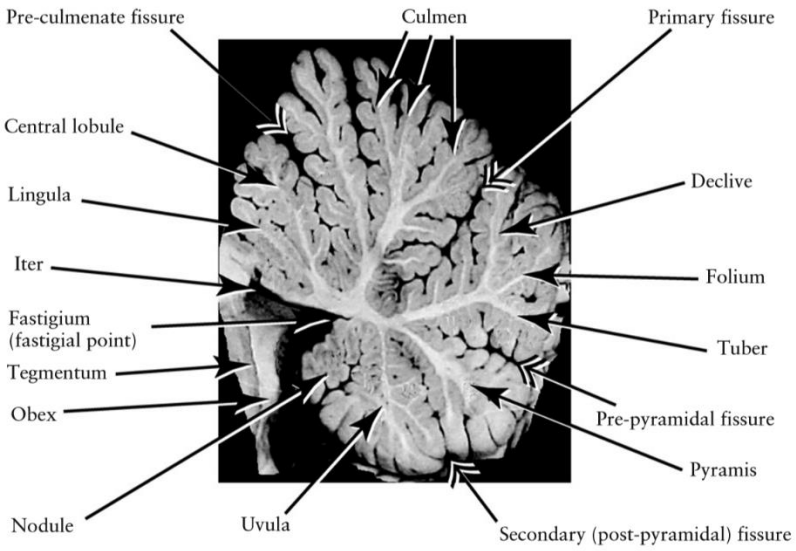

Fig. 9. Gross adult specimen with all fissures and lobules of the cerebellar vermis labelled (modified from Robinson AJ. Inferior vermian hypoplasia – preconception, misconception. Ultrasound Obstet Gynecol 2014; 43: 123–136).

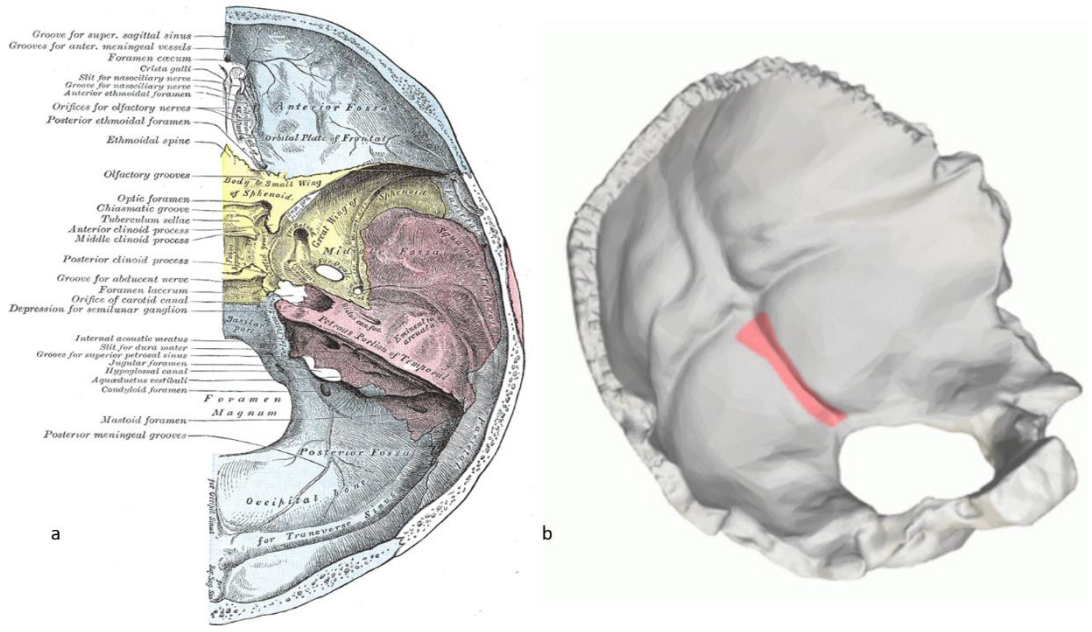

Fig. 10. (a) Axial view of the adult cranial fossae, with the posterior fossa coloured in grey (b) The internal occipital crest, labelled in red (modified from F.H. Netter. Atlas of Human Anatomy. Elsevier, 2014).

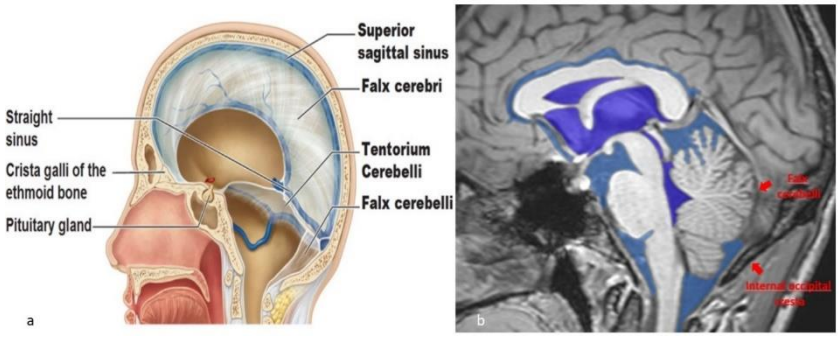

Fig. 11. (a) Graphic and (b) MRI midsagittal view of the adult cranium, with its membranous structures. In particular, the falx cerebelli is a small sickle shaped fold of dura mater, projecting forwards into the posterior cerebellar notch (modified from http://www.radioanatomie.com/29_citernes/citernes_ventricules.php?vue=1&langue=it).

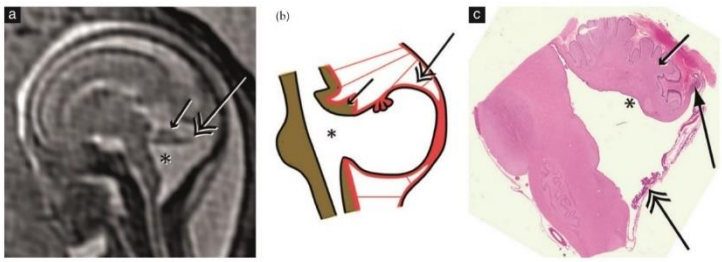

Fig. 12. (a) In Dandy–Walker continuum, the vermis is elevated and abnormally lobulated (small arrow), with enlargement of the fourth ventricle (*) and Blake's pouch. The elongated nodulus and displaced germinal matrix can be seen in the superior margin of Blake's pouch (double arrow). (b) Diagrammatic representation showing the

small vermis (small arrow), enlarged Blake's pouch (double arrow) and fourth ventricle (*). (c) Histological specimen showing abnormal vermis (small arrow) and choroid plexus (double arrow) displaced into the inferior wall of Blake's pouch, which remains intact. The fastigial recess is abnormally formed (*) and the germinal matrix (large arrow) is displaced from its normal position just below the fastigial recess into the superior margin of Blake's pouch (modified from Robinson AJ. Inferior vermian hypoplasia – preconception, misconception. Ultrasound Obstet Gynecol 2014; 43: 123–136).

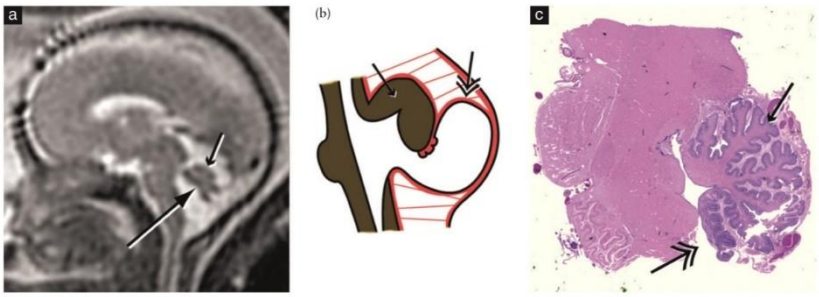

Fig. 13. (a) In persistent Blake's pouch, the vermis is elevated away from the brainstem but the major landmarks of the primary fissure (small arrow) and fastigial recess (large arrow) appear normal and the lobulation appears normal. (b) Diagrammatic representation showing Blake's pouch (double arrow) elevating a normal vermis (small arrow). (c) Pathological specimen of the same fetus with Blake's pouch collapsed (double arrow) and vermian lobulation apparently normal (arrow) (modified from Robinson AJ. Inferior vermian hypoplasia – preconception, misconception. Ultrasound Obstet Gynecol 2014; 43: 123–136).

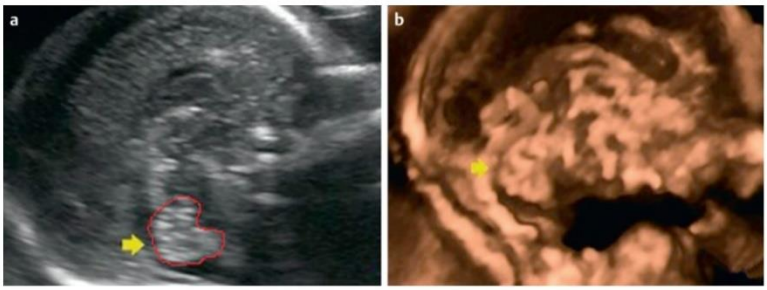

Fig. 14. Ultrasound images showing the cerebellar vermis (yellow arrow) obtained by two-dimensional ultrasound at 22 weeks of gestation (a) and three-dimensional ultrasound at 24 weeks of gestation (b) Vermis circumference (VC) is outlined in red (a).

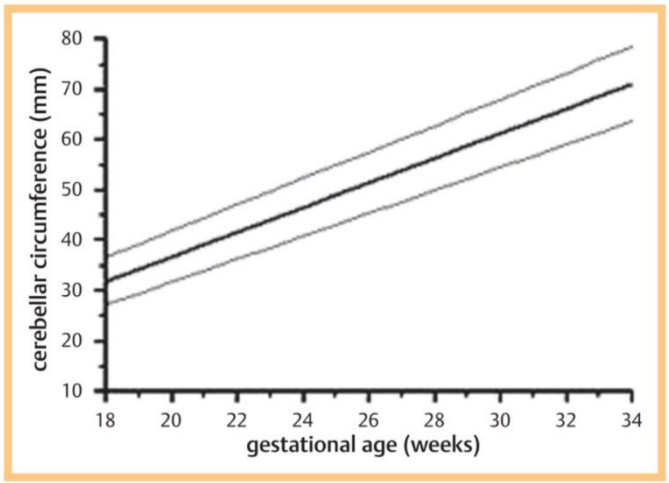

Fig. 15. Plot showing the cerebellar circumference observed measurements and the fitted 10th , 50th , and 90th percentiles for gestational age.

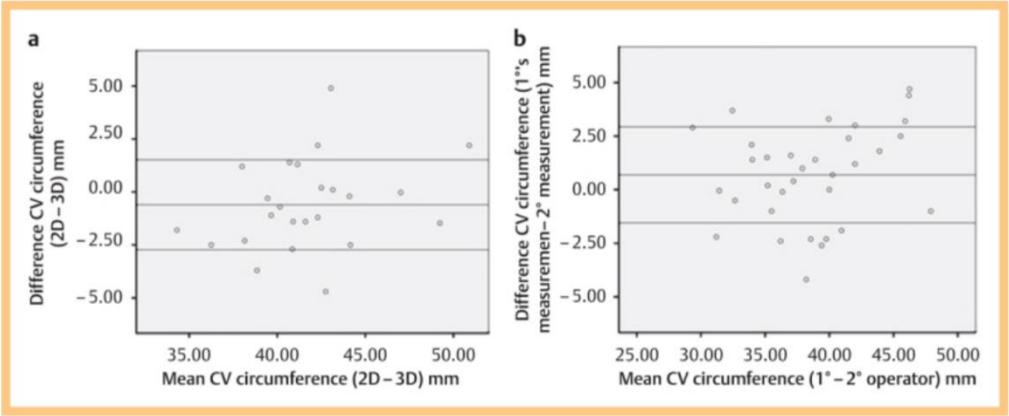

Fig. 16. Bland-Altman plots of the paired measurement obtained by 2D and 3D ultrasound (a) and by two different examiners (b).

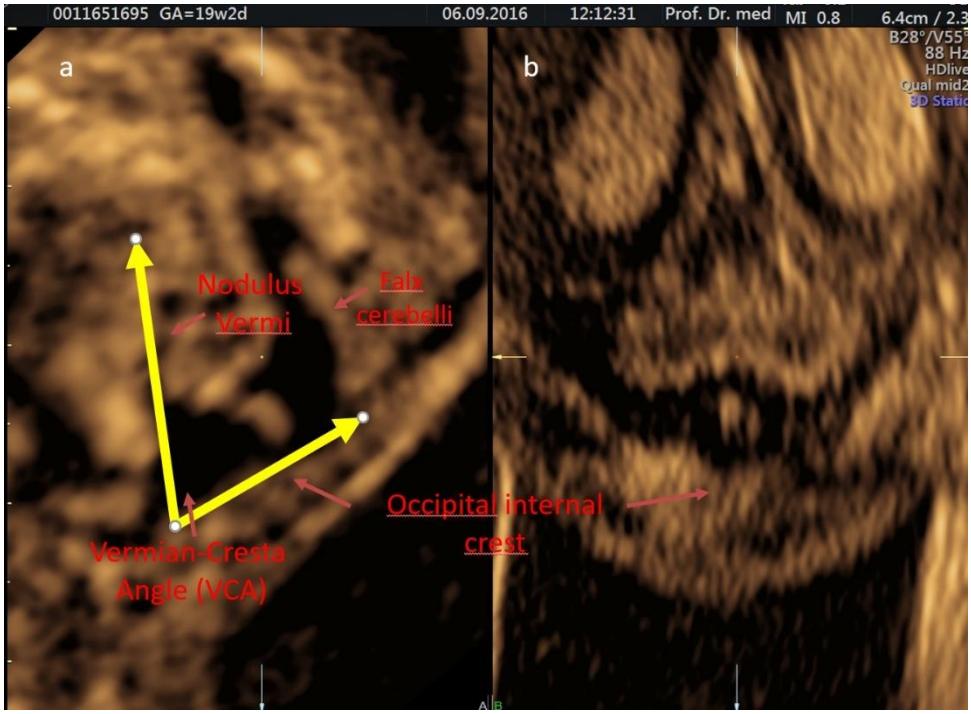

Fig. 17. Midsagittal (a) and midcoronal (b) view of the posterior fossa at ultrasonographic three-dimensional reconstructed planes in a 20 weeks fetus. The vermian-cresta angle (VCA) is labelled in yellow. Landmarks have been highlighted.

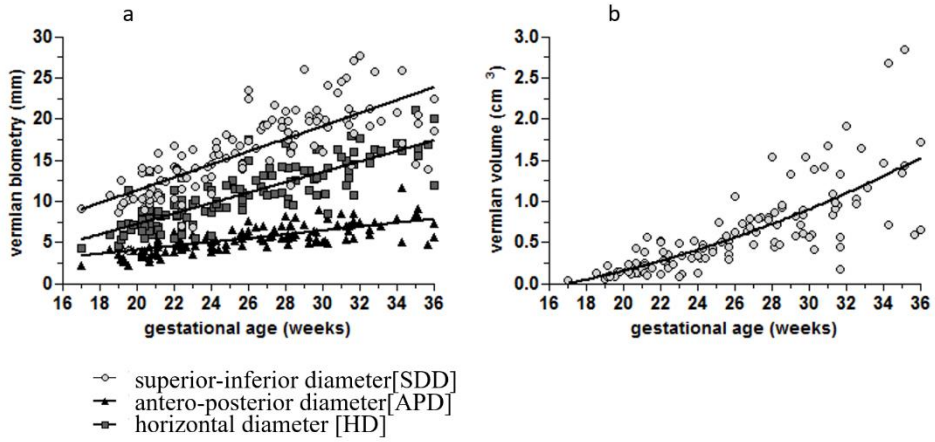

Fig. 18. Plots showing the vermian biometries (a) and volume (b) observed measurements for gestational age.

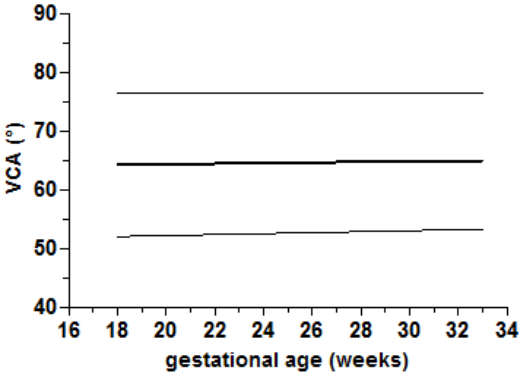

Fig. 19. Plot showing the vermian-cresta angle (VCA) observed measurements and the fitted 10th , 50th , and 90th percentiles for gestational age.

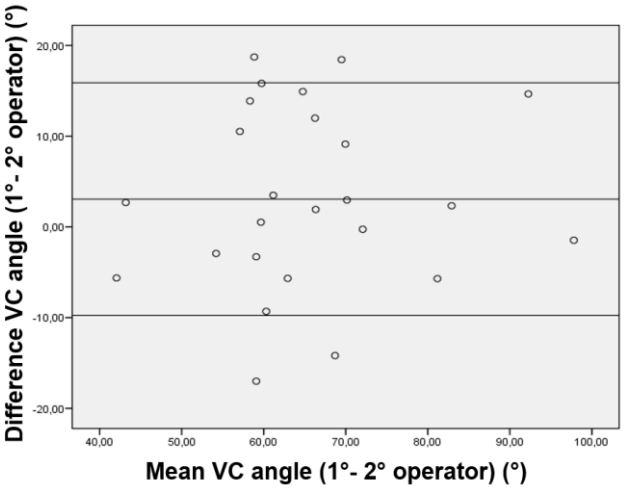

Fig. 20. Bland-Altman plots of the paired measurement obtained by two different examiners (study A 3.b)

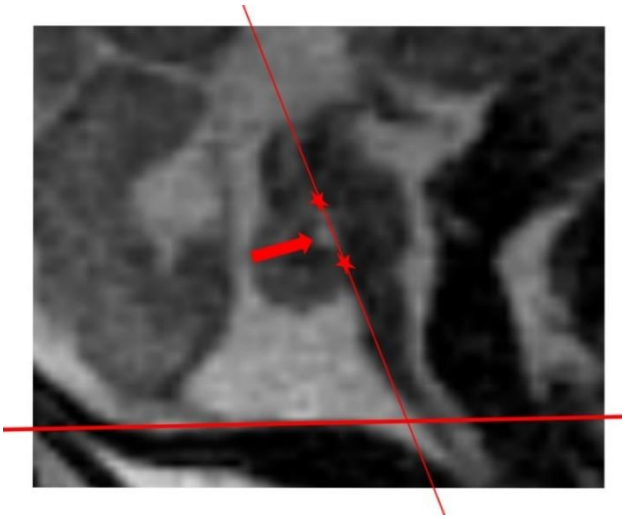

Fig. 21. MRI midsagittal view of the posterior fossa in a 25 weeks fetus. The vermian-cresta angle (VCA) is labelled in red. The red arrow with the two star-shaped markers delimitate the fastigium cerebelli.

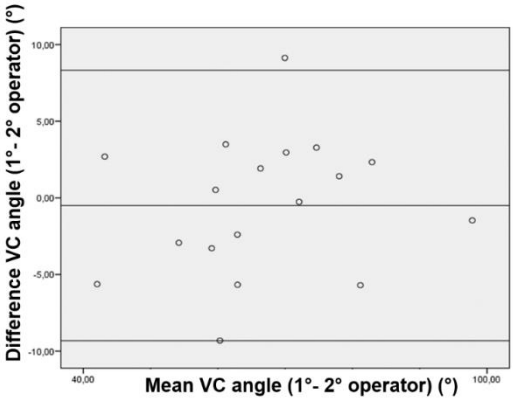

Fig. 22. Bland-Altman plots of the paired measurement obtained by two different examiners (study A 3.c)

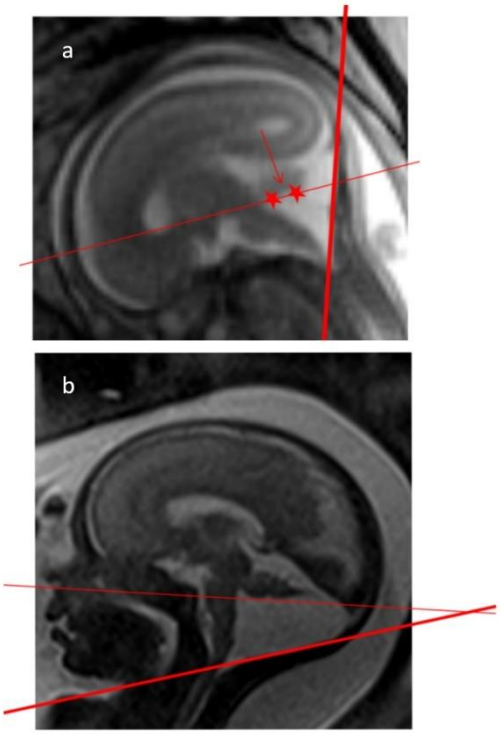

Fig. 23. Measurement of Vermian Crest angle (VCA) in fetuses with: (a) Blake's pouch cyst; (b) Dandy–Walker malformation. The BV angles are 101° and 157 °, respectively.

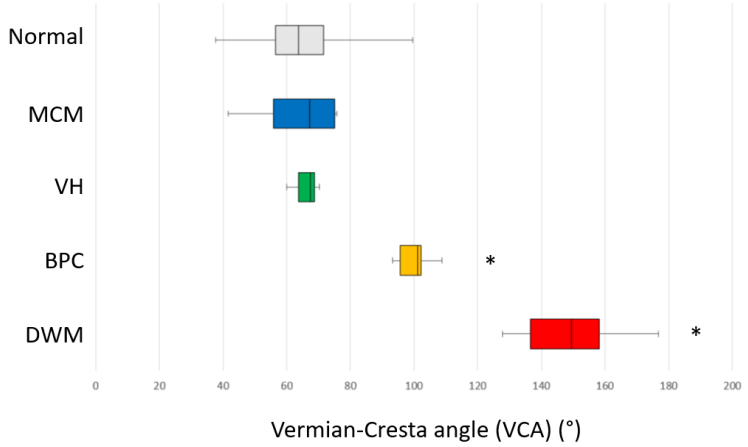

Fig. 24. Box-and-whisker plot of distribution of Vermian-Crest angle (A) in controls and in fetuses with mega cisterna magna (MCM), vermian hypoplasia (VH), Blake's pouch cyst (BPC) and Dandy-Walker Malformation (DWM). Medians are indicated by a line inside each box, 25th and 75th percentiles by box limits and 5th and 95th percentiles by lower and upper bars, respectively. VCA increased significantly (*) in both BPC and DWM compared with controls.

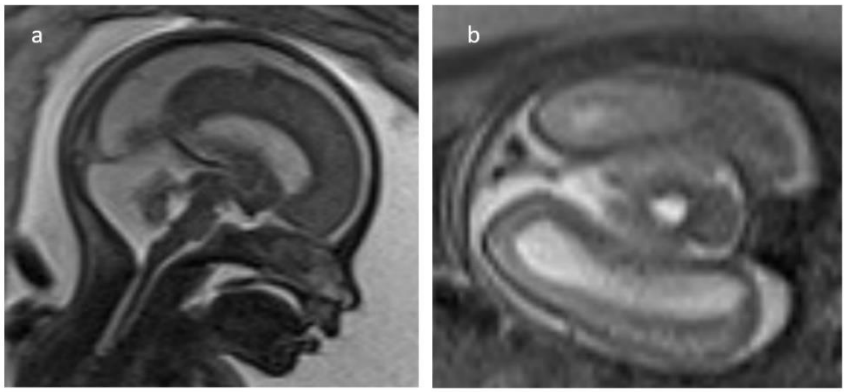

Fig. 25. Case 1. Cerebellar hypoplasia, with rhomboencephalosynapsis. Hydrocephalus. FSE/T2-weighted images. (a) Midsagittal plane; (b) Axial plane.

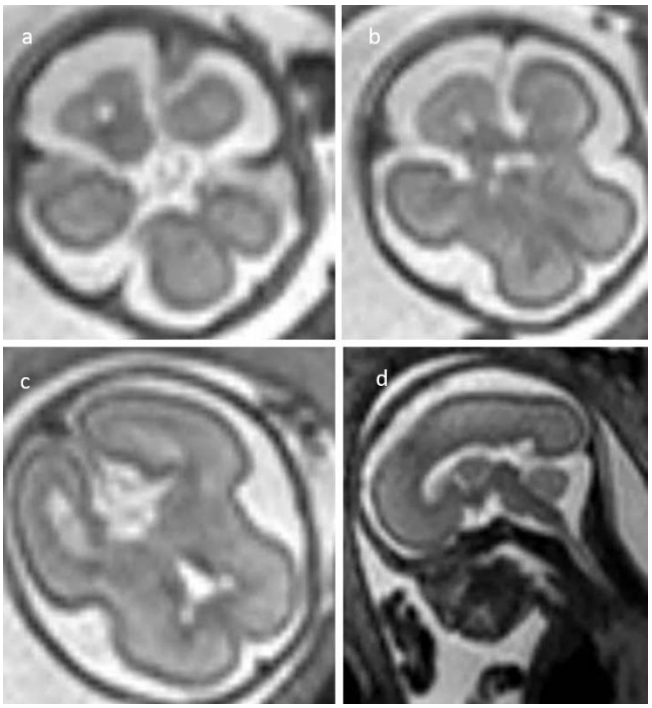

Fig. 26. Case 2. Agenesis of the cerebellar vermis, dorsal fusion of the cerebellar hemispheres, which appears without the normal cerebellar sulci, and a reduction of the fourth ventricle. No other brain anomalies. FSE/T2-weighted images. (a, b, c) Axial plane; (d) Mid-sagittal plane.

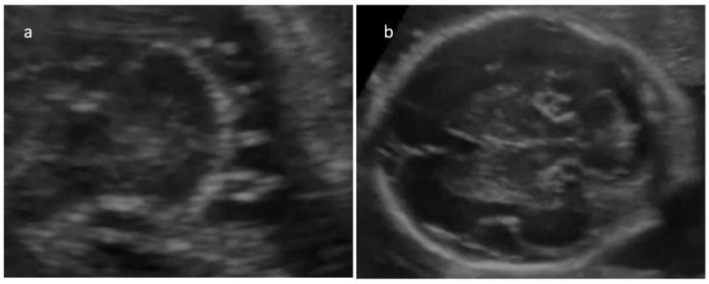

Fig. 27. Case 3. Absent visualization of the vermis, fusion of the cerebellar hemispheres with a reduction of the trans-cerebellar diameter below the fifth centiles, without demonstration of any communication between the fourth ventricle and the cisterna magna. No other brain anomalies. Two-dimensional ultrasound scan. (a) Axial plane, with magnification of the posterior fossa; (d) Axial plane.

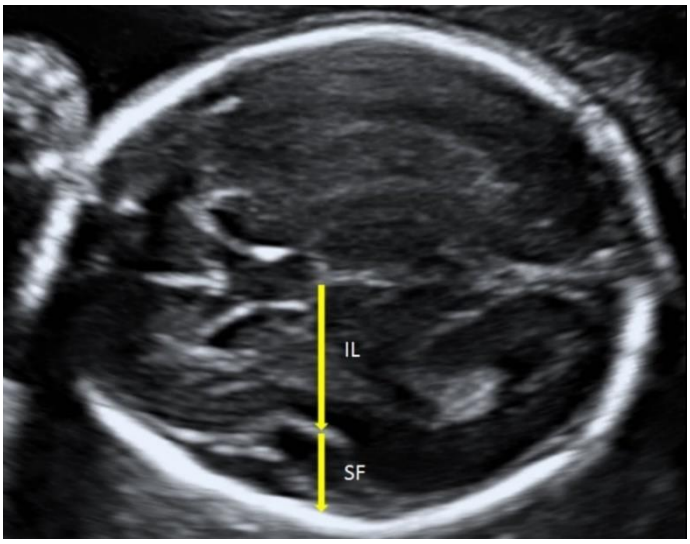

Fig. 28. demonstrates a standard trans-thalamic view of the fetal head obtained by trans-abdominal 2D-US showing the SF (Sylvian fissure) and IL (insula lobe) measurements, and adjacent anatomical landmarks at 23 weeks of gestational age.

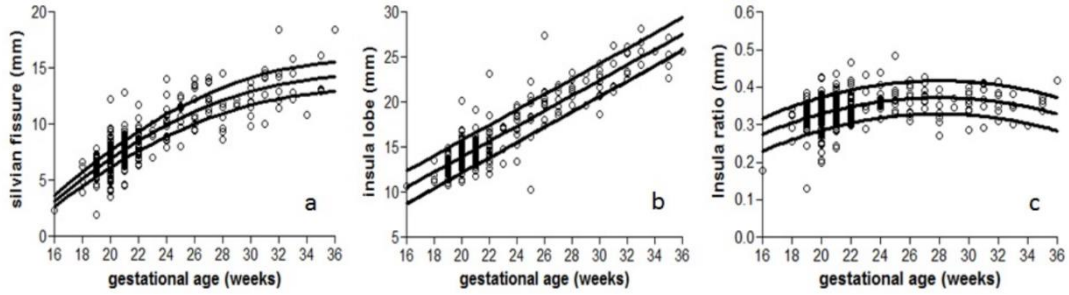

Fig. 29. Scatterplot showing the correlation of depth of sylvian fissure (a), the insula lobe (b) and the insula ratio (c) with gestational age.

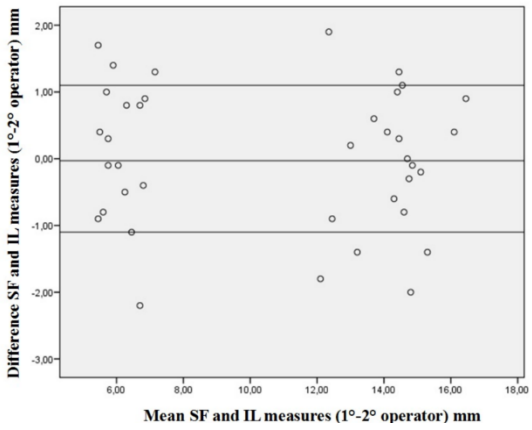

Fig. 30. Bland-Altman plots of the paired measurement obtained by two different examiners.

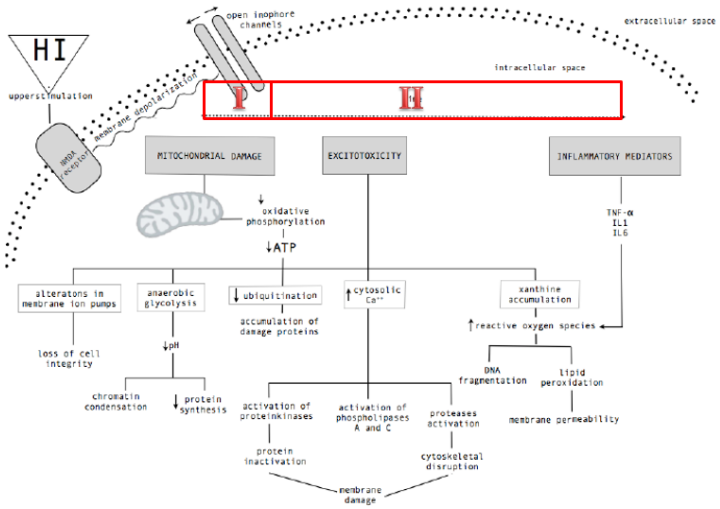

Fig. 31. Cascade of biochemical mechanism after hypoxic-ischemic brain injury. A schematic diagram that summarizes the cellular and molecular events triggered after hypoxic-ischemic injury in the developing brain. The first phase (I) include glucose depletion with mitochondrial damage, while later (II) the cytotoxic levels of intracellular calcium and the release of inflammatory mediators cause metabolic failure, oxidative stress and ultimately the cell death (modified from Cerio F.G. et al. 2013).

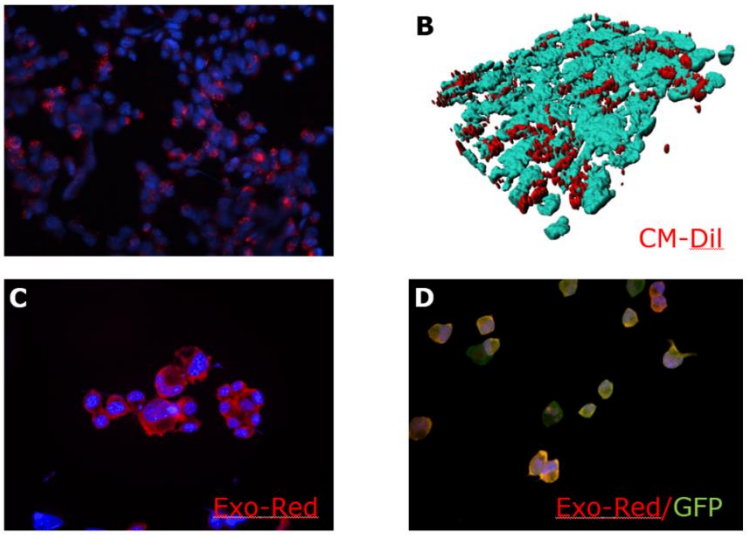

Fig. 32. Wharton's jelly mesenchymal stem cell-derived exosomes interact with N2a cells and hippocampal rNPC. Exosomes labelled with the membrane dye DiI (red) co-localize with N2a cells (DAPI, blue) after 24 hours of co-culture (A,B). Analysis was done by conventional fluorescence (A) and confocal microscopy (3D visualization by Imaris software) (B). Furthermore, exosomal RNA fluorescently labelled with Exo-Red was detected in the cytoplasma of N2a cells (C) and GFP-expressing hippocampal rNPC (D) after 2 hours of co-culture.

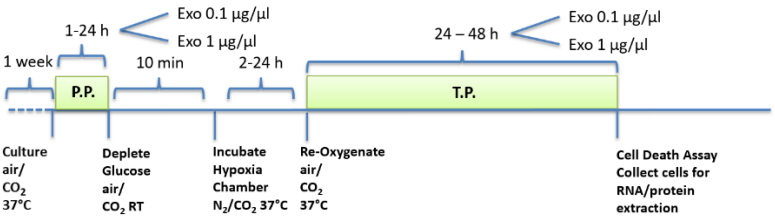

Fig. 33. Our OGD-R protocol. OGD duration is set at different time points, varying from 2 to 24h. Exosomes are given either before (prevention) or after (treatment) the OGD ad different concentrations. The prevention period (P.P.) is either 1h or 24h before OGD. Treatment period (T.P.) includes two time points: 24h and 48h after OGD.

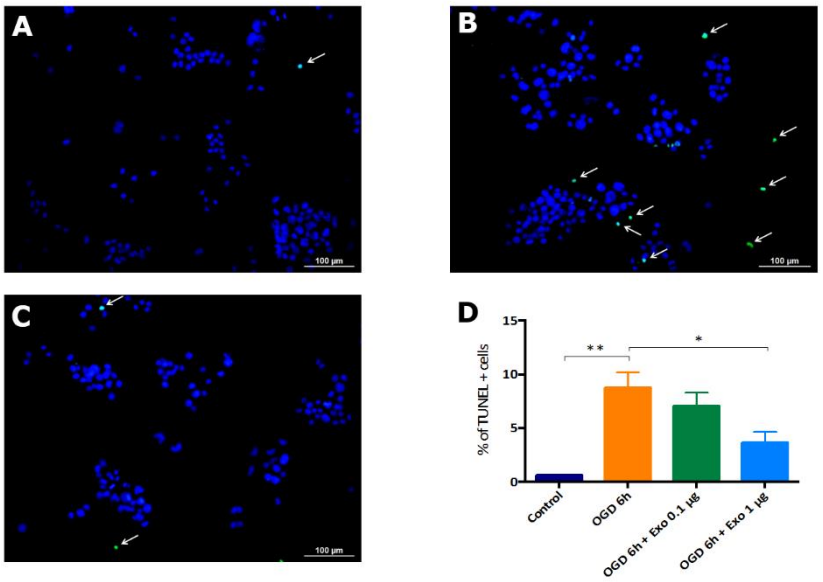

Fig. 34. Wharton's jelly mesenchymal stem cell-derived exosomes reduce OGD-R triggered apoptosis in N2a cells. N2a cells (DAPI, blue) were subjected to TUNEL test after 24 hours of control culture (A), 6 hours of OGD followed by 24 hours of reoxygenation without (B) and with the addition of 1 µg/ml exosomes (C). TUNEL-positive N2a cells are indicated by white arrows (A, B, C). The percentage of TUNEL-positive N2a cells were calculated relative to DAPI (D).

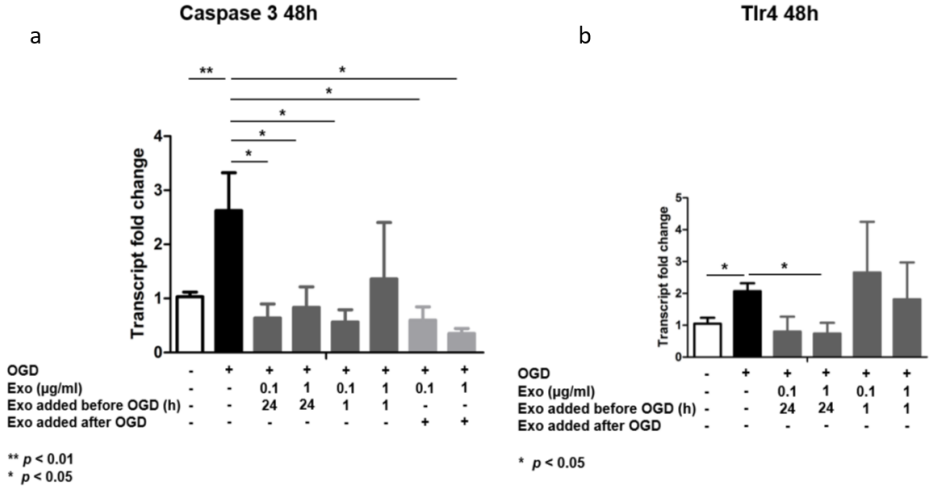

Fig. 35. Wharton's jelly mesenchymal stem cell-derived exosomes reduce OGD-R triggered increased expression of markers of apoptosis (Caspase 3) (a) and inflammation (Tlr4) (b) at the level of RNA in N2a cells in a dose- and timing- dependent manner. N2a cells were collected and RNA extracted after 6 hours of OGD followed by 48 hours of reoxygenation without and with the addition of 0.1 and 1 µg/ml exosomes at 3 different time points: 24h before OGD, 1h before OGD and immediately after OGD.

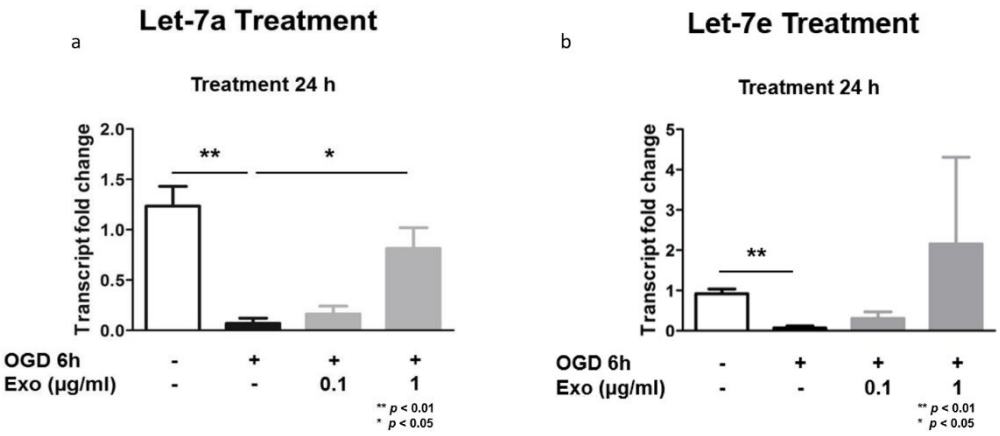

Fig. 36. Wharton's jelly mesenchymal stem cell-derived exosomes increase the expression of microRNAs associated with neuronal differentiation and modulation of inflammation Let 7a (a) and Let7e (b) in N2a cells in a dose-dependent manner. N2a cells were collected and RNA extracted after 6 hours of OGD followed by 24 hours of reoxygenation without and with the addition of 0.1 and 1 µg/ml exosomes immediately after OGD.